Assessing whether human oligodendrocytes go senescent: a cell culture and transcriptomic interrogation of human white matter

Joseph Voth

A dissertation

submitted in partial fulfillment of the

requirements for the degree of

Doctor of Philosophy

University of Washington

2025

Reading Committee:

Christopher D. Keene, Chair

Brian C. Kraemer

Jeffrey J. Iliff

Program Authorized to Offer Degree:

Neuroscience

University of Washington

Abstract

Assessing whether human oligodendrocytes go senescent: a cell culture and transcriptomic interrogation of human white matter

Joseph Voth

Chair of the Supervisory Committee:

Christopher D. Keene

Department of Laboratory Medicine & Pathology

White matter (WM) atrophy is an early sign of Alzheimer's Disease pathophysiology. However, our understanding of the main cell type that comprises white matter, the oligodendrocyte (OL), is far less understood than other neural cell types. Senescence is a phenotype associated with aging where damaging stimuli cause permanent cell cycle arrest. To date, it is unclear whether OLs become senescent or not. Understanding OL functions in both WM and gray matter (GM), and whether OLs become senescent, will help incorporate these cells into the complex physiology of the human brain. We developed human OLs from induced-pluripotent stem cells and found little evidence of senescence after exposure to typical senescence-inducing agents. Next, we generated a single nucleus RNA sequencing dataset on human WM, using spatial transcriptomics provide further information. We integrated our WM OLs to an overlapping dataset on GM and identified that GM OLs are producing more machinery for synapse formation and neurotransmitter cycling, while WM OLs are producing more immune and autophagy transcripts. Further, we identified a unique OL phenotype in high AD pathology donors with elevated transcripts related to cytokine production, cytoplasmic chaperone proteins, DNA damage repair, and ferritin accumulation. Together, we have identified a possible senescent OL phenotype and generated a highly valuable resource for further studies.

Dedication

To my Dad for enabling me to follow my passion

To Walter Low for showing me how interesting research can be

To Dirk for enabling me to study Oligodendrocytes

Table of Contents

Table of Figures

Introduction

I. Human White Matter

The human brain is comprised of two general tissue types, white matter (WM) and gray matter (GM), with vastly different cellular compositions and functionalities. GM is the primary location of neuron cell bodies that have a grayish hue while WM is where these neurons project their axons to connect to other regions of CNS. While GM is primarily composed of neurons and the glia that support them, the WM is nearly all glial cells, with oligodendrocytes representing over half of all cells producing myelin with a characteristic white hue. Although all mammals have WM, the proportion of WM generally increases with increased brain size, with the human brain containing 40-50% WM compared with the 10-15% in the mouse[1,2]. A larger brain, especially one with more gyration, requires more and typically longer axon projections to connect various regions, which necessitates expansion of the WM to both provide the trophic support and path which these projections traverse[3,4]. WM is found in deep cortical areas surrounded by GM and is organized into tracts or bundles of axon fibers that run parallel to each other. This structure is most obvious to visualize in MRI-diffuse tensor imaging, where water diffusion is measured and quantified. Water typically diffuses in down fiber tracts, rather than perpendicular to them, thus highlighting the WM tracts and their connectivity[5]. Since the human brain is nearly half WM, it is important to understand how WM functions and how these functionalities can be augmented in the context of aging and disease.

II. Cytoarchitecture of Human White Matter - Myelination

Human WM is primarily composed of oligodendrocytes (OLs), their precursors (oligodendrocyte precursor cells, OPCs), microglia, astrocytes, and vascular cells, together known as glial cells. In addition, the axons projecting from GM traverse through WM and are ensheathed by highly organized, lipid-rich concentric wrappings known as myelin. Myelination occurs in two phases, the first being the expansion and wrapping phase where the cell membrane extends and forms concentric wrappings around an axon[6]. Thus, the myelin sheath is a massive and highly specialized extension of the OL plasma membrane and cytoplasm. After the concentric wraps are formed, the myelin compacts, ingesting (through autophagy[7]) nearly all cytoplasm to form tight layers of myelin[8]. Myelin is produced exclusively by OLs in the central nervous system (CNS) and is crucial to rapid action potential propagation, and thus neural communication. Being lipid-rich, myelin insulates the axon in a manner similar to rubber coating on a wire, preventing current flow perpendicular to the axon by its high resistance and low conductance[9]. In addition to this insulating function, myelin also plays a pivotal role in stabilization and maintenance of neural connections in both the developing and adult brain. Myelination is crucial for memory formation and stability by ensheathing new and active connections during new synapse formation, ensuring their preservation[10]. However, myelination is a dynamic process that will respond to neural activity. If a neuron is more active, it will likely induce myelin production in the ensheathing OL, thus producing more insulation for the axon[11]. While the total number of OLs is largely maintained throughout human adulthood, the myelin itself is reworked and replaced frequently, suggesting myelination remains an active process after initial development[12].

Thus, myelination is a crucial component to both the formation and stability of the CNS circuitry while also playing a central role in its robust ability to adapt. One OL can ensheathe anywhere from one to hundreds of different neurons, meaning the loss of one OL can have an outsized impact on CNS functionality[6]. Fortunately, OPCs are maintained in a tile-like distribution throughout the brain parenchyma to replace these OLs that are worn out[13]. These OPCs comprise around 5-8% of all CNS cells (distributed in both GM and WM)[14], and have crucial roles in OL population maintenance, amongst other potential functionalities (OPCs will be discussed in a separate section). OLs and OPCs comprise the majority of cells in WM and are the most prevalent glial type overall[15].

III. Oligodendrocytes – Functionalities beyond Myelination

In addition to myelination, OLs also provide crucial trophic support to the axons/neurons they ensheathe[16]. This support manifests in multiple ways from direct metabolic support, stimulating axon mitochondria to produce more ATP, and growth factor support. Neurons primarily rely on glucose as an energy substrate, consuming around 25% of all glucose in the body[17]. When glucose supply is depleted or blocked, alternative energy sources in the form of ketones or lactate are used[17]. OLs are a primary source of lactate in the CNS (along with astrocytes), providing energy-starved axons and neurons with lactate via monocarboxylate transporter 1, 2, and 4 (MCT1/2/4)[18–20]. Knocking out MCT1 in OLs from aging mice results in significant axon degeneration and hypomyelination[19]. Further, action potential depolarization results in elevated extraceullar K+ ion concentrations that are detected by Kir4.1 channels on OLs, which seem to be the primary sensor responsible for OL-driven metabolic support

for the axons[21]. This metabolic support comes in two forms, the lactate shuttle, and an extracellular vesicle delivery of SIRT2 from the myelin sheath to the axon[22]. SIRT2 is a NAD-dependent deacetylase that directly stimulates axon mitochondria to metabolize glucose by removing acetyl groups from mitochondrial proteins resulting in a boost in energy production locally[22]. Together, this lactate delivery and SIRT2-mediated mitochondrial stimulation provide rapid and dynamic control over energy production, highlighting how integrally-connected the OL is to the neurons they ensheathe. It also hints at how this complex system can become dysfunctional with age, namely through decreased expression of SIRT2, glucose availability, or lactate transportation.

Beyond direct metabolic support, OLs also produce various growth factors that are involved in modulating neural functionality. Particularly, brain-derived neurotrophic factor (BDNF) is produced by OLs and binds to presynaptic tropomyosin receptor kinase B (TrkB) to stimulate glutamate release in the developing CNS[23]. Glial cell line-derived growth factor (GDNF) is also produced by OLs and plays a role in axon growth and survival[24]. While OLs can secrete growth factors, they are also able to detect and respond to them, a process that is crucial to OL development in initial development and throughout the lifespan[25].

IV. OPCs as the Precursor Pool for OLs

OPCs are the precursor population responsible for replacing OLs that are lost from disease, damage, or age-related attrition. In the mouse, there are three primary sequential waves of OPC development and migration, the first originating from the medial ganglionic eminence at E12.5, the second from the lateral ganglionic eminence at E15.5, and the final wave after birth and originating from the ventricular zone of the

cortical regions[26]. The first two waves are largely replaced by the cortically-derived OPCs in the adult mouse[26]. In humans, these waves are not as clearly defined. In addition to the ganglionic eminence-derived OPCs, a subtype of radial glia called outer radial glia comprise an additional pool of OPCs that contribute to the expanded OPC/OL population unique to the primate cortex[27].

Two key characteristics of OPCs are their ability to migrate and symmetrically divide, thus enabling them to both move to the location needed and expand rapidly to myelinate[27]. Newly divided OPCs will repel each other and migrate away via PCDH15 and DSCAM, seemingly to promote their distribution throughout the parenchyma in a manner similar to how these molecules contribute to dendrite self-avoidance[27]. OPCs use these self-avoidance molecules to form unique, non-overlapping domains in which they surveil and respond as needed. OLs turnover is estimated at around 0.33% a year and theoretically can occur anywhere in the parenchyma[12]. Thus, these non-overlapping domains cover the entire CNS, ensuring an OPC will be available to divide and replace lost OLs. It seems that PCDH15 in particular is crucial for symmetric division, as knockdown of PCDH15 by shRNA will result in only one of the two daughter cells continuing to proliferate[27]. In the adult parenchyma, non-symmetric OPC division (i.e. via downregulation of PCDH15) may maintain their population in the adult after initial myelination is completed, but this is unconfirmed at present. At this point, OPC to OL differentiation is localized and directed to either replace lost OLs or myelinate new connections rather than whole cortex myelination.

In addition to this OL attrition, new OLs are needed to myelinate newly formed axons and their synapses, particularly in the context of new memory formation[10]. In fact,

methods to enhance myelin renewal *in vivo* can reverse cognitive decline in mouse models of Alzheimer's Disease (AD)[28]. In the context of demyelinating disease or ischemic injury the OPC population can be depleted, but it can take years for this depletion to occur[29]. This suggests that the OPC population has a large, but not infinite, division and replacement potential that may be constrained by the different division pattern in the adult compared to initial development. However, recent evidence suggests that rather than a loss of replicative potential itself, the inability of OPCs to migrate properly into lesion sites may drive the remyelination failure seen in chronic demyelinating disease[30]. The cause of the migration failure is an area of active research, but one interesting hypothesis is that the remaining OLs and OPCs within the lesion site are inhibiting the recruitment and differentiation of other OPCs[29]. This type of inhibition is commonly seen in a phenomenon called cellular senescence, a topic that will be discussed later.

V. Aging, OLs, and OPCs

Aging is an attritional process that affects every aspect of the human body, including the WM. WM volume peaks around the age of 40-45 in the human brain, after which it steadily declines[31,32]. This decline is exacerbated in disease states like AD, suggesting the WM and OLs in particular may be especially susceptible to age- and disease-related stressors[32]. A 2023 review (updated from 2013) in *Cell* summarizes the "hallmarks of aging" as follows: chronic inflammation, altered intercellular communication, stem cell exhaustion, cellular senescence, mitochondrial dysfunction, deregulated nutrient-sensing, disabled macroautophagy, loss of proteostasis, epigenetic alterations, telomere attrition, genomic instability, and dysbiosis[33,34]. In particular, altered

intercellular communication, disabled macroautophagy, stem cell exhaustion, cellular senescence, and chronic inflammation have interesting implications in aging WM.

OLs and OPCs in aged WM show signs of altered intercellular communication. First, there is evidence of myelin abnormalities in normal aging, specifically “myelin balloons” where fluid pockets accumulate between the axon and myelin sheath, causing a billowing outward of the myelin sheath[35]. This ballooning likely inhibits proper OL-derived metabolic support, as only the innermost layers of myelin are in contact with the axon, while the others are pushed away by fluid. This phenomenon was primarily characterized in aged macaques, but it is very likely present in humans as well and seems to be relatively common with age. Aged OPCs also show clear signs of altered intercellular communication. In the aged brain, recruitment of OPCs to sites of demyelination is less efficient in both “normal” physiological context (i.e. OL turnover and new neural network myelination[36]) and in demyelinating disease[29]. In fact, this ineffectual OPC recruitment and subsequent molecular signaling to initiate differentiation and myelination has been suggested to be a primary driver of reduced myelination with age[36]. Supporting this, myelin formed later in life is thinner, more fragile, and contains more nodes of shorter width than myelin formed during initial development[37]. Together, this suggests the communication between the OPC/OL and the neurons it intends to ensheathe are altered in the aged brain, with recruitment being reduced and the necessary myelin content being reduced as well. Generating a knock out of muscarinic acetylcholine receptor 1 (Chrm1), a negative regulator of myelination and OPC differentiation, in aged mice can reverse this decline in myelin production[36].

Disabled macroautophagy is the next hallmark of aging particularly relevant to OLs and WM. Autophagy, the process of recycling components of a cell, is the primary mechanism employed during myelin compaction[7,38]. Impairment of this process results in malformed and non-compacted myelin. In fact, this could be a cause of myelin ballooning seen in aged OLs, but this has not been studied to date. However, a knock-out of ATG5, a key component of the autophagic complex in OLs, results in myelin sheaths with cytoplasm remaining between layers in pockets, supporting this hypothesis[7]. Autophagy seems to be a primary mechanism by which the OL can rapidly change its number of wraps as well. The number and thickness of myelin wraps changes in response to neural and astrocyte activity[39], and autophagy seems to be a primary mechanism by which wraps are removed or even forming new wraps[38]. Beyond the OL, autophagy is a key process of debris removal in the parenchyma, a process primarily carried out by microglia[40]. When an OL is lost, the myelin debris needs to be removed from the environment, and microglia will phagocytose this debris[40]. In the aged mouse WM, there is an increase in microglia and an increase in microglia in contact with myelin[41]. Beyond this, these WM microglia show an increase in lysosomes containing myelin debris and accumulate undigestible and insoluble aggregates relative to GM microglia[41]. They directly showed that aged microglia generate lipofuscin from myelin aggregates, suggesting that myelin debris may be a key contributor to lysosomal accumulation of lipofuscin and insoluble aggregates seen in aging and disease[41]. Interestingly, they also showed that a single demyelinating event in young mice was sufficient to initiate age-associated immune activation earlier, suggesting that events

that cause myelin loss may be directly priming the CNS pro-inflammatory environment seen in aging (a topic we will return to)[41].

Stem cell exhaustion and cellular senescence are the next topic of interest for WM OLs and OPCs. OPCs are the most prevalent proliferative cell type in the adult brain[42] and are required to remain proliferative throughout the entire lifespan of a human. OPC exhaustion is hypothesized to be a key component of the pathophysiology of demyelinating lesions, especially following repeated insults[29]. While the OPC population displays a robust ability to respond and adapt, repeated demyelinating events such as those in multiple sclerosis tax this capacity to the point where remyelination is no longer sufficient to repair the damage inflicted, resulting in areas of sparse or incomplete remyelination that persist[30,43]. However, OPC populations are largely maintained in the non-demyelinating disease brain regardless of age[44]. Even within the demyelinating lesion, there is heterogeneity in OPC numbers, with active demyelinated regions more likely to have elevated OPC numbers while chronic demyelinated regions tend to have reduced OPC numbers[30]. However, OPC exhaustion could take a different form than a simple reduction in total numbers. If the remaining OPCs and OLs are sufficiently damaged, this could result in inadequate or abnormal responses to demyelination. A potential way this damage could manifest is in cellular senescence.

VI. Cellular Senescence in OLs and OPCs

Cellular senescence is the process by which typically proliferative cells lose their proliferative capacity. Senescent are unable to differentiate properly into their usual mature cell type(s), while also acquiring novel (and typically aberrant) functions. While

senescence is classically associated with proliferative cell types, newer studies are associating the term to non-proliferative cells that lose (or reduce) their primary functions while acquiring new and abnormal ones[45,46]. Similar to aging, there is a wonderful review that highlights the “hallmarks of cellular senescence”: nuclear changes like LaminB1 loss, accumulation of lysosomal content, dysfunctional and large mitochondria, the presence of chromatin fragments in the cytoplasm, plasma membrane deformation, and overall cell size increase and misshaping[47]. In addition, there are molecular pathways that indicate senescence, including upregulation of the DNA-damage response (especially gamma-H2AX accumulation signifying unrepaired DNA damage), cell cycle arrest, a secretory phenotype that typically releases cytokines and metalloproteinases, apoptosis resistance, and endoplasmic reticulum stress through unfolded protein responses[47]. While senescence was initially characterized in tumors, nearly every proliferative cell type has been reported to exhibit senescence as the population ages. Beyond this, recent studies are beginning to assess whether terminally differentiated cells can become senescent as well, at least sharing common features of proliferative senescence minus the cell cycle arrest that is assumed in a terminally differentiated cell[45]. The profile of senescence in each cell type varies and may emphasize certain aspects while minimizing others, likely a result of both the intrinsic and extrinsic influences that push these cells to senescence. This means the senescence profile for one cell type may not be applicable to another.

Surprisingly, it is unclear whether OPCs become senescent or not and what the specific OPC senescence phenotype would be. One study on this topic found that Sox2+ neural precursor cells from primary progressive multiple sclerosis fail to

differentiate into OPCs and identify these NPCs in the WM lesions of these patients[42]. They propose that these senescent NPCs (not OPCs themselves) are inhibiting OPC differentiation via HMGB1 inhibition. Another study that showed that neurodegenerative disease is driven by the accumulation of senescent glial cells that promote hyper-phosphorylated tau aggregate formation in a tauopathy mouse model[48]. This study highlighted astrocyte and microglia senescence, but it is possible NPCs and OPCs were involved as well since they did not address this. Importantly, using a senolytic agent to selectively kill senescent cells restored cognitive function in these mice, suggesting the removal of these senescent subpopulations can drastically alter the entire brain. In fact, there is a clinical trial specifically looking at the effects of dasatinib and quercitin, two common senolytic agents, to alter the accelerated aging in AD[49]. Only two studies have directly studied OPCs and senescence. The first studied OPCs in both human AD patients and amyloid-beta plaque mouse models, showing that OPCs that express two cyclin dependent kinases associated with senescence (p16 and p21, CDKN2A and CDKN1A respectively) were localized around amyloid-beta plaques[50]. They were also able to induce senescence of embryonic stem cell-derived mouse OPCs after exposure to amyloid-beta fibrils. Further they showed that senolytic therapy (dasatinib and quercetin) in these mice also kills these p16- and p21-expressing OPCs, suggesting they may be senescent[50]. The final study on OPC senescence reinforces the idea that mouse OPCs become senescent in the aged brain, taking it a step further by comparing WM to GM OPCs[51]. First, they highlight that WM OPCs are larger, localized to microglia, and less prevalent in the aged mouse WM compared to hippocampal GM OPCs. Second, these WM OPCs are expressing p16 and other senescence-related pathways

like cell cycle inhibition, MHC-1 antigen processing and presentation, ubiquitination and neddylation indicative of protein degradation, and unfolded protein response pathways indicative of ER stress[51]. Finally, they highlight that WM OPCs that appear senescent have a different profile than GM OPCs from the same mice, implying that senescence in these cells may vary by region. However, they do not show successful induction of senescence in human cells, leaving the question of whether human OPCs can become senescent unclear. That being said, these studies provide a potential profile of what a senescent WM OPC may look like in the human. They may show evidence of cell cycle arrest as evidenced by p16 and p21, localization near microglia, DNA-damage repair machinery, and endoplasmic reticulum stress, increased ubiquitination and neddylation, and aberrant immune activity.

VII. Alzheimer's Disease

Alzheimer's Disease is the most prevalent neurodegenerative disease with 55 million people affected worldwide, with estimates projecting upwards of 139 million people being affected by 2050[52]. Within the United States, an estimated 6.9 million people suffer from AD, with two-thirds being women[53]. In addition to disproportionate sex prevalence, there is also an ethnic difference in the U.S. with multiple studies showing Black adults are roughly twice as likely to develop AD than White adults[54,55]. First described in 1906 by Alois Alzheimer, AD is characterized by memory loss, cognitive dysfunction, difficulty executing daily tasks, and personality changes (especially depression and rapid mood swings)[56]. While AD has been studied extensively, the most significant risk factor is simply age, with the prevalence of AD around 1.7% in ages 65-74 increasing to 13.1% in ages 85+[57]. However, there are other

socioeconomic factors that seem to be protective against AD development, particularly higher educational attainment and family income reducing the risk of AD development[57]. It is important to note that most studies on AD include predominantly white people, and this lack of representation from other populations is an important limitation of our current understanding of the disease. Further, more work is needed to determine how the interplay of socioeconomic status and health inequity contributes to AD.

The pathological hallmarks of AD are amyloid-beta plaques and hyper-phosphorylated tau tangles. Amyloid-beta plaques are extracellular protein aggregates primarily composed of a cleavage product of the amyloid precursor protein (APP), a transmembrane protein of unclear healthy physiological function[58]. APP can be cleaved by three different enzymes named alpha-, beta-, and gamma-secretase, which produce peptide fragments between 37 to 49 amino acids in length. There are two primary APP processing pathways, the first being a non-amyloidogenic pathway where alpha and gamma secretase cleave APP forming either 3 or 4kDa protein fragments called P3 peptides that are non-toxic[58]. The pathological amyloidogenic pathway involves cleavage of APP by beta- and gamma-secretase, producing a fragment that is either 40 or 42 residues in length[58]. These 40 and 42 residue fragments are referred to as amyloid-beta (Aβ), and individual monomers will aggregate spontaneously to form amyloid oligomers, protofibrils and fibrils, with only oligomeric forms being soluble[58]. Aβ fibrils will aggregate to form extracellular plaques that are maintained long-term in the parenchyma[58]. While these amyloid plaques are the form of amyloid detected by histology and used in the diagnosis of dementia, the oligomeric and other soluble forms of Aβ are the more cytotoxic[59]. There is evidence that these soluble forms can bind

extracellular receptors to promote a plethora of intracellular functions from initiating a pro-inflammatory response (e.g. through Ephrin B2 and microglia binding), reactive oxygen species formation and mitochondrial dysfunction (e.g. through mGluR5 receptor binding), and contribution to hyper-phosphorylation of tau protein, initiating aggregate formation[58]. However, recent human trials to clear Aβ aggregates from the CNS parenchyma via monoclonal antibody administration have only shown miniscule improvements in AD progression suggesting that amyloid aggregation and clearance alone is insufficient to explain AD pathophysiology[60]. Adding to this, the accumulation of Aβ aggregates does not correlate with AD severity, further suggesting that Aβ aggregation is insufficient to be the sole cause of AD.

The other pathological finding in AD is intra-neuronal hyper-phosphorylated tau aggregates. Tau, the protein translated from the MAPT gene, is a microtubule associated protein that typically localizes to the axon in healthy neurons[61]. It's primary function is to stabilize microtubules directly and indirectly by acting as a cross-bridge between microtubules and other cytoskeletal elements[62]. While the primary location of tau is in axons, it is also found in dendrites and synapses at low levels, suggesting a diverse range of roles throughout the neuron[62]. Beyond neurons, tau is found in glia as well where it has been found in mature oligodendrocytes but not OPCs[63]. Recent evidence has identified astrocytes and microglia containing intracellular tau oligomers as a result of synapse elimination[64]. Interestingly, tau does not seem to have a consistent folding structure but rather is flexible and mobile, a phenomenon coined "natively unfolded or intrinsically disordered"[65]. This flexibility enables tau to possess a diverse range of interactions and functions. Adding to this complexity, tau can be

phosphorylated or other post-translational modifications at many residues (at least 80 sites have been identified thus far), further complicating the ability to discern various functions of tau in health and disease[61]. There are two main groups of tau divided by the number of microtubule-binding repeats, known as 3R and 4R tau species. The distribution of 3R and 4R tau varies throughout development and disease with the ratio roughly 50:50 in the healthy adult brain, implying these types drive different physiological functions[62,66]. AD typically contains a mixture of both variants with either a relative increase in 4R tau or decrease in 3R to produce a roughly 2:1 4R:3R ratio[66], while tauopathies can be predominantly 4R (e.g. progressive supranuclear palsy) or 3R (e.g. Pick's Disease).

In AD, an early pathological change is mislocalization of tau from the axon to the soma and/or dendrite, a process that is in part initiated by amyloid-beta[67]. This aberrant localization hinders microtubule transport of necessary cargo and causes dendritic spine atrophy through modulated calcium ion influx[65]. The phosphorylation state of tau is variable depending on age, with fetal tau being phosphorylated 7 times on average, while adult tau only contains 2 phosphates[68]. In contrast, the tau from AD patients has 8 phosphates on average, and it seems this excess phosphorylation is what causes tau to shift from physiological to pathological[62,69]. Whether aggregation of tau is itself cytotoxic or a protective mechanism of sequestering abnormal or excess tau (a concept proposed for amyloid beta as well) is unclear and an area of active research.

VIII. Pathological Scoring of AD

In AD, scales have been developed based on the observation that both amyloid and tau aggregation progresses in a specific pattern. For Aβ, the primary scale used is

Thal phasing, named after Dr. Dietmar R. Thal, who first characterized this progression. Thal phasing measures amyloid burden in general rather than in the context of vascular amyloid on a progressive 1-5 point scale. Phase 1 = amyloid localized only to neocortex, phase 2 = amyloid in neocortex and allocortex (i.e. hippocampus and olfactory regions), phase 3 = thalamic and striatal deposition, phase 4 = some brain stem regions (substantia nigra, red nucleus, colliculi, central gray, olivary nuclei, reticular zone, and phase 5 = cerebellum and other brain stem regions[70]. While these scales measure amyloid in concrete and objective ways, they do not predict AD severity very effectively[71], implying that amyloid burden alone is insufficient for AD pathophysiology.

In contrast to Aβ, tau aggregation does correlate strongly with AD severity[72]. Tau burden and spread is classified by Braak staging on 1-6 levels. These levels are: 1= exclusive localization to transentorhinal region near rhinal sulcus, 2= extension into layer 2 of entorhinal region and hippocampal infiltration, 3 = involvement of entire hippocampus and entorhinal cortex with extension into the occipito-temporal gyrus and lingual gyru4= insular cortex and middle temporal gyrus inclusions without superior temporal gyrus involvement, 5= superior temporal gyrus and mild infiltration into premotor and sensory association regions, possibility of parastriate inclusions, 6 = strong tau labeling in primary sensory, striate areas, and occipital cortex, and Heschl's gyrus[73,74]. Of note, tau spreads to anatomically connected regions, giving credence to a prion-like spreading hypothesis where an initial seeding event steadily progresses[75].

Because both amyloid and tau aggregation are associated with AD, efforts to integrate these metrics to provide a holistic view of AD-related neuropathological

change. This has resulted in the Alzheimer's Disease Neuropathological Change rank (ADNC), which considers Aβ plaque score (modified Thal phase where A0 = no amyloid plaques, A1 = Thal 1/2, A2 = Thal 3, and A3 = Thal 4/5), NFT stage (modified Braak staging where B0 = no NFTs, B1 = Braak 1/2, B2 = Braak 3/4, and B3 = Braak 5/6), and a neuritic plaque score (modified from the Consortium to Establish a Registry for Alzheimer's Disease, CERAD) where C0 = no neuritic plaques, C1 = CERAD score sparse, C2 = CERAD score moderate, and C3 = CERAD score frequent)[76]. CERAD is scale developed to incorporate both neuropsychological testing and neuropathology to holistically characterize AD[77,78]. The ADNC ranking uses the semi-quantitative assessment of amyloid plaque burden from the CERAD scoring of neuritic plaque density in the middle frontal gyrus and inferior parietal lobule[78]. Together, these scores are reported as an "ABC" score that is consolidated into a 4 levels (Not, Low, Intermediate, and High) that represent whether AD neuropathological change is sufficient for dementia[76].

IX. AD and OLs

While AD is classically considered a disease of the GM and neurons, there is convincing evidence that OLs and WM are integrally involved with AD pathophysiology. The first evidence of WM abnormalities in aging was published a year after Dr. Alois Alzheimer's publication, with Dr. Theodor Kaes identified that WM volume peaked around 35-45 years of age and steadily declined after that[31]. However, AD increased the rate of WM atrophy beyond that seen with aging alone, suggesting the processes involved in AD are resulting in WM and myelin loss[79]. In fact, recent studies have identified that WM and myelin loss may be an early aspect of AD development. MRI

evidence has found that myelin changes are widespread in preclinical AD patients, with areas myelinated later in initial development are more substantially effected[80]. In particular, they found the most significant WM decline in frontal WM and the genu of the corpus callosum. Further, elevations of sAPPb/Ab42 via PET imaging were associated with further decreases in WM, directly connecting AD pathology to WM loss. Notably, the people assessed did not have AD and were cognitively intact with MMSE scores of 27+. This implies that WM loss is occurring before AD progression. Other MRI studies have corroborated these findings, with one study showing WM atrophy in middle temporal regions in late-onset AD patients[81], and another showing atrophy of fronto-hippocampal connectivity in patients with mild cognitive impairment and early AD[82]. White matter hyperintensity formation has been detected in autosomal dominant genetic mutation AD patients as early as 20 years prior to onset of symptoms, suggesting WM may be a core feature of AD, at least in early-onset cases[83].

Beyond MRI evidence, other studies have supported the hypothesis that later myelinated areas in initial development (e.g. frontal cortex and association regions) are the areas affected first in AD pathophysiology[32,84]. Amyloid plaque spread progresses in a sequence that mirrors the sequence of myelination[84]. Myelin formation later in life, through replacement of lost OLs and new network myelination, is thinner than initial developmental myelination, a finding so robust it has been proposed as a hallmark feature of remyelination events[85]. Since the hippocampus is a primary site of new synapse formation and memory formation, these later formed connections are likely myelinated with thinner sheaths that are less supportive[10]. Evidence for less myelin renewal and more myelin degradation directly causing memory deficits in mice has

been shown in the context of aging[36], and is likely a contributing factor in AD memory insufficiency as well. Recent evidence suggests that exercise is neuroprotective in AD[86]. Exercise has also been directly shown to increase myelination in aging, especially cardiovascular training[87]. While 20-30% of AD patients have major depression symptoms[88], a single major depressive event before signs of cognitive impairment increases the risk of AD development by more than two-fold[89]. Further, inducing early-life stress in mice causes premature OL differentiation and lasting behavioral augmentations throughout adulthood, implying that OL myelination is preserved long-term and can substantially alter circuit functionality far-removed from the initial myelinating event[90]. Major depression patients have reduced global myelin content than non-depressed controls as assessed by MRI[91], providing a potential connection between altered myelination, depression, and AD development. Together, these pieces of information all point to aberrant myelination and OL dysfunction as early and predisposing aspects of AD pathophysiology rather than being a simple result of neuronal loss.

On the cellular level, transcriptomic data has implicated OL and OPC-related transcripts in AD patients. OLs show the highest levels of APP, beta-, and gamma-secretases of all cell types in the brain[92]. Further, myelin dysfunction resulting in OL loss and microglia processing of myelin debris promotes amyloid-beta deposition in mouse models of AD, suggesting that OLs and myelin may themselves be a main initiator of amyloid aggregation[93]. This has been further supported by OLs directly forming Aβ plaques in AD mouse models[94]. APOE4, an apolipoprotein E allele involved in lipid and cholesterol transport, is the highest genetic risk factor identified for late-onset AD

development and impairs the ability of OLs to myelinate by disrupting cholesterol utilization[95]. *In vitro* work has shown that both amyloid-beta[96] is cytotoxic to OLs and tau from OLs can initiate tau seeding and spreading[97], further providing evidence that OLs are able to interact with these pathological proteins and this interaction is maladaptive. Together, all of these findings support the idea of OL and myelin dysfunction as an early process in AD pathophysiology.

X. Why the OL is exceptionally vulnerable

OLs have a host of characteristics that make them uniquely vulnerable to age- and AD-related dysfunction. First, OLs have the highest iron content of all CNS cells (70% of all CNS iron is associated with myelin[98]), with over double the amount of other glia and nearly 5-fold that of neurons[99]. In fact, iron levels have been documented to increase in OLs as a result of age and even further in AD OLs[100]. Iron is a necessary cofactor for lipid synthesis, and OLs produce massive amounts of lipid during myelination, myelin restoration, and remyelination[101]. While this accumulation of iron is necessary for myelination, it also greatly increases the oxidative stress the OL must manage. Iron directly generates free radicals via the Fenton reaction, where iron ions oxidize hydrogen peroxide (a common byproduct of mitochondrial ATP generation) to form free radicals[102]. These free radicals proceed to impact a diverse range of cell functions from directly inducing DNA strand breaks, lipid peroxidation, and protein misfolding amongst many others[102,103]. To counteract this, OLs must produce high concentrations of ferritin, the main protein complex that sequesters free iron[103]. Beyond iron content itself, the process of making the lipid necessary for myelination requires substantial amounts of energy, increasing the burden on mitochondria further[32,79,104].

OLs (and other CNS cell types) produce nearly all cholesterol *de novo*[105]. 28% of all lipid of the brain is cholesterol, and 40% of myelin is cholesterol[106]. Thus, OLs are responsible for making large amounts of cholesterol intracellularly, a process that may even provide cholesterol for other CNS cell types via apolipoprotein delivery. In fact, APOE4 alleles impair myelination directly by dysregulation cholesterol transportation[95]. These two processes, lipid production/mitochondrial stress and elevated iron/ROS production set the stage for a unique “snowball” effect where iron induces free radicals that damage mitochondria and lipids, further increasing ROS production. While the younger adult OL can manage this oxidative stress, the aged and diseased OL is less likely to control this. Multiple studies have shown ROS increases in AD in both mouse models and humans, suggesting the ability to neutralize these free radicals is impaired[107].

The metabolic demand of OLs is 2-3 fold higher than other CNS cell types[103]. This is primarily a result of the lipid production needed for myelination, metabolic support for the axons they ensheathe (recall the lactate shuttle and extracellular vesicle delivery of SIRT2), and the need to maintain OL homeostasis of iron, ROS, and other stressors. To this end, the myelin sheath results in a plasma membrane surface area 600x larger than the soma of the OL, with a weight 100x that of the soma[108]. This amount of lipid must be maintained and repaired, a process that requires constant lipid and cholesterol production to properly function. The OPC is even more metabolically burdened, with the OPC estimated to produce 3x their own weight in myelination lipids each day during differentiation[108]. Damage to the lipids in the myelin sheath from ROS

will increase this burden of lipid production, both requiring autophagy of the damaged lipid and production of new lipids[38].

Another unique aspect of OLs and WM in general is its anatomical location within the brain. WM typically resides in deep cortical regions, areas at the extreme ends of the CNS vascular network. These areas have been termed “watershed regions”, as they are the areas impacted first and most-severely during ischemia[109]. These deep WM regions tend to lack redundant blood supply and rely on smaller artery perfusion, so any insult like occlusion or age-related stenosis results in reduced blood supply and the nutrients it carries[110]. Average CNS blood flow decreases with age, and even further in AD[111]. Further, vascular contributions to AD have been well documented, and there is a vascular subtype of dementia that is predominantly driven by vascular abnormalities[112]. Thus, WM OLS are especially adversely affected by this reduction in blood flow.

While OLs are adversely affected by age-related changes, OPCs are also sensitive to these same processes. OPCs need to remain proliferative and actively surveying the parenchyma throughout the entire lifespan of the individual. Beyond the stressors identified for OLs that OPCs also endure, OPCs also experience additional stress from having to divide and differentiate in the context of reduced blood flow and elevated oxidative stress. While the replicative potential of OPCs is remarkable, it is not infinite. This is most evident in the MS literature, where chronic demyelination can result in incomplete and insufficient remyelination[29]. WM hyperintensities have been detected as early as 20 years prior to onset of AD symptoms, suggesting the WM (and both OLs and OPCs) is being challenged early in AD progression[83]. It is possible this gradual attrition may result in insufficient remyelination akin to that seen in chronic MS lesions[83].

This is why senescence is especially interesting in OPC biology, as chronic MS lesions show that OPCs are less likely to infiltrate into a demyelinated site and remyelinate[29], suggesting some mechanism is inhibiting their recruitment activation. Senescence could explain this phenomenon by the remaining OPCs (or other cell types) secreting repulsive cues, effectively keeping OPCs out of these sites. It is also possible that OPCs are exhausted through a combination of telomeric attrition, DNA damage, ROS accumulation, and pro-inflammatory inhibition, resulting in dysfunctional (albeit not dead) OPCs that no longer are able to myelinate.

XI. Inflammation and Oligodendroglia

While OLs and OPCs are not considered primary immune cells, they do express immune receptors and participate in the immune environment of the CNS. In particular, OPCs have been documented to secret cytokines[113], process and present antigen via MHC-II complexes[114], and respond to inflammatory signals[115,116]. OPCs seem to respond to both anti- and pro-inflammatory signals, including IL-4 and IL-10 (anti-inflammatory markers that reduce antigen phagocytosis and presentation as well as OPC differentiation) and TNF-alpha and IFN-gamma (inflammatory cytokines which enhance OPC phagocytosis)[117]. Because these immunomodulatory OPC functions are relatively recent discoveries, our understanding of the breadth and scale of their involvement is still unclear. However, there is evidence that that OPCs contribute to the pro-inflammatory environment of demyelinating MS lesions as well. Contact between an OPC and a T-cell can induce the OPC to produce MHC-I and -II complexes to present antigen, increasing T-cell cytotoxic activity and promoting OL degeneration[116]. Together,

this emerging evidence suggests that OPCs can play roles in both innate and adaptive immunity processes, depending on context.

XII. Gray Matter OLs and OPCs

While WM earns its name from the off-white color of myelin produced by OLs, GM also contains OLs. The myelination pattern of GM OLs is very different from that of WM. WM OLs form concentric, compact myelin sheaths, that while varying in number of wraps, typically surround the axon. GM OLs can form a variety of different myelination patterns including full wraps with compaction, full wraps without compaction, partial and incomplete wraps, and even processes that seem to place a small amount of myelin on a single surface of an axon[118,119]. Further, GM axons can be left entirely unmyelinated, even large caliber axons that would almost certainly be myelinated in WM[118]. There is also evidence of GM axons having thin wrappings of myelin that are followed by large spaces of unmyelinated axon, a phenomenal rarely seen in WM[119]. Considering the primary role of an OL in general is to myelinate the axon and provide support, it is likely that this different myelination pattern is still involved in tuning the speed of action potential propagation, but this has not been conclusively shown. Since GM OLs seem to make far less myelin than their WM counterparts, a relatively new question in the field is what these GM OLs are doing. Little research has addressed this topic but is of importance for both general neurobiology and the neurobiology of aging and disease considering OLs and OPCs are active players in the system. One of the few studies focused on GM OLs identified that GM OLs showed a propensity to degenerate and inadequately regenerate in the context of ALS[120], opening the door for future studies to investigate how these cells contribute to other disease.

XIII. Summary and Hypothesis

OLs and OPCs seem to be early contributors to aging and AD-related pathophysiology, but key questions remain unanswered. First, are human OPCs able to become senescent, and what does a senescent OPC look like? Evidence has suggested murine OPCs become senescent, and nearly every other proliferative cell type in the human can as well. However, it has yet to be shown conclusively that human OPCs share this capability and what exactly this phenotype encompasses. Further, while AD is classically considered a disease of neurons and GM, there is strong and harmonious evidence that WM is affected early in AD development. Nearly all transcriptomic studies on AD have focused on human GM tissues exclusively, with the direct consequence that any disease contribution from WM is largely undetected and unassessed. Finally, while GM OLs and OPCs exist, their functionalities are largely unknown. This has also been an unintended consequence of nearly all transcriptomic papers being focused on GM regions. Without WM samples, it is challenging if not impossible to accurately assess OL functionalities and how these are altered in disease.

The focus of this thesis is to address these three questions, and the following sections will be separated into three main chapters on the following topics:

1. Generation of OPCs/OLs from human induced-pluripotent stem cells to induce a cellular senescence profile.
2. Generation of an unbiased WM transcriptomic dataset using both single nucleus RNA sequencing and RNA-based spatial transcriptomics to understand OL and OPC functionalities in young, aged low AD pathology, and aged high AD pathology WM.

3. Compare the aged WM OLs and OPCs to aged GM OLs and OPCs from the same tissue bank with similar inclusion/exclusion criteria to understand how GM OLs differ from WM OLs.

Through these chapters, a potential profile for senescent human OPCs will be proposed, how young and old WM OLs/OPCs differ, and how GM OLs differ from WM OLs will be addressed.

Chapter 1: Generating human OPCs from iPSCs to assess cellular senescence

1.I. Background and Context

Since the few existing studies to identify senescent OPCs/OLs were in murine models, my first goal was attempting to induce senescence directly in iPSC-derived human OPCs. To my knowledge, one study has directly induced senescence in OPCs in culture, but this was done on embryonic stem cell-derived mouse OPCs after exposure to amyloid-beta fibrils[50]. However, translating this methodology to human iPSC-derived OPCs would require multiple steps and adaptations. First, generation of human OPCs is a long process requiring 75-90 days. Second, inducing senescence in a reproducible way requires identification of the proper stressor method and dosage to detect senescence. Third, since the phenotype of a senescent human OPC is unknown, determining which outputs to use and assess is vital. Since nearly every human proliferative cell type has been documented to go senescent, and there is literature evidence of murine OPCs going senescent as well, I hypothesized that human OPCs would become senescent in a dose-response manner following exposure to a stressful stimulus. Exactly what the dosage and modality of stimulus, as well as the read-out method to detect senescence, would require some experimentation.

1.II. Generation of human OPCs from iPSCs

The first step in this process was to effectively generate human OPCs. Commercial iPSCs were used with no particular genetic background to minimize risk of genetic abnormalities that would prevent or skew OPC differentiation. For this purpose, the first line used was the GM25430 cell line (also known as CViA2), a line derived from

a 62-year-old male (J. Craig Venter). These cells were initially skin fibroblasts reprogrammed using retroviral reprogramming to pluripotency. These cells were maintained in mTESR1 medium on Matrigel-coated plates, passaged at 80%+ confluency, and differentiations were initiated prior to passage number 20 to minimize risk of genetic drift or mutation. The protocol for iPSC differentiation to OPCs followed the “long” protocol published in Nature Methods in 2015[121], and is visualized in Figure 1a. This protocol has four main stages, initial neuralization, ventralization of NSCs, driving ventral NSCs to OPCs, then OPC to OL differentiation. These steps largely replicate the general steps in OL development *in vivo*.

Prior to differentiation, iPSCs are seeded on Matrigel 6-well plates at 100-200k cells per well and maintained at 37°C and 5% CO_2 (these incubator settings are maintained throughout the entire process). These cells proliferate in mTESR1 until colony sizes are between 150-300μm in diameter, then differentiation can begin. First, neuralization of iPSCs uses F12/DMEM base medium with a combination of SB431542 (a TGF-B inhibitor), LDN193189 (a small molecule inhibitor of bone morphogen protein (BMP)), and all-trans retinoic acid (ATRA). Recall in neurodevelopment how opposing gradients of Sonic Hedgehog released from the notochord and BMPs from ectoderm/roof plate create opposing gradients that define unique niches along the neural tube[122]. OL-lineage cells are derived from the ventral region called pMN, which derives both OLs and motor neurons (interestingly, both of these cell types are *OLIG2+* as well). This ventral origin also explains why the next step after neuralization is to “ventralize” these cells via the addition of smoothened agonist (SAG) and maintained ATRA. Smoothened is a downstream component of the Sonic Hedgehog pathway[123],

and thus this combination simulates a ventral input from the notochord. By day 8-9, most cells should be *PAX6+*, an indication of their neural precursor identity. This neural precursor identity was assessed during the differentiation via qPCR where cells were *PAX6+* by day 9 relative to day 0 (figure 1B, middle panel). While the first 12 days are Matrigel adhered, days 12 to 30 are in cell suspension. This suspension phase emulates the synchronization of the early OPC niche, where *OLIG2+* cells in the ganglionic eminence signal in a wave-like pattern to harmonize all the cells in the niche to the same phase[26]. In line with this, I typically would see elevation of *OLIG2* during this suspension phase with decreased Pax6, a sign that the NPCs are beginning to narrow toward an OPC lineage (Fig. 1B, right panel). The initial suspension was created by cutting and scraping each well of the 6-well plate and transferring to an uncoated 6-well plate that was placed on a revolving shaker in the incubator. Ventral NPCs/early OPCs would aggregate spontaneously while other cells would remain unaggregated and is subsequently in media changes. Shaking was necessary to maintain suspension as cells would sink and adhere otherwise. After 20 days, SAG and ATRA are replaced by a cocktail of OPC-specific cues that are maintained until the end of OPC differentiation. These signals are all later stage OPC cues that drive the early OPCs to a fulminant OPC phenotype and include thyroid T3 hormone, insulin, cAMP, biotin, platelet-derived growth factor AA, insulin growth factor 1, hepatocyte growth factor, and neurotrophin 3. Following the switch to the OPC-specific cocktail, aggregates are removed from the shaker and transferred to poly-lysine and laminin coated wells and allowed to adhere at day 30. After the adhesion of the aggregates, OPCs begin to migrate out of the aggregates and onto the plate (Figure 2A shows brightfield images of

this process in action). By day 75, the entire well surface will be covered with multiple layers of cells. A typical differentiation with three wells of a 6-well plate would yield between 100-150 million OPCs.

To initiate terminal differentiation of OPCs to OLs, the pro-OPC cocktail of PDGFaa, HGC, IGF-1 and NT3 was replaced by ascorbic acid, a potent signal to induce myelination[124]. Following dissociation of the OPCs using accutase and p1000 pipette agitation, cells could either be placed on poly-lysine and laminin coated coverslips or seeded onto poly-lactide electrospun nanofibers. These nanofibers were developed to simulate an axon using prior studies that assessed what characteristics OPCs/OLs use during differentiation to determine where to myelinate. These studies elucidated that OLs primarily rely on the size/caliber of the fiber to dictate which fibers become myelinated or not, rather than activity or signaling molecules[125]. They determined that the ideal caliber to induce myelination was 2μm, and that the smaller or larger the fiber was beyond 2μm decreased myelination[126]. Thus, inert (non-living) nanofibers are sufficient to induce myelination, simplifying the system by avoiding co-culture with neurons. However, electrical activity (i.e. depolarization from an axon) may be required to form compact myelin, although this is not entirely clear at present[127]. Thus, these nanofibers, while simplifying the experimental system, may not entirely recapitulate mature myelination. However, to address whether OPCs become senescent and lose their ability to differentiate and form myelin, this was deemed a sufficient compromise. Following seeding of dissociated OPCs onto coverslips (Figure 2B) and nanofibers coated with laminin (Figure 2C), I saw myelin production in all cells that remained 14 days after seeding. Interestingly, the coverslip cells did not seem to proliferate but did

form myelin (as evidenced by myelin basic protein ICC). In contrast, nanofiber-seeded OPCs differentiated to produce myelin and proliferated extensively. An optimal seeding density of OPCs for nanofibers was experimentally determined by doing a serial seeding by orders of magnitude to determine the ideal amount needed to produce myelination “webs” that were not overgrown by day 14. Interestingly, too few OPCs seeded would result in death of all cells, while too many would result in overgrown fibers where no individual cells could be delineated. This low OPC density resulting in wholesale cell death suggests OPCs require some sort of contact or interaction with other OPCs, which aligns with studies that suggest OPC differentiation in development occurs when OPCs distribute and myelinate together[128,129]. If the critical density is not met, then they die.

After around day 60, qPCR should reveal a classic OPC phenotype with elevated *PDGFRA* and *NG2* (Figure 1C). It is worth mentioning that *GFAP* and *S100B* were commonly upregulated as well, either indicating a subset of cells that have an astrocyte lineage or potentially OPC-derived expression. Both *GFAP* and *S100B* expression has been documented in OPCs[130], and attempts to purify OPCs from presumed astrocytes using flow cytometry proved unsuccessful. However, it is also possible that my iPSC-OPCs were some hybrid form of OPC-astrocyte, especially considering these two cell types share a precursor *in vivo*[130,131]. However, OPCs were able to differentiate and produce myelin when plated on poly-lysine and laminin coated coverslips (Figure 2B) and when seeded onto poly-lactide electrospun 2μm fibers (Figure 2C), suggesting they are more likely OPCs. Further, I ran these iPSC-OPCs in single nucleus RNA sequencing to see how they mapped relative to various WM cell types, and both the

OPCs and OPCs differentiated towards OLs in pro myelination medium clustered with myelinating OLs (Figure 3). Interestingly, these iPSC-derived OLs also displayed a “smear” clustering phenomenon from the myelinating OLs to the neuronal subclusters. This is typically qualitative evidence that these cells are exhibiting some aspects of both cell types to the point where dimensional reductions maintain these differences. It is unclear whether these “smear” cells and cells that are within the neuronal clusters are in fact neurons, or OLs that express transcripts similar to neurons.

This iPSC to OPC protocol was attempted on three different iPSC lines, the CViA2 line, CViB5 (another line derived from J Craig Venter), and GM25256 (a commercial line derived from a 30-year-old Japanese male with no known medical history). CViA2 was the most effective for downstream analysis, as these cells were robust and able to be passaged, frozen, and rethawed successfully. CViB5 cells failed to aggregate into spheres when they were removed from the plate for some reason. These cells looked similar to CViA2 until then in both morphology and qPCR, but then failed to aggregate. GM25256 was able to differentiate into hOPCs that looked similar to CViA2 by qPCR, but these cells failed to dissociate at the end of the protocol, so they were unusable for downstream analysis. Using different dissociation methods than Accutase (I tried both papain and trypsin) did not remedy this situation.

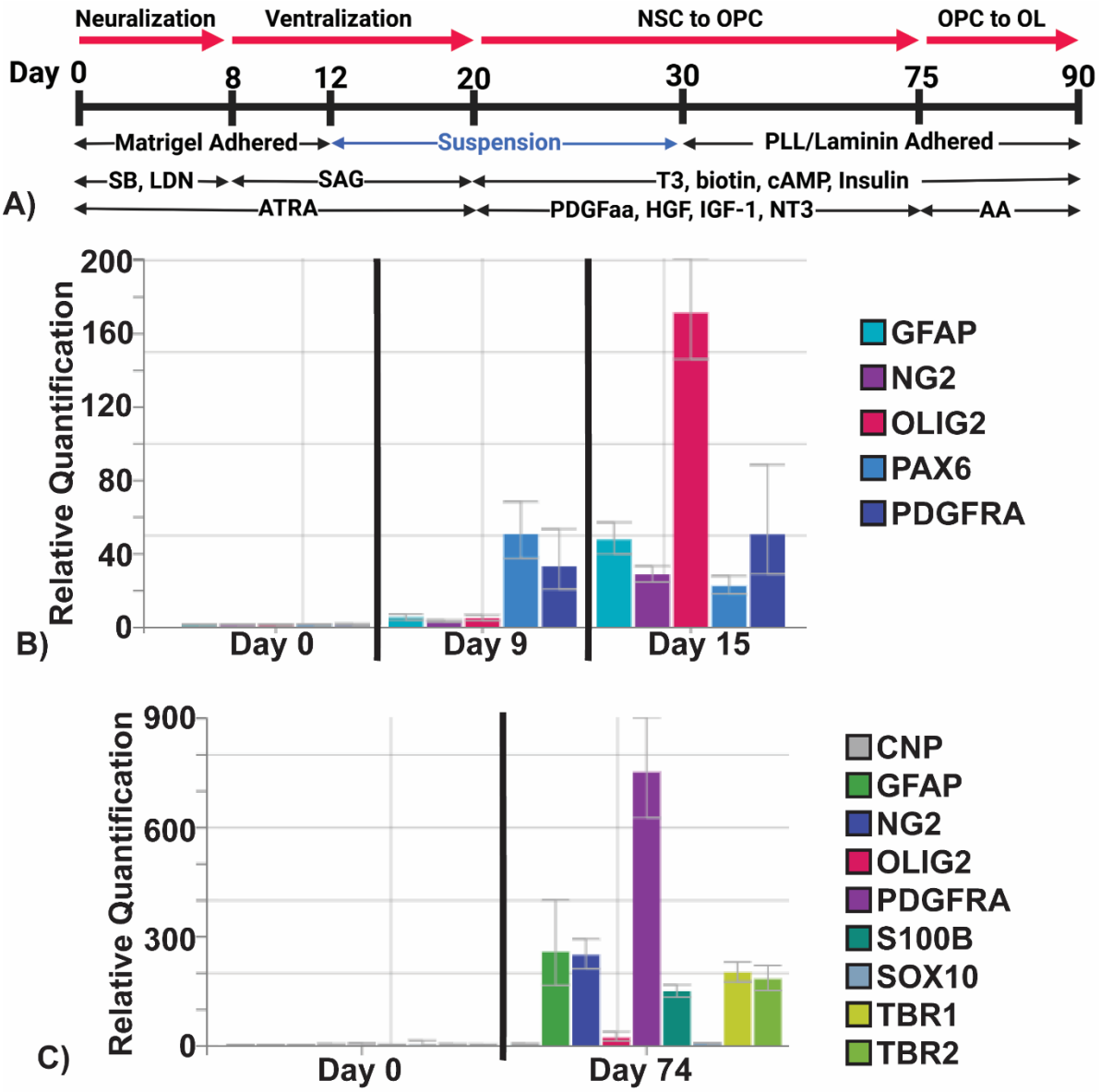

Figure 1. Protocol to produce human OPCs from iPSCs. 1A) Schematic of the protocol followed to produce OPCs from iPSCs, adapted from Douvaras and Fossati[121]. **1B)** qPCR results from a representative differentiation at day 9 showing *PAX6* upregulation and day 15 showing *OLIG2* upregulation relative to day zero. **1C)** qPCR results showing final differentiation expression of genes representing OPCs/OLs (*PDGFRA, NG2, SOX10, CNP*), astrocytes (*S100B* and *GFAP*), neural precursors (*TBR2*) and neurons (*TBR1*). Error bars represent standard error for technical replicates (three individual wells were ran of each transcript from the same RNA isolation).

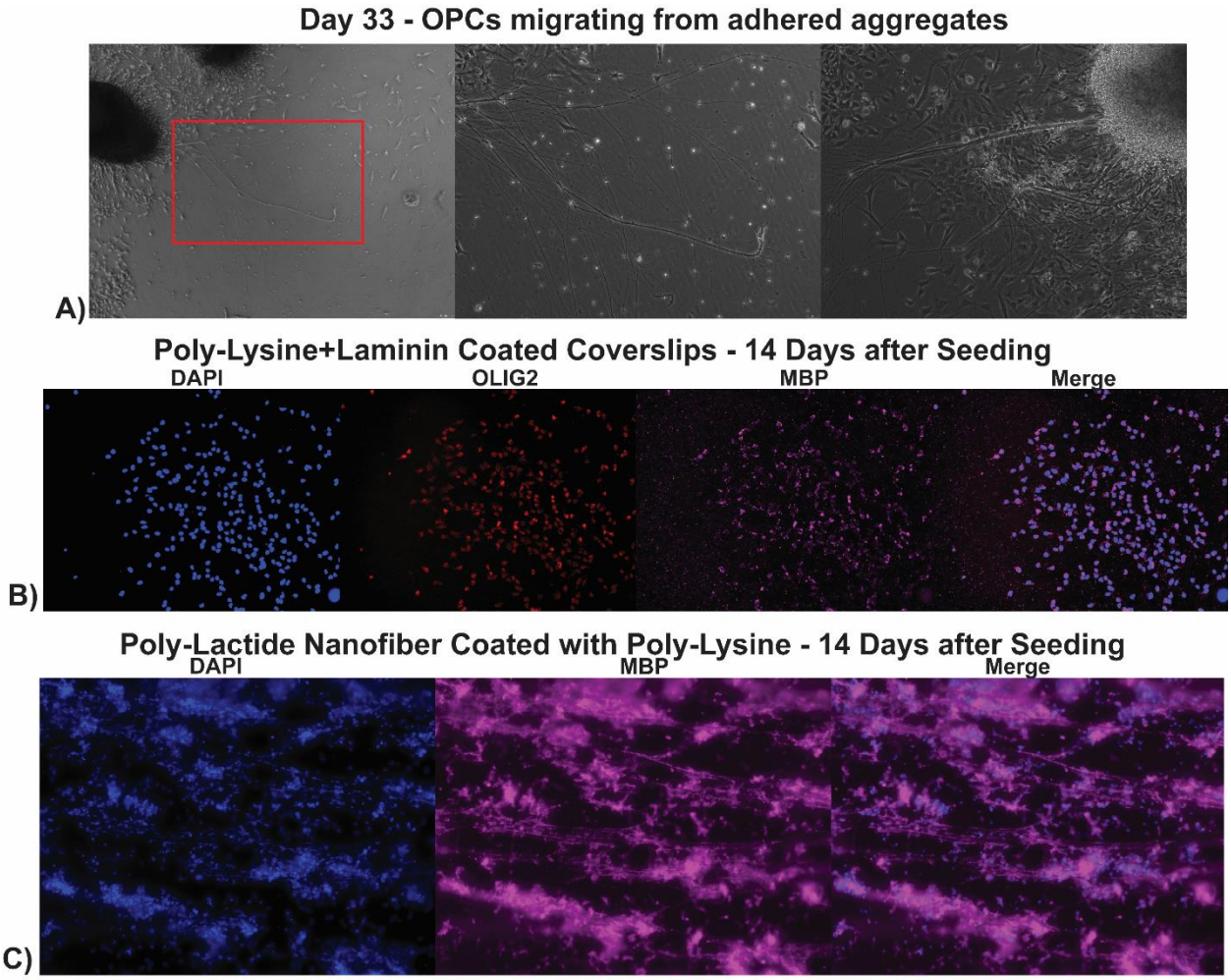

Figure 2. Microscopy and Immunocytochemistry of OPCs and OLs. 2A) Phase-contrast microscopy images at day 33 in differentiation protocol showing aggregates (dark ovals) with OPCs migrating out onto the plate. The red box in the left-most image shows the region enlarged in the middle frame. Note how the aggregates extend long processes from the aggregate out towards the open areas of the plate in a way reminiscent of radial glia. The Over time, the OPCs spread from both the aggregate itself and these extensions. **2B)** Following dissociation of OPCs after day 75, OPCs were plated onto poly-lysine and laminin coated coverslips and pro-myelinating medium introduced. After 14 days, ICC was conducted using OLIG2 and myelin basic protein (MBP) antibodies to identify whether myelin was produced. Secondary only slides were ran and showed no labeling besides DAPI. All cells that remained at 14 days were OLIG2+ and MBP+, suggesting they were OLs. **2C)** OPCs seeded onto 2um diameter

poly-lactide electrospun fibers coated in poly-lysine induce both proliferation/expansion of seeded OPCs and myelination. Using the same MBP antibody, I show that nearly all cells on the fibers at 14 days were MBP+, with cells producing myelin reminiscent of myelin sheaths (compare MBP pattern from 2B and 2C). Individual OPCs extend their processes and elongate to enwrap the fibers, with clear processes emanating from the cell body to the fibers.

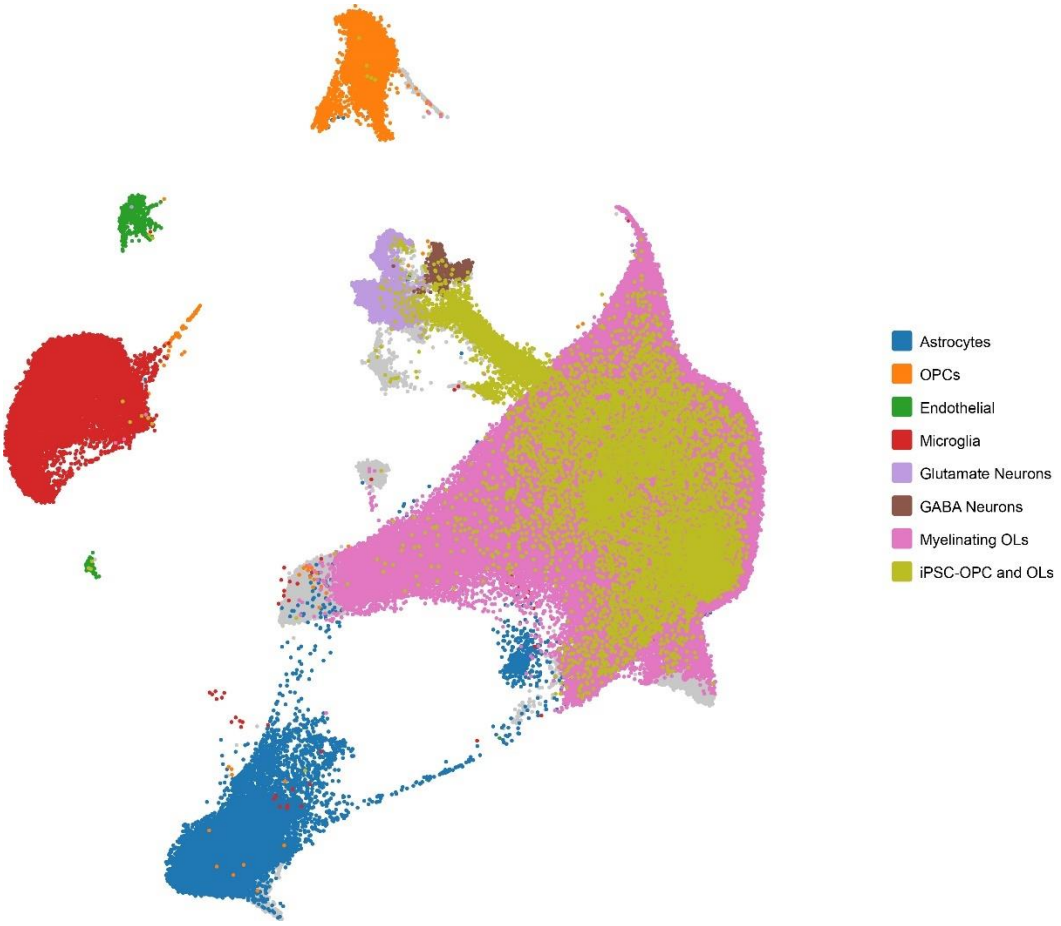

Figure 3. Human iPSC-derived OPCs and OLs cluster with the myelinating OL and neuronal clusters. hiPSC-OLs were derived from hiPSC-OPCs with 10 days in promyelinating medium (see text for components of this media). Following snRNAseq. and integration, my OPCs and OLs both clustered together, and predominantly overlapped with the myelinating OL clusters from human WM samples (see subsequent chapters for more information on the WM datasets). There was a “smear” clustering from the myelinating OLs to the neural subtype clusters as well, suggesting these iPSC-derived OLs are also expressing neural transcripts. However, it is possible there are a

subset of neurons being derived during differentiation as well. We found elevations of neural markers like TBR1/2 in qPCR as well (Figure 1C).

1.III. Inducing senescence in human meningeal fibroblast primary cultures and human iPSC-OPCs

Once OPCs were reliably made, the next step was to develop an assay to induce senescence and measure whether cells became senescent. In general, the main way senescence assay *in vitro* involves plating an equal number of cells per well of a 6-well plate, then exposing each well to a different concentration of a toxin for a determined amount of time. One challenge is to determine what agent to induce senescence with. The literature has documented many agents as senescence inducers from DNA double-strand breaking agents like etoposide, free radical producers like hydrogen peroxide, and disease-specific agents like amyloid-beta oligomers to name a few[132]. Because aged OPCs are likely exposed to elevated levels of free radicals and DNA damage, etoposide and hydrogen peroxide were selected as senescence-inducing agents.

The next question was at what concentration and for how long to expose OPCs to these agents to induce senescence. It was expected that each cell type would require a different range and duration of exposure, and thus the experiment was designed to cover a wide range of dosages. An example of how these experiments were designed is in figure 4A. Cells were seeded at 100k cells per well of a 6-well plate and allowed to adhere and proliferate to 50-60% confluence. This was important, as by the end of exposure the well needed to be near confluence but not overgrown to ensure the beta-galactosidase assay could properly label cells. Each well received a precise amount of

etoposide (or hydrogen peroxide) for 3 or 7 days. The dosage range for the initial experiment of a given cell type would encompass a range from 1nM to 100,000nM to narrow down the optimal senescence induction range. In addition to etoposide wells, a DMSO vehicle well and a well that received etoposide (typically a moderate dose) and no X-gal were included as negative controls. Following 3- or 7-day exposure, cells were fixed and the beta-galactosidase assay conducted, a procedure that incubates overnight.

The beta-galactosidase was selected as the primary read-out for senescence as this assay was used for identification of other senescent cells (including mouse OPCs exposed to amyloid-beta[50]) and thus was a reasonable and quick way to assess senescence[132]. Beta-galactosidase itself is a proxy measure of overall lysosomal content, and lysosomal content increases in senescent cells[47]. To quantify senescence, three random 10x fields were captured per well and cells that had turned blue (indicating X-gal cleavage by beta-galactosidase, producing a blue color) were quantified manually using ImageJ's counter feature. DAPI was added to each well and cells were semi-autonomously quantified using ImageJ to determine the total number of cells in the fields of view.

This protocol was first tested on human meningeal fibroblasts obtained from post-mortem meningeal samples. These cells were already isolated and expanded from the meningeal tissue by Shannon Rose, a member of Dr. Jessica Young's lab at the University of Washington. Because these are primary cultures, they were low passage cells (typically 3-5 passages total). Leptomeningeal fibroblasts were selected because they required no differentiation and have been senescence-induced in the literature

(albeit typically dermal fibroblasts)[133]. Following three days of etoposide exposure, the percentage of cells positive for beta-galactosidase were found to increase from around 3-5% in 10-100nM etoposide doses, peaking around 750-1000nM, and declining after that point (figure 4B). Note, in the same fields of view, the total number of cells declines with increasing dose of etoposide beyond 10nM, implying that doses beyond this cause cell death in a subset of leptomeningeal fibroblasts as well (Figure 4C). However, I still saw a dose-response curve as expected in leptomeningeal fibroblasts with increased senescence until a critical dosage, after which they die rather than become senescent. When this protocol was extended to 7 days of exposure, the dosages needed to be lowered as longer etoposide exposure resulted in cell death at a lower concentration (figure 4E). However, a similar dose-response relationship between etoposide concentration and senescent cells was present, implying that fibroblasts indeed will become senescent, or at minimum beta-galactosidase positive (Figure 4D).

Since both 3- and 7-day exposure induced senescence in leptomeningeal fibroblasts, it was time to induce senescence in human iPSC-derived OPCs. The protocol was similar for OPCs, with the dosage range between 1nM and 100nM, like that used for the 7-day fibroblast exposure. However, while fibroblasts showed widespread death after 10nM of etoposide exposure for 7 days, hiPSC-OPCs showed a precipitous decline in cell number between 40-50nM (Figure 4F). This is visualized with representative brightfield images of each well in figure 3G. While the hiPSC-OPCs died off, there was a total of 4 beta-galactosidase positive cells found across all wells. If hiPSC-OPCs were becoming senescent, this implies that they are not accumulating lysosomes (and beta-galactosidase). After replicating this experiment to confirm it was

not a technical issue, I attempted this same experimental paradigm with hydrogen peroxide instead of etoposide. However, I saw a similar result to etoposide where human fibroblasts would become senescent while hiPSC-OPCs would die with no concurrent beta-galactosidase accumulation (data not shown).

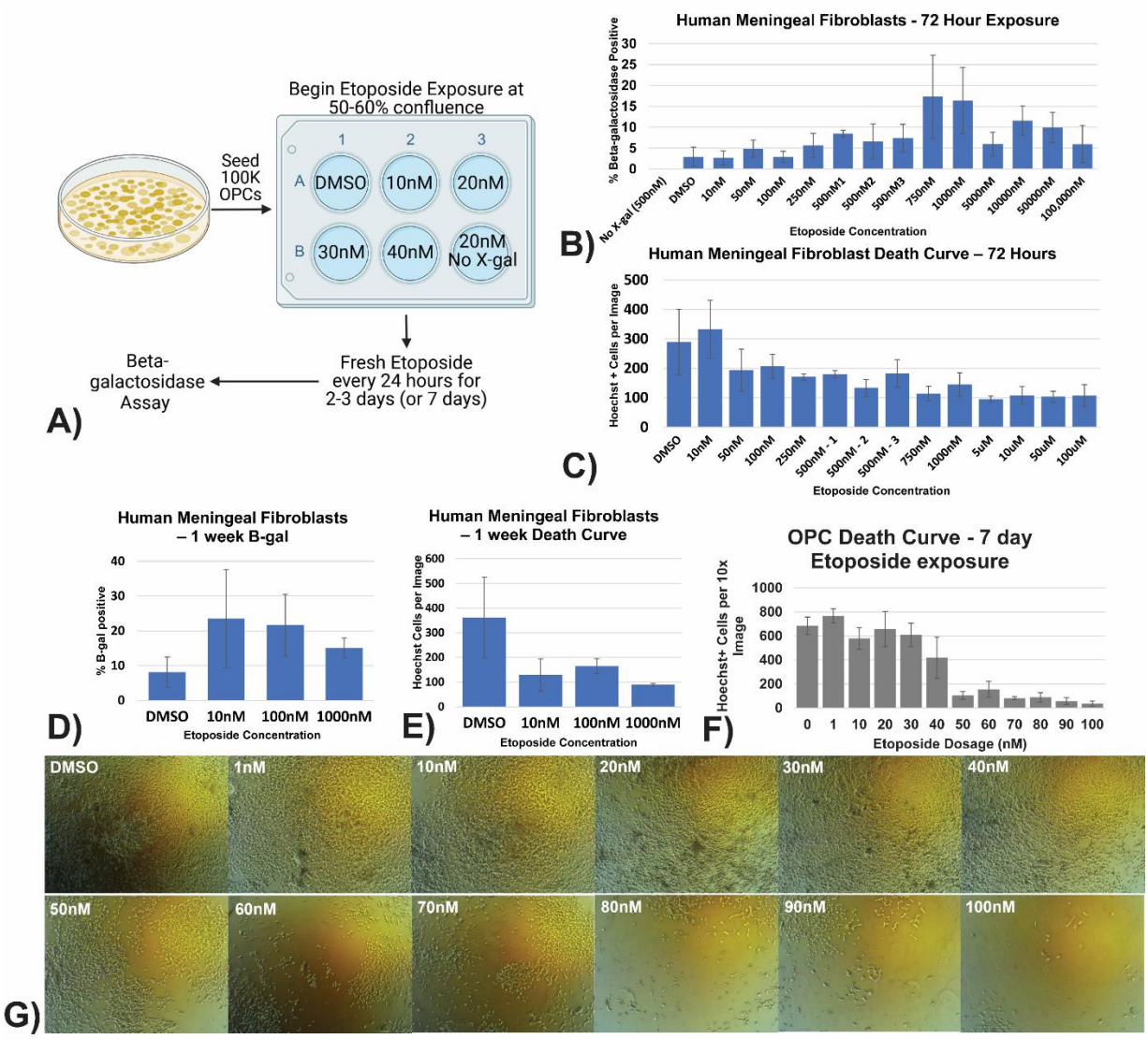

Figure 4. Inducing senescence via etoposide exposure in human leptomeningeal fibroblasts and hiPSC-OPCs. 4A) Schematic depicting the protocol used to induce senescence. This schematic was generated in BioRender. **4B-C)** Human leptomeningeal fibroblasts show elevated percentages of beta-galactosidase positive cells around 750nM and 1000nM exposure for 72 hours. During this same time, the

number of cells per field of view declined as etoposide dose increased (4C). **4D-E)** When exposure was extended to 7 days, there was a substantial increase in beta-galactosidase positive cells in all etoposide exposure groups (4D). This coincided with a reduction in total cell numbers in each of the etoposide groups as well (4E). **4F-G)** When this etoposide exposure protocol was conducted on hiPSC-OPCs for 7 days, there was a precipitous reduction in total cell number between 40-50nM dosage. This is visually displayed with representative 10x fields of view in 4G. In contrast to the increase in beta-galactosidase cells in leptomeningeal cells with etoposide exposure, a total of 4 beta-galactosidase positive cells were detected across all exposures. Error bars signify standard error from three fields of view from one experiment (n=1). Note: each experiment was conducted two times to confirm similar results, but results were not combined for these graphs.

1.IV. Discussion

In this chapter, I show that I could create human OPCs from CViA2 iPSCs. When this protocol was used on CViB5 and GM25256, there were issues that prevented these iPSC lines from being used for further analysis. CViA2 OPCs were able to myelinate on both coverslips and 2μm poly-lactide nanofibers, supporting their identity as OPCs/OLs. Etoposide exposure of hiPSC-OPCs for 7 days revealed no accumulation of beta-galactosidase but did show a death curve. This is in contrast to the human leptomeningeal fibroblasts, which in addition to showing a dose-response death curve at both 3 and 7 days, also showed an increase in beta-galactosidase-positive cells between 750-1000nM etoposide (after 3 days of exposure) and 10-100nM etoposide exposure (after 7 days of exposure). Together, this suggests that the meningeal fibroblasts were able to become senescent, while the human iPSC-derived OPCs were

not, at least the senescent phenotype that includes an accumulation of lysosomes and beta-galactosidase.

The initial hypothesis was that iPSC-OPCs could be pushed to a senescent phenotype that would look similar to other senescent profiles identified. This was a reasonable hypothesis because mouse OPCs have been shown to accumulate beta-galactosidase when exposed to amyloid-beta oligomers. However, we did not see this beta-galactosidase accumulation when exposed to etoposide or hydrogen peroxide. Rather, we see that human OPCs remain alive and non-beta-galactosidase reactive until a critical concentration, at which point they simply die, bypassing this senescent stage. While this evidence suggests that senescent human OPCs may not be inducible, there are multiple reasons why such strong conclusions were not drawn here. First, as mentioned, there is evidence of mouse OPCs becoming senescent, or at least acquiring senescent characteristics. Second, there are a multitude of methods to induce senescence[132]. While etoposide and hydrogen peroxide are two of the most common agents used, amyloid-beta oligomers[50], radiation, other chemotherapy agents, and UV light are also used[132]. Third, senescence is not homogenous, and the phenotype of one senescent cell type will encompass different aspects than another senescent cell type[47]. Senescent cells were first identified in tumor biology, where a subset of senescent cells would accumulate within the tumor and modulate the tumor as a whole[134]. Beyond this, nearly all proliferative cell types have been documented to go senescent one way or another, and the way this senescence manifests is highly variable. It is plausible that OPC senescence is unconventional, as OPCs and OLs themselves are highly specialized and unique cells within the CNS (for an interesting review on OL origins

during evolution, see Hines 2022[135]). Because I did not know exactly what this human OPC senescent profile would look like I chose the beta-galactosidase assay, one of the more common and reliable methods of detecting senescent cells, as my proxy measure. But this is only sensitive to lysosome accumulation, one aspect of many associated with senescence. Finally, because my OPCs were derived from iPSCs, it is possible this reprogramming and differentiation creating a unique *in vitro* OPC phenotype that was resilient to senescence. This is less-likely to be the issue, as embryonic stem cells were driven to an OPC phenotype and induced to become senescence using mouse ESCs[50], but it is still a possibility.

Because there were so many different viable options to induce and detect senescence, including exactly what aspects the human OPC would acquire or not, this line of research reached an impasse. On the one hand, there was the option of continuing to evaluate various other senescence-inducing agents to see if any of these could induce senescence. Alternatively, I could change the read-out methods to other modalities like detecting cytokine secretion (a sign of the senescence-associated secretory phenotype) using ELISA, qPCR to detect upregulation of senescent transcripts, or electrophoresis of individual cell genomes to show elevated fractioning and damage that is a key aspect of senescence (to name but a few). However, this process would require a large amount of time and effort, and the reality is it is reliant on the existing senescence literature, which may or may not represent the actual human OPC senescent profile, if one were to exist. Thus, the decision was made to take a step back and approach this question from a different angle. What if I could generate a single nucleus RNA sequencing and spatial transcriptomic dataset on human WM that would

include all cell types present in WM? Could I identify a subset of cells that showed enrichment for senescence-associated pathways and transcripts? Further, could I identify unique aspects the damaged OPC and OL assumes that are not characterized with the senescent profile of other cell types? This was the intent of the rest of this thesis. In the final thesis discussion, a roadmap of a plausible future iPSC-based workflow to identify senescent cells will be elucidated, incorporating the findings from the single cell datasets discussed next.

Chapter 2: Generation of a single nucleus RNA sequencing and spatial transcriptomics dataset on post-mortem human deep anterior frontal white matter and dorsolateral prefrontal cortex

2.I. Background and Cohort Selection

The human brain is 40-50% WM, but to date there are only a couple small single cell RNA sequencing datasets that exclusively focus on WM. Further, these datasets are focused on specific questions like white matter hyperintensities[136], multiple sclerosis[137], or chronic traumatic encephalopathy[138], skewing the resulting dataset towards disease states at the expense of characterizing typical WM. To that end, no dataset has simply characterized how young adult WM and old adult WM change at the transcriptomic level. This was one goal of this project. Beyond this, I aimed to also contrast this typical WM aging to WM from donors with high AD pathology. When designing RNA sequencing experiments, cohort selection is crucial. Defining which characteristics to include versus exclude is vital to controlling confounding variables and generating data is as representative as possible. Because the Allen Institute recently published a dataset on 90 donors from our brain biorepository (18 of which were included in this study as well as the Allen Institute's project known as Seattle Alzheimer's Disease Brain Cell Atlas, SEA-AD)[92], I intended to merge and compare my WM dataset to the SEA-AD to understand how human WM OLs differ from GM OLs, especially in the context of aging and AD. To this end, we generated a spatial transcriptomics dataset that used Nanostring's CosMx platform on 6 cases that were included in both my and the Allen Institute's datasets, 3 high ADNC and 3 no/low ADNC cases, to provide more information and confirm my findings.

When selecting young donors, I only included samples that were beyond 27 years of age. This cutoff was selected to ensure that the area being sampled, deep anterior periventricular WM, was fully myelinated, a process that can take until the late 20's to complete in normal development[139]. This region is one of the last regions to myelinate (consequentially, one of the first to be affected in AD as discussed in the introduction[84]), and I wanted to avoid donors who were still finishing initial myelination. Beyond this, I selected cases that were at or below the age of 50 that had no AD pathology or other identified psychiatric diagnoses. The main exceptions to these criteria were drug use, with half of the donors selected having died from acute fentanyl overdose, suicide, and depression diagnoses. These exceptions were made not because they were ideal, but rather they were practical. If I excluded cases with these criteria, I would have had zero cases that met the criteria. 50 was chosen as the upper age limit because it was separated from the old cohort by at least 15 years, hopefully minimizing the inclusion of any mild cognitive impairment or pre-AD prodromal donors. While this cannot be definitively concluded, I am confident it was a reasonable compromise.

For the aged WM donors, I selected two separate groups, one with low ADNC rank (No/Low) and one with high ADNC rank (High). This excluded ADNC = Moderate cases to clearly separate the low and high pathology cases. A unique challenge to designing AD-specific studies is whether to use clinical metrics like impaired cognitive function as assessed by neuropsychiatric tests (e.g. mini mental status exam and Montreal Cognitive Assessment (MoCA)), clinical diagnosis of probable AD, or pathological burden to delineate AD cases. While some groups use clinical diagnosis

(e.g. the SEA-AD project), I decided to use AD pathological burden exclusively. This decision primarily rested on the fact that pathological assessment is standardized, semi-quantitative, and based on concrete tissue abnormalities. Since the goal is to single cell transcriptomic data, I concluded that AD pathology would most likely result in differences in expression on the transcriptomic level. However, it would have been reasonable to stratify by whether donors had clinical diagnoses of AD as well, although AD diagnoses have classically only been confirmed upon post-mortem analysis, thus relying on pathological burden anyways[57]. For my cohort, I stratified primarily using ADNC rank, which considers both amyloid and tau pathology in its ranking scale, thus encompassing both primary pathological abnormalities required for AD diagnosis. A secondary stratification metric (and one that was ultimately ignored in the final analyses) was vascular pathological burden. Initially, this was deemed necessary to determine whether AD pathology was being driven by vascular contribution specifically. However, one of these subgroups was underpowered (n=3), and this challenge was unresolvable as no additional cases that met the criteria were available. Further, the analyses I conducted were more general and this level of granularity was unnecessary, so my final cohort was stratified into only “Low AD” pathology (representing ADNC = No/Low) and “High AD” pathology (representing ADNC = High). I excluded donors with LATE-NC stage 3, indicative of TDP-43 pathology extending into middle frontal gyrus[140], Lewy body disease extending into limbic zone, fronto-temporal dementia, chronic traumatic encephalopathy, hippocampal sclerosis, and amyotrophic lateral sclerosis/motor neuron disease. For the Low AD group, I also excluded any cases that had Braak staging 5-6, CERAD score 2-3, and Thal phasing of 3-5. These were excluded to further ensure

pathological burden was stratified between the low and high AD groups as these high scores in any one category indicate that at least one of the pathological proteins is aberrantly present, even though the overall ADNC rank was still 0-1. The final cohort selection is summarized in Table 1. Note, the Allen Institute's dorsolateral prefrontal cortex GM samples were included in this table, as this will be compared to my WM dataset in the next chapter.

Group	Sex	Age at Death	ADNC Rank	Thal Phase	Braak Stage	CAA Score	CERAD	Microinfarcts
Low AD WM	8F/5M	87.7 (72-102)	0.54 (0-1)	0.77 (0-2)	2.77 (0-4)	0.46 (0-2)	0.23 (0-1)	0.69 (0-2)
High AD WM	11F/8M	86.6 (73-99)	3 (3)	4.63 (4-5)	5.47 (5-6)	1.26 (0-2)	2.68 (2-3)	3.74 (0-26)
Young	6F/10M	39 (27-50)	0.067 (0-1)	0.125 (0-1)	0	0	0	0
DLPFC GM Low AD	24F/17M	89.76 (72-102)	1.61 (0-3)	2.5 (0-5)	4 (0-6)	0.92 (0-2)	1.24 (0-3)	1.02 (0-8)
DLPFC GM AD	24F/15M	87.69 (70-99)	2.64 (1-3)	4.17 (1-5)	5 (2-6)	1.24 (0-3)	2.43 (0-3)	0.95 (0-10)
CosMx – Low AD	2F/1M	86, 87, 98	0.33 (0-1)	4.33 (4-5)	5.33 (5-6)	0.66(0-2)	0.33 (0-1)	0.33 (0-1)
CosMx – High AD	2F/1M	84, 83, 98	3	1 (0-2)	3 (2-4)	1 (0-2)	2.67 (2-3)	5.67 (1-8)

Table 1. Summary statistics for pathology metrics for the snRNAseq. WM cohort, the Allen's SEA-AD project, and the CosMx samples. Mean values are presented with the range in parentheses.

2.II. Generation of snRNA sequencing dataset on human WM

To generate the single nucleus RNA sequencing (snRNAseq) dataset, we began by dissecting deep anterior periventricular WM from fresh frozen (unfixed) 0.5mm brain slabs stored at -80°C. The area of dissection was determined by selecting the slab immediately anterior to the termination point of the lateral ventricle in the frontal cortex. The slab was removed from freezer, placed on dry ice, and dissected using a 5-10mm sterile biopsy punch. The dissected tissue was bisected and placed in two tubes, one half for bulk RNA extraction and RIN value calculation and the other for the snRNAseq.

process. RIN values were calculated on all samples and a RIN at or above 5.9 was deemed sufficient to proceed. Typical RIN cutoff values for RNA sequencing are around 7 for GM tissues, but RIN values were consistently a point below those calculated on GM from the same brain, requiring the threshold to be reduced. In addition, visual inspection of the Bioanalyzer gel was conducted to ensure RNA degradation was not visually apparent.

The snRNAseq. procedure can be broken into three main parts: isolation and purification of nuclei, 10x chip loading and downstream cDNA clean up, and cDNA library preparation for sequencing. The general workflow is displayed in Figure 5A. First, the samples are dounced in microcentrifuge tubes using sterile, single use dounces designed to fit the tube. Throughout the entire nuclei purification process, samples are maintained on wet ice. Following douncing, samples are filtered to remove any debris beyond 30um. After numerous wash steps, the nuclei are mixed with equal parts 42% iodixanol/resuspension solution and layered onto a 25% iodixanol solution. This is spun at 10,000x*g* for 10 minutes, resulting in a pure nuclei pellet at the bottom of the tube with a thick layer of myelin on top. This myelin is pulled off with a pipette and/or Q-tip, at which point the nuclei are quantified. This quantification resulted in a typical nuclei purity of 70+%, and Figure 5B shows a representative image of brightfield and DAPI labeling. To proceed to the 10x Genomics process, nuclei needed to be pure with at least 60% DAPI-positive nuclei, and the concentration needed to be sufficiently high to avoid blockage of microfluidic channels or overloading of the chip wells. The 10x procedure can work on both nuclei or whole cells, and for human WM I relied on nuclei exclusively. Isolating full, intact cells from human WM is extremely challenging since OLs wrap

around many different axons. Successfully isolating the full OL without rupture would be impractical, so nuclei were the more reasonable target. The douncing process effectively destroys the myelin and breaks up the cell while preserving the nucleus intact. While this certainly skews the resulting sequencing results since cytoplasmic RNA is being lost, at least all cells would be stripped to their nuclei rather than the selective whole cell bias that would result from attempting to purify whole cells from WM.

The 10x procedure followed the 10x Genomics 3' GEM v3.1 Dual-Index protocol (CG000315). I targeted 8,000 cells captured per sample with the intent of balancing the total number of cells captured and number of multiplets that were generated. The more cells/nuclei loaded in the chip, the higher the percentage of multiplets captured. This multiplet rate is a result of the way 10x snRNAseq. generates an emulsion akin to a soap bubble emulsion, where each bubble contains all the necessary components to do reverse transcription of RNA to cDNA, a bead with unique molecular sequences that serve as primers to bind poly-A tail (hence the 3') RNA sequences, and a single nucleus. This emulsion is created via a microfluidics chip that pushes the nuclei suspension and reagents through a small passage into an oil. After the emulsion is created, reverse transcription is completed in a thermocycler, at which point cDNA is created. This process results in each nucleus's RNA being converted to cDNA with a unique genetic sequence that acts as a barcode that can be used to correlate individually sequenced reads to each cell. Since the number of individual bubbles generated is roughly the same each run, the more nuclei you load initially, the more of these bubbles will receive two or more nuclei. Following reverse transcription, the

emulsion is dissolved and cDNA cleaned up. At this point, a small amount of the cDNA is run on a Bioanalyzer chip to confirm that cDNA was produced, and to determine how much and what sizes the cDNA is. The left two tracings in Figure 5C show an example of the cDNA product from a single sample at this step (bottom tracing), with the 10x-provided example Bioanalyzer result at this stage above it. The final stage of the snRNAseq. process before sequencing is to generate the cDNA library, which involves cleaving the cDNA into smaller fragments and selectively purifying these fragments and amplifying them via PCR. This process removes low base pair sequences that are likely primers and high base pair sequences. This selection process is optimized to provide individual reads between 200-600 base pairs, the ideal amount of sequence to capture the barcode and enough genetic sequence to map it to a reference genome during analysis. Any larger fragments are essentially excessive, and may indicate fragments that were unfragmented transcripts or abnormal PCR products, both of which are removed. The two tracings on the right side of Figure 5C show representative tracing of a single cDNA library (bottom tracing) with the 10x-provided sample tracing above.

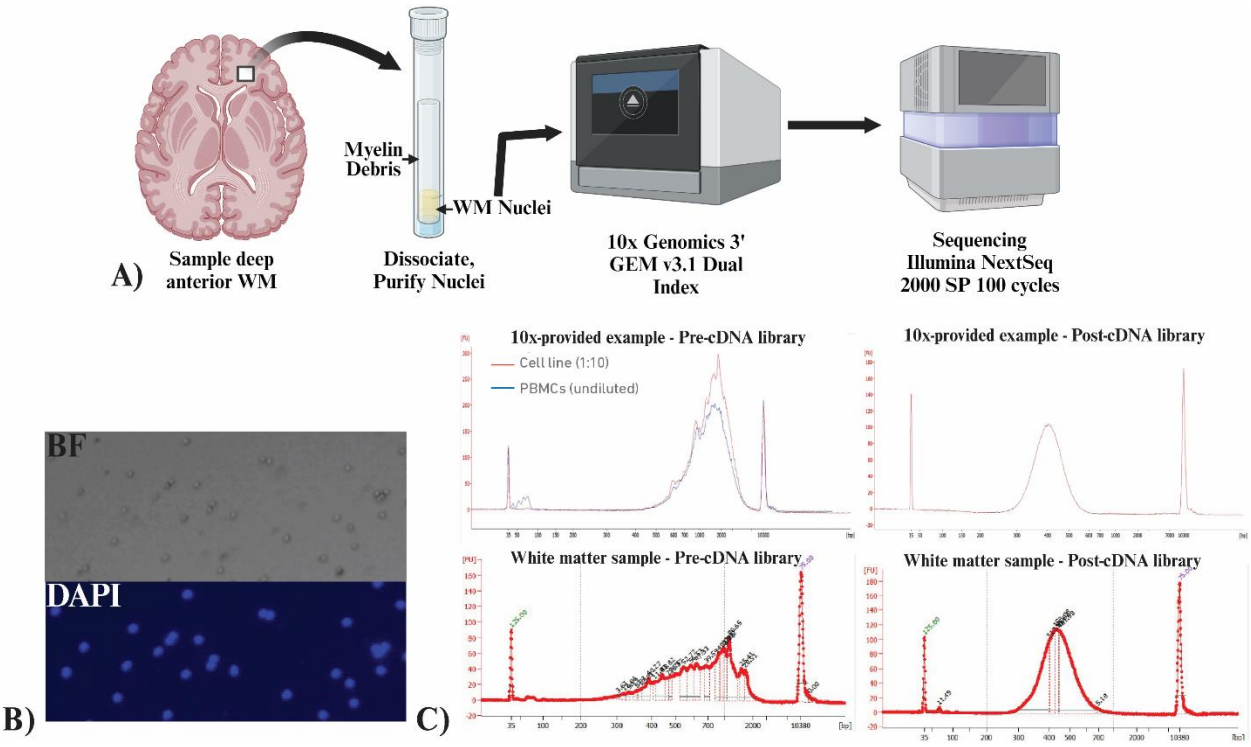

Figure 5. Generation of a snRNAseq. dataset. 5A) Cartoon schematic showing the general steps involved in creating a snRNAseq. dataset. This schematic was generated in BioRender. **5B)** Representative images of nuclei following purification, prior to loading on 10x chip. Note how nearly all objects are nuclei (DAPI+) and maintain their circular shape, indicating the nuclei are intact. **5C)** Bioanalyzer cDNA tracing following purification prior to (left) and after (right) cDNA library generation. Top tracing is the 10x-provided example while the bottom tracing is a single WM sample's tracing.

Following cDNA library preparation, samples are pooled and sequenced. Sequencing was done on the Illumina NovaSeq. 6000 SP Reagent Kit v1.5 (100 cycle) (PN:20028401) sequencing kits. The raw sequencing data was run through 10x's CellRanger (v7.2) pipeline to map to the Human reference genome (Human GRCh38 (GENCODE v32/Ensembl98)), demultiplex each sample, and provide initial quality control on samples. All cells with less than 200 features (genes) and greater than 5%

mitochondrial reads were removed. Sequencing metrics like RIN values, cells captured, median genes per cell, and mean reads per cell are depicted in Figure 6.

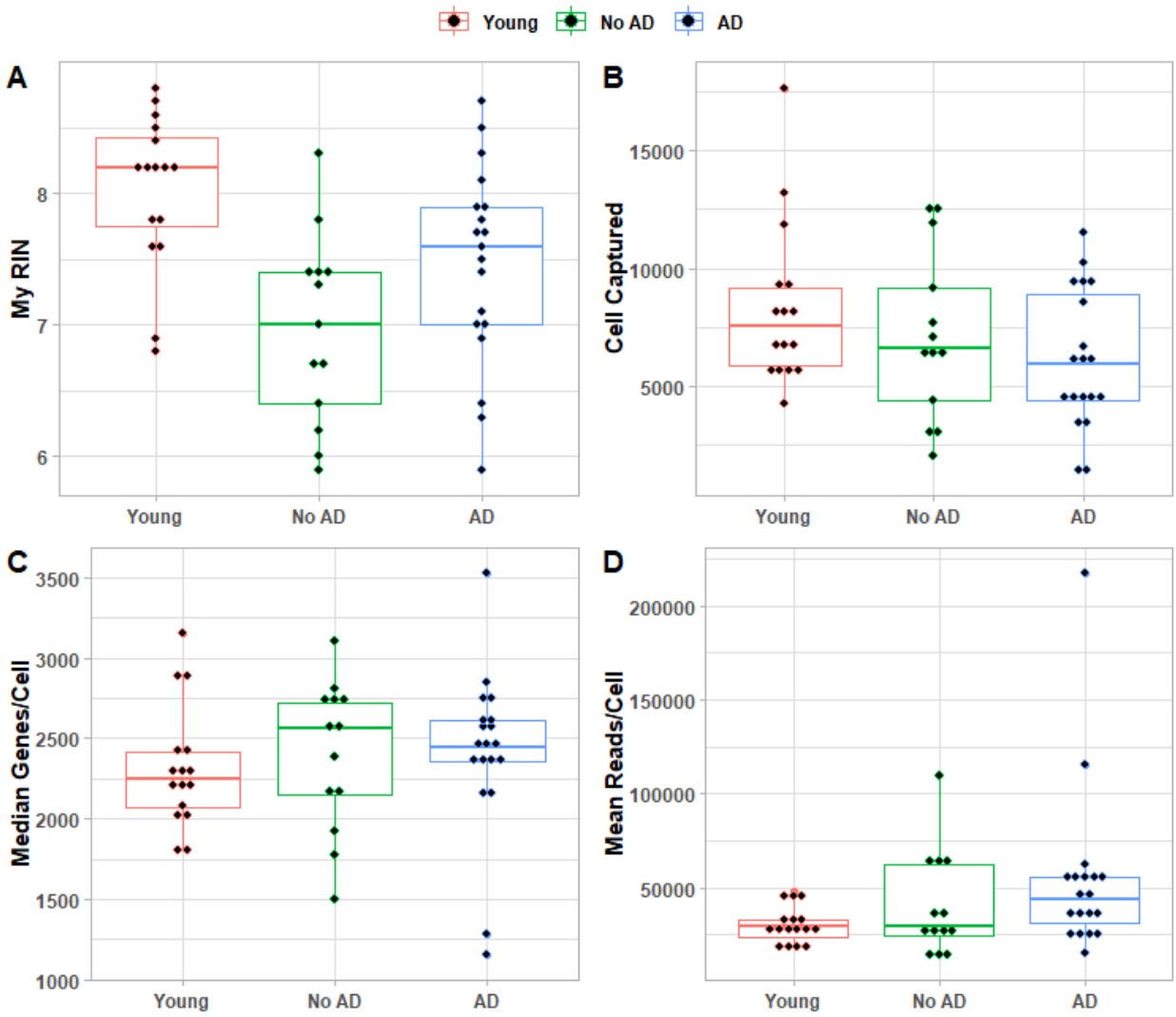

Figure 6. Quality control and sequencing metrics for the WM snRNAseq. dataset. **6A)** RIN values as measured by bulk RNA extraction and analysis via Bioanalyzer. RIN values at or above 5.9 were used for snRNAseq. **6B)** The number of cells captured following demultiplex in CellRanger. A target of 8,000 nuclei were loaded per run. **6C)** The median number of unique genes sequenced per cell. **6D)** The mean number of reads per cell. A general trend exists where there were more reads/cell and unique genes captured when less nuclei were loaded. This is due to the sequencing depth (i.e. number of transcripts sequenced per sample) being consistent for all samples.

2.III. Procedure to generate spatial transcriptomics dataset

Because the literature is sparse on GM OLs and I intended to merge my WM OLs to the SEA-AD's GM OLs, validation of the merging process and GM OL findings was deemed necessary. Beyond validation, spatial transcriptomics also provides spatial localization of mRNA molecules within the cell and overall tissue, providing useful information not obtainable via snRNAseq. To do this I used Nanostring's CosMx platform, a method that uses a combination of antibody-based morphology marker localization and RNA-based *in situ* hybridization to assess 6,000 separate RNA transcripts while maintaining spatial resolution. A key limitation of snRNAseq. methodology is the requirement of destroying the tissue cytoarchitecture to purify the nuclei. Further, all cytoplasmic expression is lost, potentially skewing the outputs. CosMx preserves the tissue structure by labeling RNA sequences directly on the slide and imaging with high resolution to provide an image of the tissue and spatial coordinates for each transcript. Rather than snRNAseq. that uses 3' poly-A tail binding and reverse transcription to sequence any transcript within a nucleus, CosMx relies on *in situ* hybridization sequences with each probe containing a unique combination of binding sites to 5 different fluorophores. These bindings sites are bound, imaged, and cleaved, one at a time to provide a unique code that is used to identify which transcript is where on the slide. So, while snRNAseq. is unbiased in regard to what it captures (beyond the requirement of the transcript being nuclear and containing a poly-A tail), CosMx will only detect sequences that have probes designed and included for them. However, because I was able to run a 6,000 probe set at one time, my read depth was

sufficient to accurately identify individual cell types and run similar downstream analyses to snRNAseq. methods.

Figure 7 outlines the general procedure for CosMx. The first step is to dissect out the regions of interest to be analyzed. For this, we selected 5-10mm biopsy cores immediately adjacent to the cores taken for 10x to minimize regional variability between my CosMx and snRNAseq. data. For the GM samples, we used the Allen Institute's dissection images to determine the precise location they dissected and collected as close to this region as possible on the contralateral hemisphere. Again, we attempted to get as close to the same region as possible to minimize the regional variability. Following dissection, these tissues were transferred to a cryostat, where each sample was placed in a block and each piece mapped to ensure proper identification during analysis. We were able to combine 4 pieces of tissue, two GM and two WM (one high AD and one low AD donor) per slide, and made a total of 3 slides. All donors for CosMx were also included in both my WM dataset and the SEA-AD dataset. Thus, my CosMx dataset contained 6 donors with one WM and one DLPFC GM piece per donor. Following cryosectioning at 5um, I stored slides at -80C until beginning the CosMx procedure. The CosMx process requires multiple steps that are summarized as follows: fixation of sections, antigen retrieval, preparation for hybridization of RNA-probes, overnight hybridization of *in situ* probes, morphology marker application, and coverslipping each slide. At this point, slides are loaded onto the CosMx machine and the experiment is run, a process that typically took seven days. The CosMx machine directly uploaded all images captured to their proprietary software (Nanostring's AtoMx Platform) that runs initial processing to identify which probes localize where as well as

segmentation of cells. Cell segmentation uses the morphology markers (DAPI, histone H3, ribosomal RNA, and GFAP) to identify individual cells and determine where cell boundaries are. This is crucial for determining which probes are localized to which cell, enabling the production of a similar count matrix to snRNAseq. While these morphology markers effectively labeled nuclei, cytoplasm and membrane segmentation was challenging. Most of the cells identified in the final dataset primarily consisted of nuclei and a portion of the surrounding cytoplasm, rather than whole cells. This lack of membrane labeling and cell boundaries results in difficulty identifying direct cell to cell contact or interaction, as well as association of cytoplasmic mRNA transcripts that localize between the segmented regions. However, this nuclear focus likely to made the resulting data more comparable to my snRNAseq. dataset since that dataset only sequences nuclei.

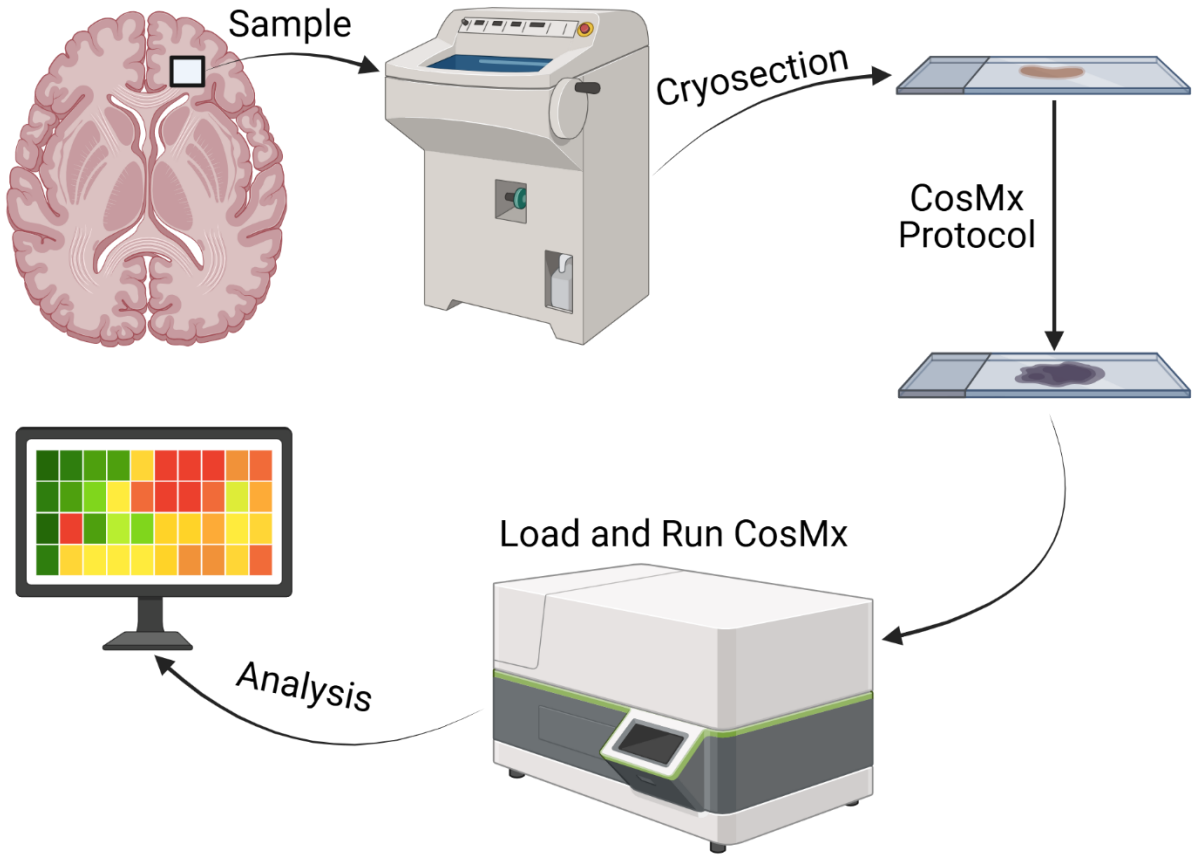

Figure 7. Spatial transcriptomics via Nanostring's CosMx platform. Deep anterior WM and DLPFC were sampled using snRNAseq. sampling as guide. Sampled regions were cryosectioned and prepared for CosMx. Slides are loaded on the machine and initial QC and demultiplexing is done automatically via Nanostring's AtoMx platform. Figure was made in BioRender.

2.IV. Initial characterization of the WM snRNAseq. dataset

Following initial QC, clustering and data integration can begin. The Seurat single cell analysis pipeline was used in RStudio to execute a sequence of steps that normalize, scale, group, cluster, and project the dataset into a dimensionally reduced UMAP. Normalization is conducted on each cell by calculating the proportion of each gene's reads relative to total number of reads, scaled by 10,000, and natural logarithm

transformed. This step accounts for the variable read depth of each cell within a sample. Scaling is used for dimensional reduction methods and sets the mean expression across all cells in a sample is zero and the variance is 1. This step adjusts for the variable cell capture by sample, allowing samples to be merged and clustered together on the same scale. Following PCA, initial clusters are identified. Because these samples were sequenced in groups of 4, there was some variability in clustering that resulted in a single cluster being composed of cells from only one or two donors. This is a typical indication that there is a “batch effect” where cells from one batch get pulled into their own cluster near the main cell type grouping. The primary purpose of dimensional reduction and UMAP projections are to identify broad cell types and groupings that can be isolated for downstream analyses. Thus, this batch effect needed to be corrected. In Seurat, there are multiple methods to do this, but the one employed here was canonical correlation analysis (CCA). CCA finds the greatest sources of variation in the entire dataset (and thus the genes most strongly representing individual cell types within the dataset) and compares individual cells within two clusters and identifies if they share the same features and levels of expression (and designates them as anchors if they align). If individual anchors are surrounded by other anchor pairs, then they are maintained. Individual anchor sets that are not surrounded by other anchors are flagged as false anchors and removed. Finally, cell expression values are transformed to integrate and align the anchor sets and representative clusters. Two important notes for this process are: 1. If a cluster is represented in one batch but not another, it will remain its own cluster. 2. Downstream analyses do not use these transformed values from CCA-

integration, rather downstream analysis (like differential expression analyses) use either raw or normalized counts.

For my dataset, I had 32 old (19 high AD, 13 low AD) and 16 young WM samples, and during this alignment step each individual donor was considered an independent sample for alignment. Following CCA-integration, clustering and UMAP projection were rerun, resulting in a UMAP where individual cell types and clusters were represented by cells from all samples. Since every sample should have the same general cell types (e.g. OLs, OPCs, astrocytes, etc.), I was confident the integration worked. Interestingly, there was one cluster that represented the “main” concentration of each cell type, and a second smaller cluster that smeared from the main concentration towards the large OL cluster. Further, these smear clusters were also positive for *MBP* and *MOBP*, two key myelination genes. Since roughly 70% of the WM cells captured were OLs, these smeared clusters likely represented doublets/multiplets, and thus these clusters were removed from the dataset as technical artifacts. These MBP/MOBP+ smear clusters accounted for 8.8% of total cells captured. Considering 10x Genomics provides an estimated multiplet rate of 6.4% for a target capture of 8,000 cells and the process of isolating nuclei from WM likely results in some contaminating myelin debris that could stick nuclei together, the slightly higher multiplet rate in my dataset is plausible. Following this multiplet removal, the UMAP in Figure 8A was generated with a similar distribution of clusters between the three groups (Figure 8B). Each cluster’s identity was determined using candidate genes representing each cell type (e.g. MBP and MOBP for myelinating OLs, GFAP and AQP4 for astrocytes, etc.), where both percent of cells expressing each transcript and the relative level of expression were

assessed (figure 8C). All major cell types were identified in WM, including neurons, although nearly 70% of cells captured were myelinating OLs.

2.V. Characterization of the spatial transcriptomics dataset on human WM and GM

Following initial processing in AtoMx, I used semi-supervised clustering to map my new dataset's clusters to previously identified CosMx cell type profiles. This process used a Nanostring-provided dataset generated on human frontal cortex using the same 6,000-plex panel in CosMx I used. However, this method only partially identified cluster identities, and I proceeded to use a similar clustering strategy to my snRNAseq. data to identify all clusters, exporting raw data to R from AtoMx. The first step was to remove low quality cells from the dataset, since AtoMx would flag cells but not remove them. Since these cells were still included in the dataset, the resulting clustering and UMAP projections were bimodal in shape, with one cluster being split into two groups. QC to remove low quality cells used the following parameters in sequence: 1. Remove any FOV with mean reads/cell below 300, 2. Remove any cell with 200 reads/cell or less, 3. Remove any cell with above 30,000 um^2 of segmented area. This process eliminated poor quality areas by FOV, sparsely represented cells within the remaining regions, and any cells that were abnormally large. While these metrics were deemed sufficient for the purpose of this project, these cutoff values were subjective as cutoff recommendations from Nanostring were insufficient. Following QC, the same CCA-integration pipeline was employed that was used for snRNAseq. to integrate the 3 different slides, accounting for batch effects in a similar manner. Following CCA-integration, the UMAP in Figure 8G was generated. The distribution of each cell type is similar to my snRNAseq. data with

most WM cells being OLs while GM is more diverse, with nearly a 50/50 split of neurons to glia (Figure 8H). Cluster identities were confirmed in the dot plot in Figure 8I, where candidate genes were used to determine each cluster's general identity. Of note, the markers used to identify clustering in the CosMx data were different than snRNAseq. because my 6,000-probe set did not include all of the genes identified in snRNAseq.

The individual clusters and cell types identified in the UMAP were mapped onto individual FOVs from both a WM and GM sample as shown in Figure 8D-F. The representation of cell types between WM and GM was starkly different, with WM being primarily composed of OLs (similar to my 10x findings), while the GM was more diverse (Figure 8D). A strength of spatial transcriptomics is the ability to map individual probes/transcripts onto the FOV to determine where the localization of these probes are relative to the cell bodies and other cells. I were able to identify that while both WM and GM OLs express transcripts classically associated with OLs (*CNP, CRYAB, MAG, PLP1*, and *SCD*, Figure 8E, especially insets), I show that only the GM OLs show substantial colocalization with synapse-related transcripts (*BASP1, CALM3, GNAS, SNAP25, SPARCL1*, and *YWHAG*, Figure 8F, especially insets). This was visual evidence that these GM OLs are contributing to synapse processes. Note that CosMx is an RNA-based technology, not protein, and thus this implies that these cells are producing mRNA for synapse machinery, not necessarily producing synapse proteins.

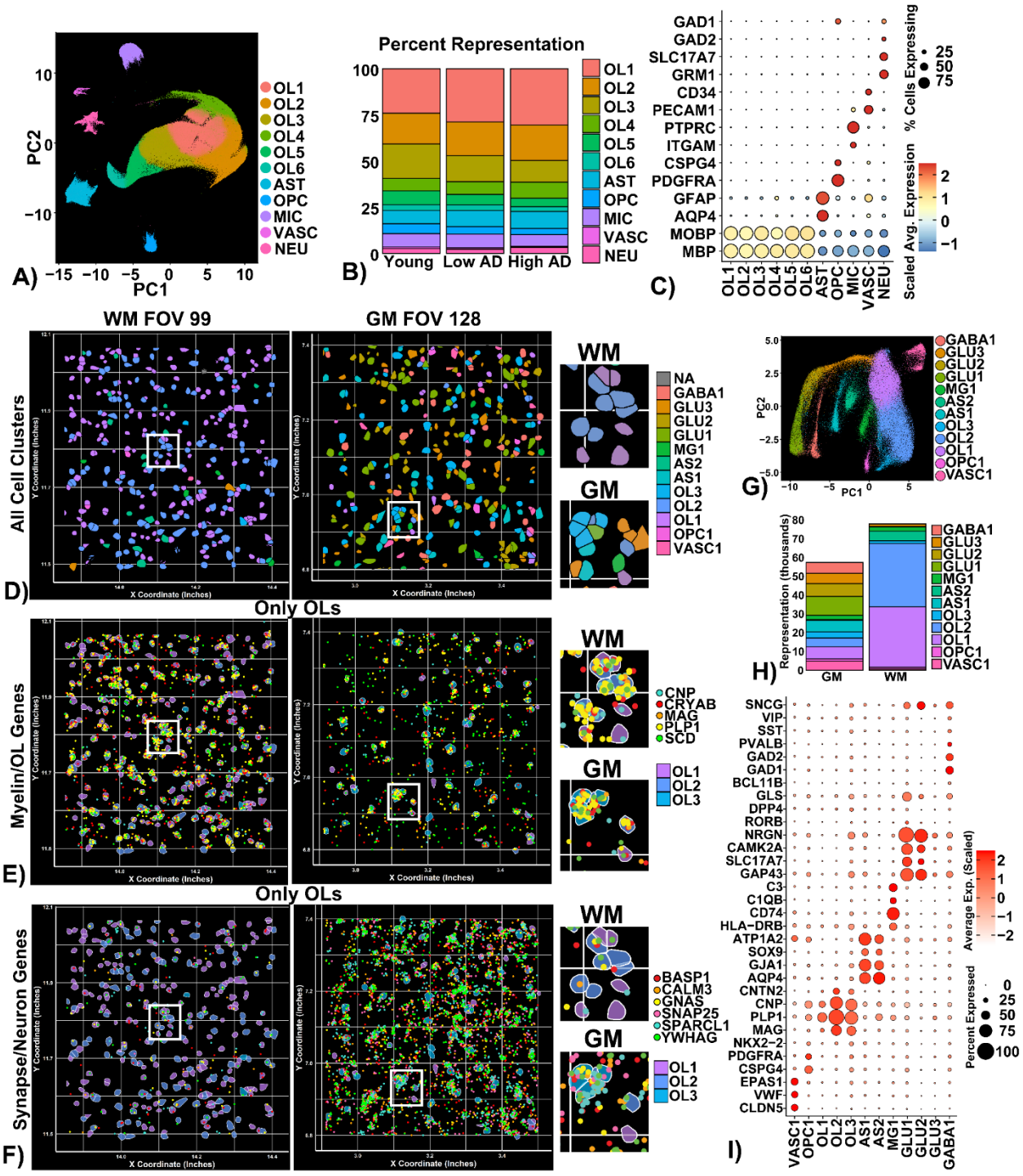

Figure 8. Characterization of the single cell RNA sequencing and CosMx datasets of human brain. 8A) UMAP following CCA-integration of all individual snRNAseq. WM samples collected show all clusters identified following k-nearest neighbors and Louvain clustering at 0.1 resolution. **8B)** Percent representation of each cluster, stratified by donor group. “Low AD” signifies donors with an ADNC stage of No/Low, while “High AD”

signifies donors with an ADNC stage of High. **8C)** Dot plot of each cluster and its expression across a list of candidate genes used to identify cell types within the snRNAseq. WM dataset. Circle size indicates the percentage of cells within the cluster expressing each gene of interest while dot color represents its scaled expression relative to all other clusters. A stronger red hue indicates this cluster expressed relatively more of that transcript than all others while blue hues represent relatively less expression. **8D)** Single FOVs from spatial transcriptomics post-segmentation representing one WM (left) and one GM (right) FOV from the same donor. The white box signifies the enlarged inset region. **8E)** OL cell segmentation with five ubiquitous OL transcripts mapped on the FOV. Each dot represents one *in situ* hybridization probe's location within the tissue. **8F)** The same OL segmentation with synapse- and neuron-related genes. **8G)** UMAP of entire CosMx dataset following QC. **8H)** Representation of each identified cluster, split between GM and WM. **8I)** Dot plot representing expression levels of each marker gene by cell cluster. The size of each dot represents the percentage of cells in each cluster that expressed the given gene, while the shade represents the level of expression, scaled relative to all other clusters in the dataset.

Chapter 3: Evidence of unique functionalities between WM- and GM-derived OLs and OPCs

3.I. OLs express synaptic machinery transcripts

Now that I have identified my OLs in both of my datasets, I was able to isolate them and run comparative analyses to see how they differ between groups. My first analysis was to assess how young WM OLs differ from the old WM OLs. In this comparison, I ran differential expression (DE) on young WM OLs versus the combined low and high AD WM OL groups. These OLs are color-coded in the UMAP in Figure 9A. After DE, I conducted gene set enrichment analysis (GSEA) using the Gene Ontology database. GSEA utilizes the DE outputs to identify what cellular processes or machinery are variable between groups, providing insights into functionalities beyond individual genes. GSEA revealed that young WM OLs are significantly enriched for pathways involving synaptic transmission, including synaptic vesicles themselves (Figure 9B). GSEA outputs are reported as inverted Log10-adjusted p-values (also known as q-values) following correction using the Benjamini-Hochberg correction method. Because DE and GSEA are comparing the expression level of many cells and genes at once (i.e. testing multiple hypotheses at the same time), respectively, the number of potential false-positive discoveries increases as well. To account for this heightened risk of false discoveries, numerous methods have been developed to adjust the significance threshold and reduce the number of false-positives identified. A classic and more conservative method is the Bonferroni correction, which adjusts each p-value by the total number of tests being conducted[141]. However, the Bonferroni method can be overly conservative, especially in datasets such as snRNAseq., where there are tens of

thousands of comparisons being tested at once. The Benjamini-Hochberg method was developed as a less conservative but still rigorous method to correct p-values[142]. This method is the most employed statistical correction method used in single cell datasets, and all significance values reported will be following this correction.

Next, I isolated the genes included in the GO pathway “regulation of trans-synaptic signaling” to see whether individual genes in this pathway were noticeably upregulated in the young relative to the old WM OLs (Figure 9C). I subset the WM OLs to only include genes in this pathway and selected the top 25 genes differentially expressed between groups. Because there were over 50,000 cells in each of the groups, I randomly subset 10,000 from each group (young and old) to provide a representative heatmap of normalized expression of these genes. The left side of the heatmap, representing the expression in 10,000 young WM OLs, shows elevated levels of these transcripts compared to the right side (the old WM OLs). Notably, the old group did still express lower levels of these transcripts, implying these transcripts are downregulated, not absent. Together, both the GSEA and gene level analyses suggest that young WM OLs are producing more synapse-related machinery than older OLs.

3.II. Integrating my WM OLs with the GM OLs identified in the SEA-AD project

The finding of WM OLs producing synaptic transcripts led to the question of whether GM OLs are doing something similar. As mentioned in the introduction, the function of GM OLs is largely unknown. However, with the Allen Institute’s SEA-AD cohort, I was able to directly compare my WM OLs to GM OLs to understand how GM OLs differ from these WM OLs. To do this, I first isolated the OLs from the SEA-AD

dataset using their cell type information in their metadata. There were four different subtypes of OLs identified in the SEA-AD dataset on dorsolateral prefrontal cortex (hereby called GM OLs for simplicity), and all four were isolated and merged into a single GM OL cohort for my analyses. Similarly, the WM OLs were treated as one single cohort to assess general functional differences between GM and WM OLs. After combining the WM and GM OLs, I performed the data integration pipeline established for my WM OL dataset. This was necessary to properly align the two datasets, and to ensure comparisons were compatible between the two similar but unique datasets.

Before explaining findings, it is important to understand how these two datasets were similar and different. The SEA-AD project included 90 donors above the age of 70, stratified by whether they had a clinical diagnosis of AD or not. 18 of these cases were shared between my WM cohort and SEA-AD. While this resulted in a similar cohort grouping to mine, they did not stratify by AD pathology metrics like my WM cohort. For analyses where no/low and high AD pathology are assessed, I exclude moderate ADNC stage cases from analysis, aligning their cohort with mine to directly compare. However, for analyses where I assessed WM versus GM cells in general, I include these moderate ADNC stage donors, as removal of them did not alter the results. Further, the inclusion of these donors increased the total number of cells being assessed which is generally beneficial in these analyses. The other key difference between SEA-AD and my WM cohort is the sequencing depth and cell capture for each individual run. While my target cell capture was 8,000 cells at 40,000 reads/cell, the SEA-AD targeted 10,000 cells at 120,000 reads/cell. This increased depth resulted in capture and inclusion of rarer transcripts and more genes captured overall than my WM dataset. However, both

my WM and SEA-AD metrics are above the 10x Genomics-provided minimum parameters. Further, normalization, scaling, and integration will aid in accounting for these differences, ensuring the datasets are compatible.

3.III. GM OLs show significant upregulation of synaptic transcripts compared to WM OLs

After integrating the WM and GM OLs together, I ran DE and GSEA analyses comparing WM OLs to GM OLs. As suspected, the GM OLs show significant enrichment of synaptic pathways (Figure 9E). The GSEA results were reinforced on the individual gene level, with GM OLs showing 1-2 fold higher expression of various genes involved in neurotransmission and synapse structure (Figure 9F). Again, these genes were downregulated in WM OLs, but not entirely absent. Considering the GM OLs are between 5-10 orders of magnitude more significant than young WM OLs (compare Figure 9E to 9B) when compared against the same old WM OLs, the old GM OLs show further upregulation of these genes than young WM OLs. Finally, I compared high ADNC stage donors to no/low ADNC stage donors in this GM cohort to see whether AD pathology modulated these pathways. I found that the no/low ADNC GM OLs showed significant enrichment of synaptic pathways relative to high ADNC GM OLs (Figure 9D).

Now that I have seen upregulation in synapse machinery in both my young WM OLs and old GM OLs, I wanted to confirm this by a second modality. This was an ideal application of the CosMx dataset, which provides similar RNA-based transcriptomic data but relies on an entirely separate method of data collection, providing mutually-supportive datasets. I conducted DE and GSEA on WM and GM OLs isolated from

CosMx and found similar trends to the snRNAseq. data. Specifically, I found that GM OLs expressed more synapse-related transcripts than WM OLs (Figure 9I). When I compared the three individual clusters of OLs identified in the CosMx dataset (of which OL3 was more represented in GM), I found that OL3 showed upregulation of synapse-related genes (Figure 9G). Finally, GSEA supports this, with OL3 showing significant enrichment for various synaptic pathways (Figure 9H). Recall that the FOV images in Figure 8 highlight synaptic machinery being more prevalent in GM OLs relative to WM OLs as well.

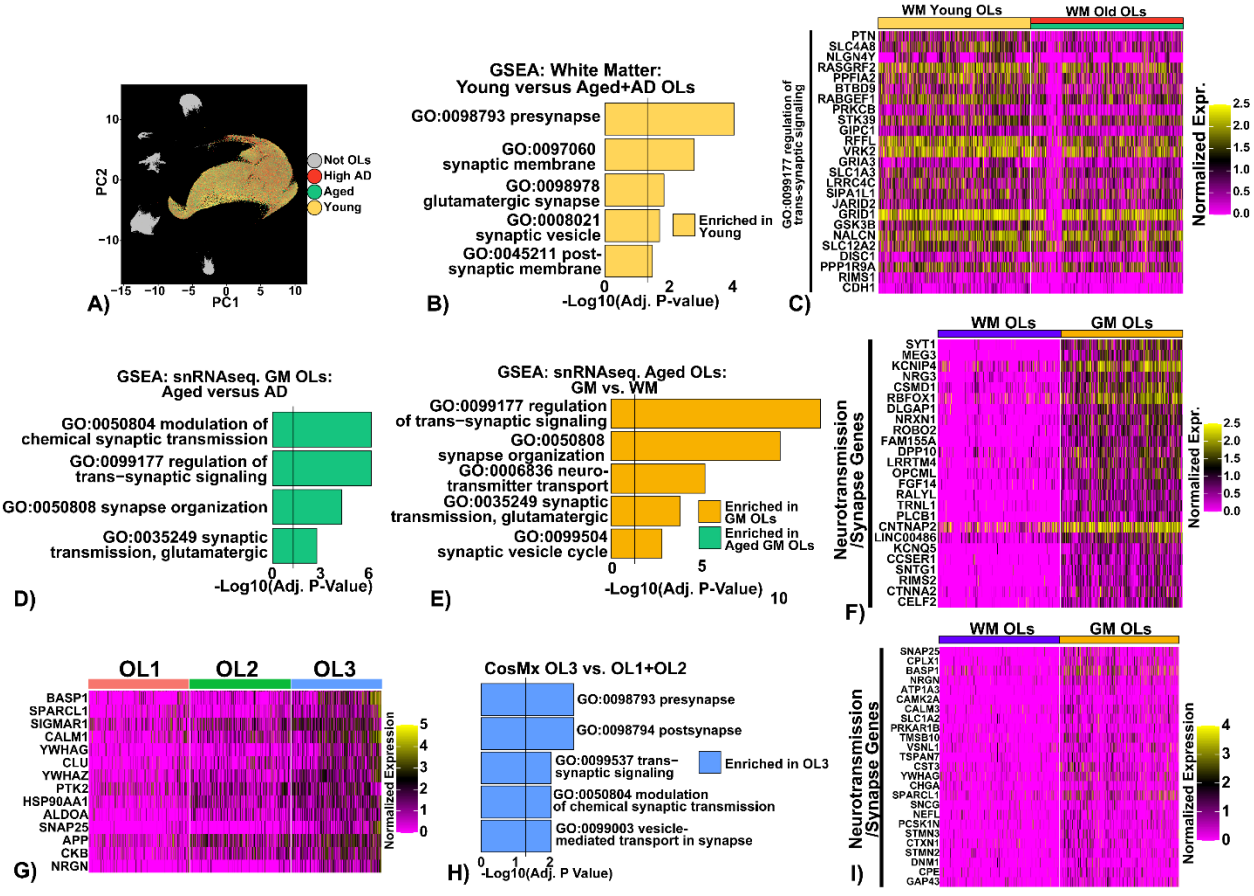

Figure 9. GM OLs show significant enrichment of synapse and neurotransmission-related transcripts. 9A) WM OLs are highlighted on the UMAP of

the WM dataset. **9B)** Young WM OLs show significant enrichment of synaptic pathways in GSEA analyses relative to old WM OLs (both aged and high AD OLs). **9C)** Young WM OLs show upregulation of transcripts included in “GO:0099177 regulation of trans-synaptic signaling” relative to old WM OLs. **9D)** Within old GM OLs, there was significant enrichment for synaptic pathways in no/low ADNC relative to high ADNC stage donors in snRNAseq. **9E)** Old GM OLs show significant enrichment of synaptic pathways relative to old WM OLs in snRNAseq. **9F)** GM OLs show upregulation of individual genes involved in neurotransmission and synapse function (right half of heatmap) relative to WM OLs (left half of heatmap). **9G)** When assessing synapse gene expression in CosMx, OL3 shows the most expression of these transcripts compared to the other clusters. **9H)** GSEA analysis supports the expression pattern in 9G, finding significant enrichment of synapse machinery in OL3 relative to OL1 and OL2. **9I)** When stratifying by WM or GM OL tissue of origin, GM OLs show upregulation of synapse-related transcripts relative to WM OLs, similar to snRNAseq. (figure 9I versus 9F). Heatmap data is colored by normalized expression values of each gene, with each vertical column representing the expression within a single cell. GSEA results are reported as $-Log_{10}$(adjusted p-values) following Benjamini-Hochberg correction. Vertical lines in GSEA plots represent an adjusted p-value of *q=0.05*.

3.IV. Both WM and GM OLs express myelin transcripts

Since the primary role of the OL is to myelinate, I assessed the expression of myelin transcripts in my WM and GM datasets to determine whether GM OLs express similar levels to WM OLs. With WM having more myelin content, I expected the myelin transcript levels to be increased in WM OLs relative to GM OLs. However, the only myelin-related significant GSEA enrichment in WM OLs was involving autophagy pathways and “glial cell development” (Figure 10B). When I assessed key genes involved with myelin (e.g. *MBP, MAG, MOG, MOBP, PLP1, APLP1*), these genes were similarly expressed in WM and GM OLs (Figure 10C).

In my CosMx data, I assessed both the three OL clusters (colored in Figure 10D and 10G), as well as WM versus GM OLs. While OL1 showed the lowest myelin/OL gene expression, OL2 showed the highest and OL3 was in-between (Figure 10E). This finding of OL2 expressing the most myelin was supported in GSEA, where OL2 showed significant enrichment for myelination and autophagy pathways (green bars, Figure 10H) relative to the other two clusters. OL1 showed significant depletion of these same pathways (salmon bars, Figure 10H). This suggests there may be multiple general phenotypes/subtypes of OLs. Notably, OL1 and OL2 were the primary WM clusters, with only a minor contribution of WM to OL3 (Figure 10G). Finally, when I assessed myelin genes in the CosMx data after stratifying for WM or GM region, I see a modest upregulation of myelin genes in WM OLs. However, there was noticeable variation between WM OLs, supporting the notion of multiple subtypes.

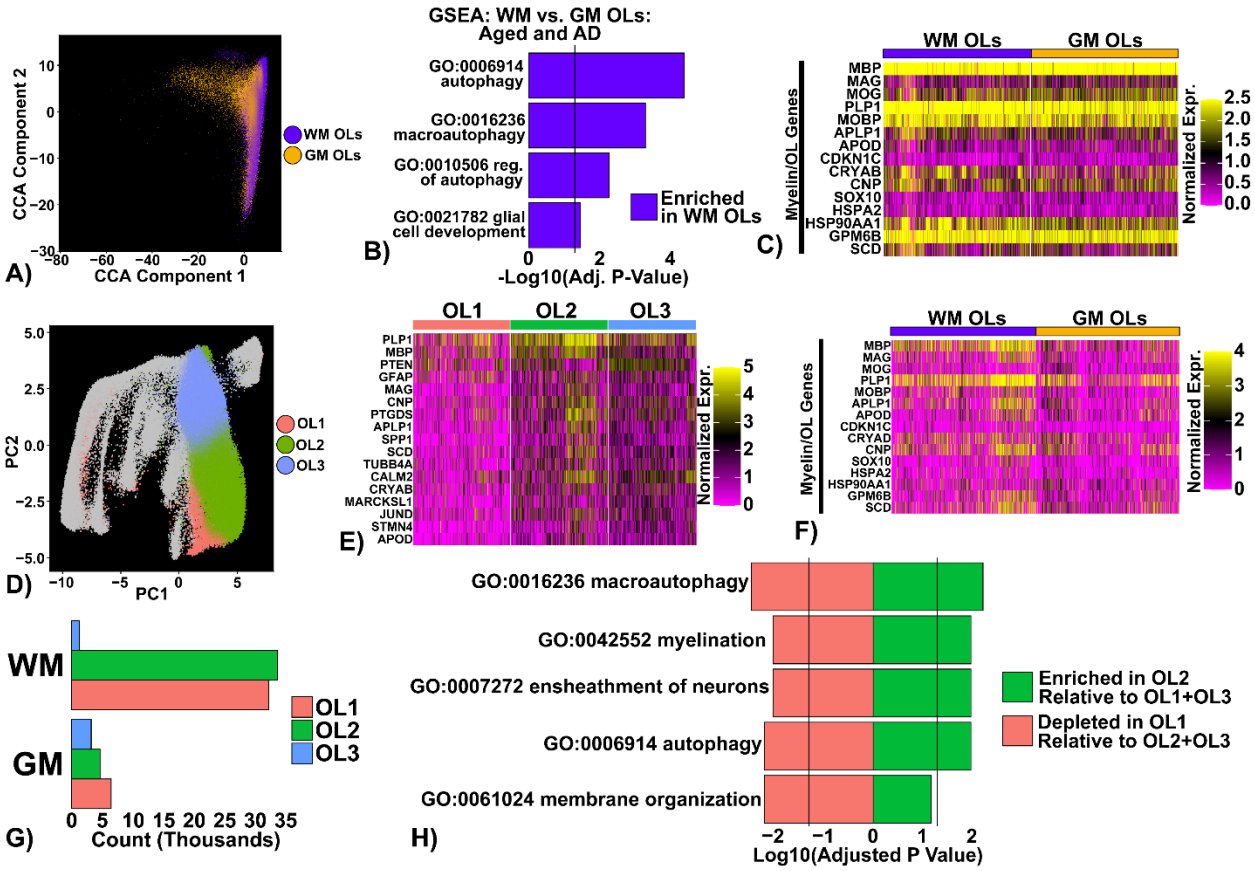

Figure 10. Myelin-related expression is similar between WM and GM OLs. 10A) UMAP following CCA-integration of old WM and GM OLs. **10B)** GSEA reveals significant enrichment of autophagy pathways in WM OLs relative to GM OLs. **10C)** Heatmap showing expression of individual genes involved with myelination or OL identity. **10D)** UMAP of CosMx dataset with OL clusters OL1, OL2, and OL3 identified. **10E)** Expression of myelin and OL genes in OL1-OL3. **10F)** Expression of myelin genes in WM and GM OLs in CosMx. **10G)** Distribution of OL1, OL2, and OL3 by tissue of origin. **10H)** GSEA reveals OL2 is significantly enriched for myelination and autophagy pathways, while OL1 is significantly depleted in these same pathways. Heatmap data is colored by normalized expression values of each gene, with each vertical column representing the expression within a single cell. GSEA results are reported as -Log_{10}(adjusted p-values) following Benjamini-Hochberg correction. Vertical lines in GSEA plots represent an adjusted p-value of *q=0.05*.

3.V. Human OLs contribute to both the innate and adaptive immune system

While I have identified what WM OLs in the young cohort are preferentially expressing relative to old WM OLs (see Figure 9B), I had yet to determine what these old WM OLs are uniquely expressing. Compared to young OLs, the aged and high AD OLs are significantly enriched for MHC complex expression, as well as cytokine activity (Figure 11B). When assessing genes included in the “GO:0034097 response to cytokine” pathway, I see that old OLs from WM show increased expression of at least a subset of these transcripts (right half, Figure 11C). Note, within the old WM OLs there is variability, with some cells showing upregulation and others showing little to no expression of these genes.

When I compared the snRNAseq. of WM and GM OLs, I found that WM OLs show significant enrichment for pathways involving antigen processing and presentation and cytokine production (typically adaptive immunity processes) and innate immune response relative to GM OLs (Figure 11E). Next, I considered whether AD pathology could explain some of this significance by stratifying my CosMx dataset by high ADNC stage and no/low ADNC stage. When I did this, I found significant enrichment for immune related pathways in both GM and WM in the high ADNC stage donors (Figure 11F, 11G). However, high ADNC stage WM OLs showed more significant enrichment than GM OLs, providing support for the previous finding of WM OLs showing GSEA enrichment of immune pathways relative to GM OLs in snRNAseq. Further, the pathways enriched in the high ADNC donor OLs were largely centered on cytokine and chemokine activity, rather than innate immunity.

To complete my analysis of the OL clusters identified in CosMx, I assessed whether any immune pathways were enriched via GSEA. I found significant enrichment of adaptive immune pathways in OL1 relative to OL2/3, both involving cytokine activity and adaptive immunity in general (Figure 11J). When I assessed OL2, I found significant depletion of nearly the same pathways (Figure 11K). Combining this information with the information presented in Figure 10H, I find that OL1 is enriched for immune pathways and depleted for myelination pathways, while OL2 is the opposite. Finally, OL3 is primarily enriched for synaptic mechanisms (Figure 9H).

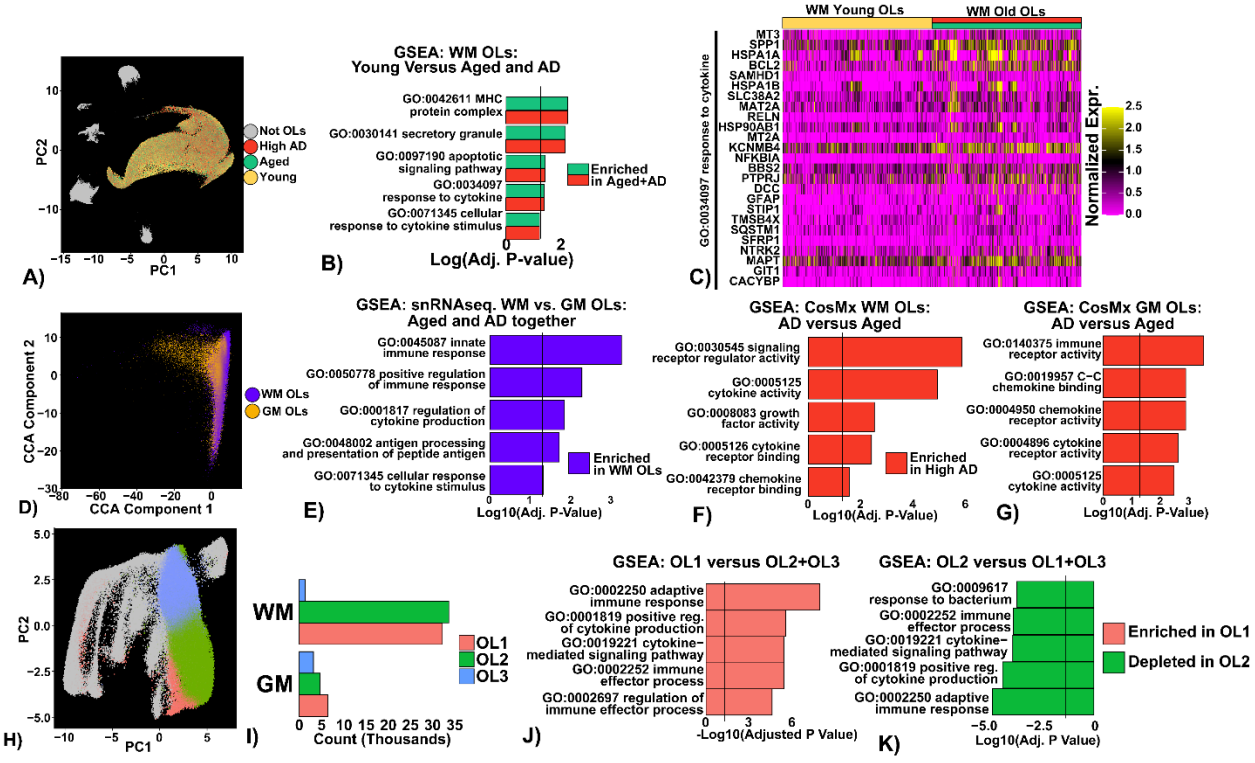

Figure 11. Human OLs are involved in immune processes, especially in the aged and AD brain. 11A) UMAP showing OLs colored by donor group. **11B)** GSEA reveals aged and AD OLs show significant enrichment of MHC complexes and cytokine activity relative to young OLs in WM. **11C)** Individual cell expression of genes included in the gene ontology pathway “GO:0035097 response to cytokine) are upregulated in a portion of the aged+AD WM OLs. **11D)** UMAP following integration of WM and GM OLs in

snRNAseq. **11E)** WM OLs show significant enrichment of innate and adaptive immunity processes compared to GM OLs in snRNAseq. **11F-G)** Following stratification of CosMx OLs by WM or GM origin, GSEA reveals that high ADNC donor OLs show enrichment for cytokine and chemokine pathways relative to no/low ADNC donor OLs in both WM **(11F)** and GM **(11G)**. **11H)** UMAP highlighting the three OL clusters identified in the CosMx dataset. **11I)** Distribution of these OL clusters by tissue of origin. **11J)** CosMx cluster OL1 shows significant enrichment for pathways involving adaptive immunity and cytokine activity. **11K)** CosMx OL2 shows depletion of immune pathways involving cytokines and the adaptive immune response. Heatmap data is colored by normalized expression values of each gene, with each vertical column representing the expression within a single cell. GSEA results are reported as $-Log_{10}$(adjusted p-values) following Benjamini-Hochberg correction. Vertical lines in GSEA plots represent an adjusted p-value of $q=0.05$.

3.VI. High AD pathology WM OLs express certain chaperone and heat shock proteins

Now that the snRNAseq. and spatial transcriptomic datasets have been characterized in general, individual targeted analyses can be conducted to identify how high AD pathology is contributing to altered cell transcription. The main analyses were to compare the high AD and low AD groups, specifically studying how the OL population changes in both my WM and the SEA-AD's GM OLs. The most prominent and significant enrichment on both the gene and pathway level were centered on the unfolded protein response (UPR) and chaperone proteins. The UPR has been identified as a component of cellular senescence in other cell types, and is more generally indicative of cellular stress, particularly manifesting as ER stress and misfolded proteins[143]. The ER UPR involves three main pathways, the IRE1, ATF6, and PERK pathways, which are typically activated together[144]. Activation of the ER UPR is

challenging to detect in classic transcriptomic data, as it largely relies on post-translational modifications and alternative splicing variants to activate, aspects that are largely undetected[144]. However, beyond the ER and UPR, there are cytoplasmic chaperone proteins that are expressed as well, especially in the context of pathological protein aggregation[145]. While every HSP and chaperone was assessed (both UPR and cytoplasmic), the shortlist in figure 12A and 12B were the ones showing significant enrichment in the high AD WM OLs. Although these genes were not exclusively expressed in high AD WM OLs, they were enriched relative to the other groups, including the GM from the high AD donors. The most differentially expressed genes are displayed in 12C in violin plots, highlighting these genes are especially enriched in the high AD WM OLs relative to other groups. The chaperones we found elevated were largely from the HSP70[146] and HSP90[147] groups, which are cytoplasmic chaperone proteins rather than ER UPR. Further, we did not see elevation in key components of the ER UPR, including ATF6, IRE1, etc. Beyond the chaperone proteins, we found elevation in ferritin heavy and light chain (FTH1 and FTL), transcripts that comprise the ferritin complex. Enrichment of the ferritin complex in the high AD WM suggests the OLs are storing more iron, although this has not been confirmed in our cases using cytochemistry. Since iron is a key cofactor in lipid synthesis, this could imply that these OLs are making more lipid or responding to a parenchymal iron overload in general, as OLs are the primary storage site of iron. However, in the context of a concurrent elevation of the cytoplasmic chaperones, elevated ferritin may signal elevated ROS and protein aggregation within the OL, a potential mechanism for how OLs and WM are reduced in AD. Beyond the gene level, GSEA identified that protein folding, UPR, and

particularly HSP binding were enriched in WM OLs from high AD pathology WM, relative to age-matched low AD pathology (figure 12D) and young WM OLs (figure 12E). While similar trends were found when comparing GM OLs from high and low AD pathology OLs (figure 12F), the HSP binding was no longer significantly enriched. Recall that GO pathways are curated to encompass specific functionalities, aspects, or components of cells. However, these pathways are typically developed to represent specific processes, sometimes only considering the cell type the curators study when compiling the pathway. Thus, when addressing OLs and other understudied cell types, these pathways can provide useful pointers but should be corroborated with individual genes known to be important in the pathways being assessed. This ensures that the flagged pathway enrichment is in fact enriched. In the case of these chaperone proteins, it seems the enriched pathways are indicative of proteostatic flux and misfolded proteins in the cytoplasm, rather than the ER UPR. Since these pathways both involve unfolded proteins, it is likely the pathway included cytoplasmic chaperones as well (in fact, cytoplasmic chaperones can aid in localizing misfolded proteins to the ER[147]).

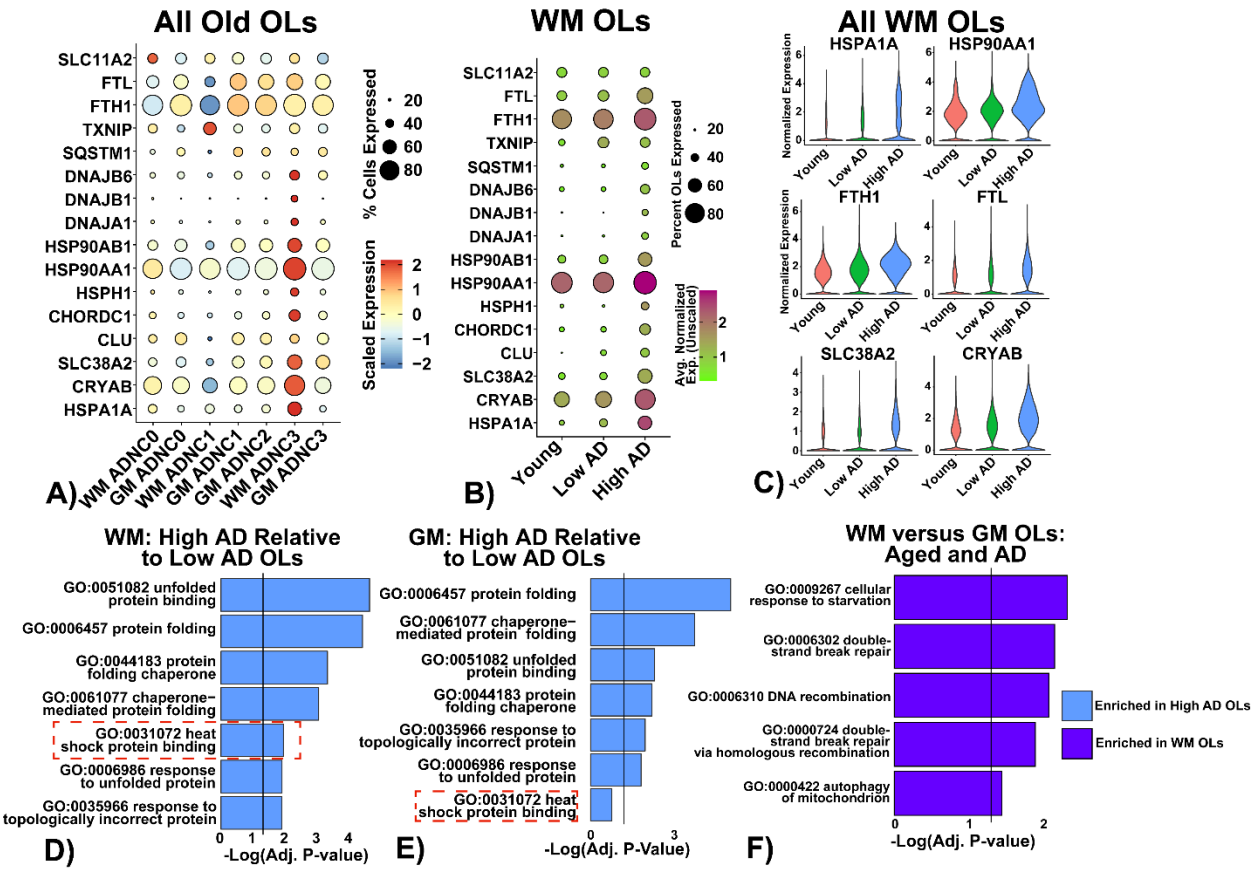

Figure 12. AD OLs show elevated chaperone proteins in both WM and GM relative to age-matched controls. 12A) Dot plot showing expression of key chaperone and heat shock protein transcripts in WM high AD OLs. OLs were stratified by GM or WM origin, then by ADNC rank (0=None, 1=Low, 2=Intermediate, 3=High AD pathology). Circle size indicates percentage of that cluster expressing each gene while color represents relative expression to all other groups. WM ADNC=3 OLs show elevated expression of most of these heat shock proteins. **12B)** Dot plot showing same HSPs across young, low AD old, and high AD old OLs. While young and low AD OLs show similar expression levels of these chaperone proteins, more high AD OLs express these transcripts and at higher levels. **12C)** Violin plots of six of the most elevated transcripts in high AD OLs. All violin plots are showing only WM OLs stratified by young, low AD, and high AD groups. **12D-E)** GO pathway enrichment in high AD WM OLs relative to young WM OLs **(12D)** and low AD WM OLs **(12E).** Both 12D/12E show significant enrichment of unfolded protein response and heat shock protein pathways in high AD WM OLs relative to young and low AD WM OLs. **12F)** GO pathway enrichment in high

AD GM OLs (ADNC=3) versus low AD GM OLs (ADNC=0-1). ADNC=2 GM OLs were excluded from this analysis. While high AD GM OLs show significant enrichment of the same unfolded protein response pathways as high AD WM OLs (blue bars), they do not show significant enrichment of heat shock proteins specifically (red dashed box), hinting at distinct un-/mis-folded protein responses in WM versus GM OLs. GSEA results are reported as $-Log_{10}$(adjusted p-values) following Benjamini-Hochberg correction. Vertical lines in GSEA plots represent an adjusted p-value of *q=0.05*.

3.VII. OPC expression in both CosMx and snRNAseq. supports elevated synaptic functioning of GM OPCs

Since my datasets contain all cell types present in GM and WM, I was able to isolate OPCs from these datasets and run similar analyses to identify unique functions of both GM and WM OPCs. Like the GM OLs, the GM OPCs show elevated gene expression for synapse machinery relative to WM OPCs (bottom half of Figure 13D and 12H). This trend was maintained at the pathway level with GSEA, where both pre- and post-synapse as well as synaptic vesicle cycling was enriched (Figure 13C and 13G). While there were no significant GSEA enrichments in the CosMx data for WM OPCs (Figure 13C) (likely due to a relatively low number of OPCs captured), there was significant enrichment of myelination and glial cell development in snRNAseq. WM OPCs are likely to form more myelin when terminally differentiated, and the snRNAseq. data supports that these WM OPCs are in the process of transcribing the necessary components (Figure 13H, top half), while the GM OPCs are not. It is interesting that the CosMx OPCs do not show as much contrast on myelination/OL gene expression as the snRNAseq., but this may be a result of the low number of OPCs captured in CosMx and

the 6,000 probes not covering the myelination processes as well as the unbiased snRNAseq.

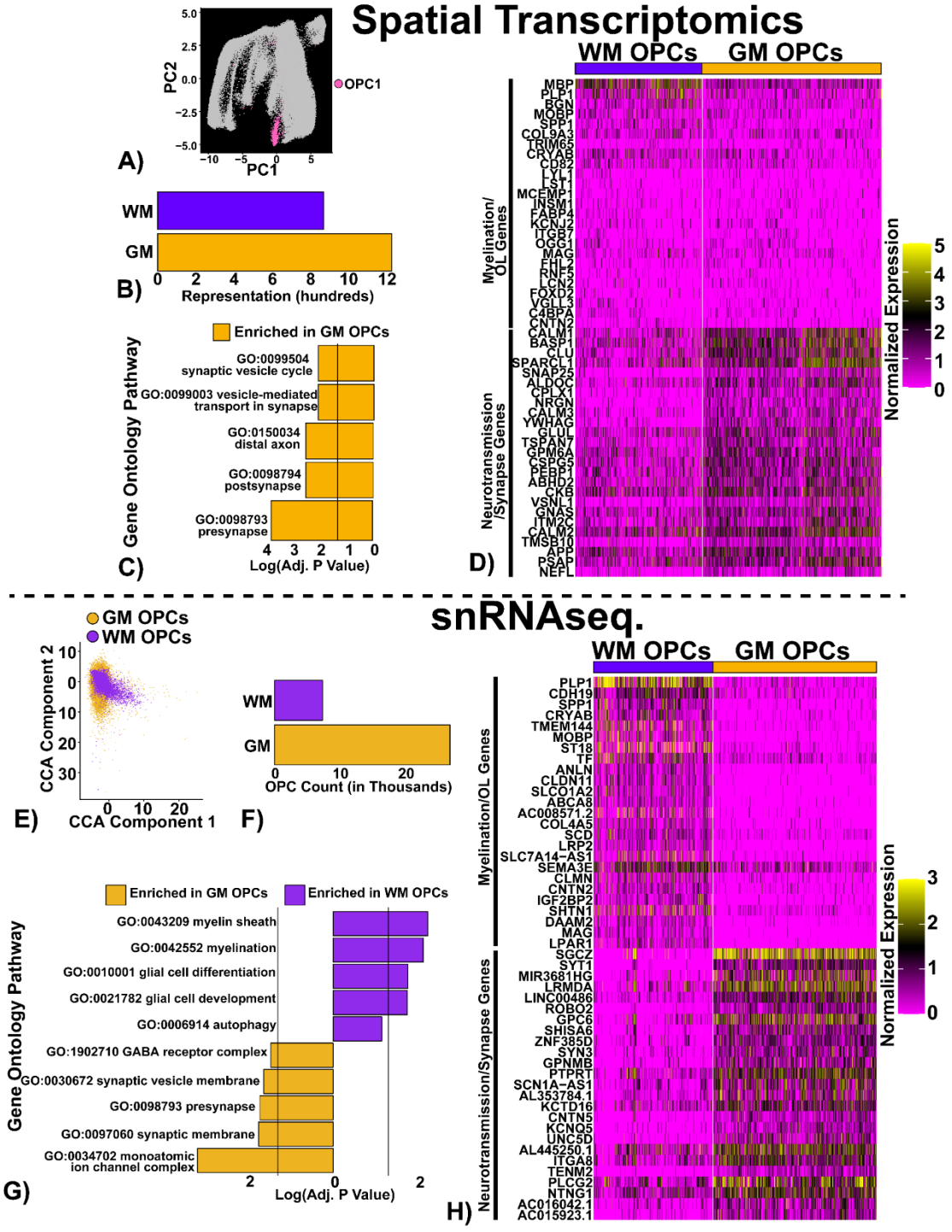

Figure 13. CosMx identifies unique synaptic functions in human GM OPCs, similar to GM OLs. 13A) OPCs highlighted on the spatial transcriptomic UMAP in pink.

13B) Distribution of OPCs between WM and GM. **13C)** GSEA analysis results with the most significant GM OPC enrichment in pre- and post-synapse and synaptic vesicle cycling. There were no significant WM OPC pathways enriched relative to GM OPCs. **13D)** Heatmap of the 25 most up-regulated WM OPC genes (top half) and GM OPC genes (bottom half). Although both GM and WM OPCs expressed synapse- and neurotransmitter-related genes, GM OPCs displayed elevated and more widespread expression than WM OPCs. **13E)** UMAP following CCA integration of all old WM and GM OPCs. **13F)** OPC count by GM or WM donor origin. **13G)** GO pathway enrichment between WM and GM OPCs. WM OPCs show elevated myelination and glial cell differentiation enrichment (purple bars) while GM OPCs show elevated synaptic and ion channel pathways (golden bars). **13H)** Heatmap showing some of the most significant differentially expressed genes in WM OPCs (top half) and GM OPCs (bottom half). WM OPC genes tend to represent key myelination genes (i.e. *PLP1, MOBP, MAG*) or lipid metabolism (i.e. *SCD, LRP2*), while GM OPC upregulated genes were synaptic (i.e. *SYT1, CNTN5, ROBO2*). GSEA results are reported as $-\text{Log}_{10}$(adjusted p-values) following Benjamini-Hochberg correction. Vertical lines in GSEA plots represent an adjusted p-value of $q=0.05$.

Chapter 4: Discussion

4.I. Brief summary of cell culture experiments and creation of transcriptomics datasets

In this thesis, I began with the hypothesis that OLs and their precursors (OPCs) could become senescent, and that this senescence partially explains the WM atrophy seen in aging and AD. To this end, I was able to produce OPCs and ultimately OLs from human iPSCs. Their identity was confirmed with both qPCR (molecularly) and their ability to form loose myelin on poly-lactide nanofibers (functionally). Next, I developed a method to induce senescence reliably in human meningeal fibroblast primary cultures using both etoposide and hydrogen peroxide, two of the most used methods of senescence induction. The accumulation of beta-galactosidase, a proxy for lysosomal accumulation and a commonly used metric for whether a cell is senescent, was employed to characterize the dose-response curve for these meningeal fibroblasts. However, when I employed this senescence assay on my hiPSC-OPCs, they showed no evidence of beta-galactosidase accumulation, regardless of dose. Rather, these hiPSC-OPCs simply died at a certain concentration with no concurrent beta-galactosidase accumulation. Because senescence in human OPCs/OLs has not been documented conclusively, it was unclear which aspects of this experiment were inadequate for detecting OPC/OL senescence, and I decided to address this question using a different approach.

This different approach was to use transcriptomic methods to identify unique changes in the OL and OPC populations as a result of age and AD status. To that end, I developed a novel single nucleus RNA sequencing dataset on exclusively post-mortem

WM, including age-matched high and low AD pathology donors and a young control group. This is the largest and most robust single cell dataset on human WM to date. To bolster this dataset, I successfully leveraged the Allen Institute's SEA-AD dataset published in 2024 to compare GM OLs and OPCs to WM OLs and OPCs. The combination of these two datasets was ideal as SEA-AD used brain tissues from the same brain repository and similar inclusion and exclusion criteria (18 cases were included in both studies). To further bolster these comparisons and datasets, I generated an RNA-based spatial transcriptomic dataset on 6 of the 18 cases included in both my WM dataset and the SEA-AD, including both WM and GM from as close to the snRNAseq. regions assessed as possible. In addition to providing the spatial component and collaborating evidence, this method included WM and GM from the same donors on the same slide, providing external validation that the methods employed to merge WM and GM OLs in snRNAseq. did not introduce technical artifacts. Because WM was primarily composed of OLs, I narrowed my analyses specifically to OLs and OPCs after initial identification of various cell types in each dataset.

4.II. OLs and synapse functions

My analyses revealed that OLs express a variety of transcripts indicating functions beyond myelination, their canonical function. I found that young WM OLs express more synapse and neurotransmitter cycling transcripts than old WM OLs. It is unclear whether these OLs are forming functional synapses, where/which cell type these synapses are forming with, and which direction the synapses are "firing". There was significant enrichment in glutamatergic synapses on GSEA (figure 9B), which suggests glutamatergic synapses may comprise at least a portion of these. The

literature on OLs forming synapses is sparse, but there are studies suggesting that OLs express synapse machinery (particularly ion channels) to detect neural activity and modulate myelin thickness accordingly[148,149]. Whether these OLs are forming fully functional synapses, or simply expressing voltage gated ion channels (potassium channels like Kir4.1 have been specifically identified in OLs[150]) or neurotransmitter receptors to detect neural activity is unclear. Since GSEA uses full pathways and is solely-correlation based, further studies are needed to detect whether OLs are forming functional synapses and what types.

While young WM OLs are expressing more synapse machinery than old WM OLs, I found further evidence of OLs contributing to synapse function in the old GM OLs, which showed even higher levels of these transcripts relative to WM OLs. This was supported by both snRNAseq. and CosMx, with clear upregulation at both the gene and pathway levels (Figure 9). Considering GM contains less myelin than WM, it is plausible that GM OLs modulate their functionality to better support the GM environment. The current evidence on OLs expressing synapse machinery and ion channels to sense neural activity supports this[149,150]. More neurons and neural activity will provoke the OL to produce more of the sensory components necessary to accurately detect the activity of these neurons as well as support them. Interestingly, GM myelination is more variable than in WM[118]. While WM myelination tends to be full concentric wrappings of myelin that tightly compact to form roughly identical wrappings, GM myelination is highly variable. This GM myelination can take the form of small myelin patches seemingly set on one side of an axon, single wraps, multiple loose wraps, a WM-like wrapping with a large unmyelinated gap, amongst other configurations[118]. This high variability may

necessitate more sensory components to accurately detect the neural activity and internalize enough information to properly myelinate these connections. So far, there is little evidence to suggest GM myelination serves any additional role beyond its roles in WM (i.e. insulation, trophic support, sensory input of neural activity).

Studies performing electrophysiology on rodent iPSC-derived OPCs that were then pushed to differentiated OLs show that OPCs express high levels of voltage-gated sodium channels sensitive to tetrodotoxin, but as these OPCs differentiate into OLs they reduce these channels to a point of being entirely unresponsive to tetrodotoxin by 3 weeks post-differentiation[151]. Further, OPCs show a “spiking” behavior that is distinct from neuronal action potentials, with a lower magnitude not crossing the 0mV threshold. In addition, OPCs also expressed both outward-rectifying and A-type potassium channels that were substantially reduced (but notably not entirely ablated) by 3 weeks post-differentiation[151]. In contrast, the inward-rectifying Kir channel expression (especially Kir4.1[150]) substantially increases in the fully-differentiated OL[151]. Together, this suggests that OPCs may use a similar ion shifting paradigm to an action potential to initiate differentiation and myelination, shifting towards inward-rectifying potassium channels to detect extra-cellular potassium as a proxy for neural activity to modulate myelination in the fully differentiated OL. Similar to my OL data, I found that OPCs from GM express more synapse-related transcripts than WM OPCs (Figure 13). Specifically, I found that “monoatomic ion channels” were the most significant GSEA pathway in GM OPCs, supporting the evidence that OPCs rely on these sodium and potassium channels.

A peculiar finding was that within the old GM OLs, I found a decrease in the synaptic machinery from high AD pathology donors compared with no/low AD pathology. This suggests AD pathology may be causing these GM OLs to decrease their sensitivity to these signals, or these OLs are losing this ability to detect neural activity somehow. It is unclear exactly how this depletion is occurring, but it is worth further study. A theoretical hypothesis is that the OL senses hyperexcitability in the neurons it interacts with, which causes it to downregulate its myelin production and trophic support while stimulating the neuron/axon to make more energy (recall the SIRT2-mediated mitochondrial stimulation from the OL to the axon[22]). This combination of reducing myelin-based insulation while also upregulating the axon's metabolic burden could intensify the stress on the already overburdened cell, resulting in cell death. In fact, new studies are suggesting that neuron death in AD may be partially through necroptosis and MEG3 (a long non-coding RNA) in particular[152]. Necroptosis has been associated with glutamate-induced hyperexcitability[153], adding some credence to this idea. I also saw MEG3 present in most GM OLs but few WM OLs (Figure 9F, second gene from top). The old WM OLs seem to express the lowest amounts of synapse-related machinery, possibly a result of myelin being thick and compacted in most cases. This means the OL would likely need sensing channels (like Kir4.1) in less places. However, WM OLs still likely express them considering myelination is not static but ever changing along with neural activity[154].

4.III. OLs and myelination

Next, I showed that both GM and WM OLs express transcripts involved in myelination, as expected (Figure 10). However, the expression levels were largely

comparable between WM and GM, while overall myelin content is far higher in WM. Since WM OLs make more myelin, it was expected these OLs would show relatively more myelin-related transcripts than GM OLs. However, this was not the case, suggesting that both WM and GM OLs require certain levels of myelination machinery to effectively create myelin, regardless of how much myelin is ultimately made. In retrospect, this is not surprising considering myelination is a primary function of the OL, and without myelination pathways it is unlikely a cell would even be identified as an OL versus some other cell type.

An interesting observation in my CosMx data was three unique OL clusters, one of which had significant enrichment for myelination and autophagy pathways, and another that was significantly depleted in these same pathways. Because these two clusters contained OLs from both WM and GM, it is unlikely (although not impossible) that these differences are simply a result of different representation between WM and GM in each group. It seems that these three groups may highlight the three main functions I have identified in OLs, synapse-related, myelination, and immune-related functions.

4.IV. OLs and the immune system

Within my OL populations, I consistently found significant GSEA hits for immune related processes, particularly adaptive immunity functions. I found consistent evidence that OLs from old donors, especially in the context of high AD pathology, expressed elevated levels of transcripts implicated in cyto-/chemokine production and antigen processing and presentation, including MHC complexes themselves. These findings were present in both GM and WM, and consistent across the datasets (Figure 11). Of

note, within WM OLs, the old OLs (AD + aged combined) showed considerable variability in expression of these immune transcripts, with some cells showing 2.5-fold higher levels of expression than other OLs from the same group. This suggests there may be further subpopulations/phenotypes of OLs within these groups.

As the human body ages, there is a commensurate pro-inflammatory shift that occurs[155]. The brain is not exempt from this pro-inflammatory shift[155]. In fact, in the context of AD, there is even further evidence of the CNS parenchyma becoming more inflammatory to the point where this is being coined the “third aspect” of AD pathophysiology along with amyloid plaques and hyperphosphorylated Tau tangles[156]. My evidence, while supporting these concepts, also extends them to include OLs as participants in the overall immune state. There is some literature on OPCs producing MHCs and processing antigen that directly activates T-cells[114], but this literature did not comment on OLs. I show that OLs themselves are directly producing these transcripts, which is a strong indication that they may be ultimately presenting antigen as well. Beyond direct MHC production, GSEA pathways involving the cytokine response were significantly enriched in high AD OLs, suggesting the pro-inflammatory milieu is directly affecting OLs as well. While the OPC has been documented to secrete cytokines[113] and respond to both pro- and anti-inflammatory signals[115,116], my evidence shows that myelinating OLs may do this as well. Future studies to address how OLs detect cytokines and how they respond will be necessary to understand exactly how these cells incorporate into the immune response, particularly in the context of AD.

As mentioned above, I identified three OL clusters in my CosMx data, in particular a cluster that was enriched for myelination/autophagy pathways and another

that was depleted for these same pathways. Interestingly, this cluster (OL1, Figure 11J) depleted for myelination pathways was enriched for immune-related processes, particularly cytokine and chemokine activity, while the myelination-enriched cluster was significantly depleted for similar immune pathways (OL2, Figure 11K). At present, there are multiple ways to interpret these findings. One option is that these groupings represent an immune-OL phenotype and a canonical/myelinating-OL phenotype, essentially two subclusters of OLs. Another is that this is more of a context-dependent finding where OLs that are detecting elevated levels of cytokines modulate their cytokine response in an attempt to remain equilibrium (akin to a feedback loop), and that this cytokine response alters myelination accordingly. Whether increased cytokine detection results in more or less receptor activity is unclear, as is whether this activity alters myelination. Regardless, my evidence suggests that OLs are at minimum sensitive to cytokines. Future studies to understand which cytokines OLs respond to, and what these responses are, will help elucidate exactly how the pro-inflammatory environment augments OL function.

4.V. OLs, AD pathology, and cytoplasmic chaperone protein elevation

A primary finding in my high versus no/low ADNC analyses were elevations of specific cytoplasmic chaperone proteins that are involved in processing aggregated proteins[157]. Typically, proteins have a specific conformation they need to both obtain and maintain to properly function. Chaperone proteins, of which the heat shock protein family is the largest, are crucial for proper protein folding[145]. Chaperones commonly use the free energy produced from the hydrolysis of ATP to ADP to undergo conformational shifts, pushing a protein from a less to more folded state[145]. Said differently, chaperone

proteins are proteins that change their conformation themselves to facilitate the folding of other proteins. However, chaperones also serve roles beyond initial folding, including identification of misfolded or newly unfolded proteins and disaggregation of misfolded and aggregated proteins[145,157,158]. There are a multitude of ways proteins can become misfolded, with some of the most common methods being incorrect translation during initial peptide formation, abnormal post-translational protein modifications, and oxidative or thermal stress (this is where the name heat shock protein originated)[145]. While translation errors are possible in all cell types, abnormal protein modifications (e.g. phosphorylation) and oxidative stress require further discussion, especially in the context of AD.

AD is characterized by two pathological proteins that form aggregates, amyloid-beta and tau. Amyloid-beta forms aggregates from cleavage of amyloid precursor protein, producing a fragment that is prone to aggregate and resist degradation. There is evidence that over-expression of HSPs can reduce amyloid-beta accumulation in mouse models of AD[159]. Further, HSPs can directly inhibit amyloid-beta 1-42 aggregation *in vitro*, but only prior to fibril formation[159]. Once fibrils are formed, HSPs show little effect on Abeta aggregation[159]. There is evidence in humans with AD that HSP expression increases, and in particular HSP90s can directly associate with APP and regulate its production and processing[158]. Further, isoforms of HSP70s and HSP90s are proven to reduce amyloid production and aggregate initiation[158]. However, not all functions of HSPs are beneficial, and there is evidence that heat shock factor 1 (HSF1) directs HSP production in response to oxidative stress, but that HSF1 induces both more APP production and release of Abeta from fibrils, processes that result in more

free or oligomeric amyloid species in the cell[158]. The oligomeric form of amyloid-beta is thought to be the most toxic, and thus this combination of more APP and release of oligomeric amyloid from plaques can be directly cytotoxic[59].

The other protein aggregation characteristic of AD are neurofibrillary tangles primarily composed of tau in a hyper-phosphorylated form. Tau is an inherently unfolded protein with only a somewhat consistent conformational region at its microtubule binding domain, which interacts with and stabilizes microtubules in the cell[62]. The unfolded region of tau, which comprises most of the peptide, is prone to phosphorylation at a multitude of sites[62]. This phosphorylation alters the structure and conformation of the inherently unfolded region of tau, a process that pushes it towards folding and cleavage events that culminate in aggregation[62]. As phosphorylation occurs and accumulates, HSPs become more involved with tau (particularly HSP27 and alphaB-crystallin) to both prevent further phosphorylation and promote degradation[157]. In fact, there are positive correlations between soluble tau and HSP expression levels in the human brain, suggesting that HSPs promote soluble tau that is able to be degraded[157]. If the tau burden exceeds the HSP capacity to process it, then tau aggregation is likely to proceed unabated. Together with amyloid, these two pathological proteins heavily tax the HSP and chaperone protein response. Since this response is adaptable but not infinite, the cell is able to adapt to an extent. However, over time, the aggregation overcomes the HSP response, resulting in aggregation. It is worth putting this into context of an entire cell as well, where in addition to these pathological proteins there is the constant production and alteration of all other proteins necessary for cell function. With the elevated tau and amyloid occupying a substantial proportion of the HSPs and

cytoplasmic chaperone activity, are other processes being ignored or inappropriately managed? At present this is speculation, but it is plausible to see how these pathological proteins could indirectly affect necessary new protein synthesis and autophagy of other misfolded proteins, a cascade that would affect every aspect of the cell from metabolism to cell signaling.

I found that HSPs are being elevated in my WM OLs in the high AD pathology context exclusively (Figure 12). Considering tau and amyloid aggregation is minimal in WM from even high AD pathology patients, somehow the WM is either removing any tau or amyloid produced before it can form aggregates or simply not being exposed. However, there is evidence of mature OLs expressing tau protein[63], and amyloid-beta oligomers are soluble[58] and form plaques extracellularly, so it is unlikely that the WM is entirely devoid of tau or amyloid. Since WM OLs upregulate their HSPs in high AD pathology, this could be a partial explanation for how these pathological proteins are processed and removed. The elevated HSPs in high AD pathology WM OLs suggests they are responding to elevated pathological protein levels, and a plausible explanation is elevated amyloid and tau exposure. However, this also could be a result of elevated oxidative stress, a process which can damage existing proteins and result in their misfolding, a process that would similarly result in elevated HSPs.

An outstanding question is why there is not a corresponding increase of HSPs in GM OLs from the high AD pathology donors. One possible explanation is an underlying dysfunction in the GM OLs HSP response. Another option is that the GM OLs I are assessing are from an area that is likely severely impacted by AD pathology at the stage I am assessing (DLPFC), and it is possible the OLs remaining are simply exhausted and

unable to adequately respond to the pathology at the time of isolation. Finally, it is possible that GM OLs (and WM OLs) are unable to internalize or access amyloid or tau aggregation, particularly tau aggregates that are inside the neuron, and thus unable to process these proteins. Further studies are needed to clarify why GM OLs in the high AD pathology context are unable to elevate their HSPs and whether the ER UPR is affected as well.

Returning to the idea of oxidative stress in WM OLs, the WM is especially vulnerable to hypoxia. This vulnerability is exacerbated with age, and even further in the context of AD where blood supply to the CNS and particularly the WM is diminished further. I found significant enrichment of GSEA pathways involving cell starvation, autophagy of mitochondrion, and double-strand DNA breaks in WM OLs relative to GM OLs. This suggests WM OLs are managing more oxidative stress than GM OLs. In addition to tenuous blood flow, OLs have to store large amounts of iron for lipid and cholesterol synthesis[103]. Iron is a well-characterized free radical generator, and more iron implies more potential for oxidative stress[102]. My data found upregulation of the two transcripts that form the ferritin “box”, the primary receptacle for free iron in the cell[160], in the WM OLs from the high AD pathology donors, a pattern similar to the HSP findings. I cannot determine whether there is more iron in these OLs in my studies, but elevated ferritin is a good indicator of elevated iron stores[161]. Further, other studies have specifically identified elevated iron levels in the OLs from AD donors[162]. While both GM and WM OLs show significant elevation of the UPR in the high AD relative to low AD pathology donors, only the WM OLs show significant elevation of the heat shock protein binding specifically. Together, my data points to the WM OL being exceptionally

burdened by oxidative stress and employing multiple mechanisms to respond to it. In particular, they are repairing double-stranded DNA breaks via homologous recombination, upregulating HSPs and other chaperones to sequester unfolded proteins, producing more ferritin to sequester free iron, and possibly using autophagy for these processes (Figure 10B, Figure 12).

4.VI. A potential senescence phenotype for the human OL?

Cellular senescence is defined as “a state of permanent cell cycle arrest in response to different damaging stimuli[47]”. While this is most commonly associated with proliferative cell types, cellular senescence is possible in any cell type. I struggled to find overt evidence of senescence in OPCs, the proliferative precursor of OLs, in both cell culture and transcriptomics interrogation. However, there is a plethora of findings in mature OLs that may suggest a senescent phenotype. In short, these aspects are accumulation and repairing double-stranded DNA breaks via homologous recombination, upregulating HSPs and other chaperones to sequester unfolded proteins, immune and cytokine activity, producing more ferritin to sequester free iron, and possibly using autophagy to destroy abnormal organelles (like mitochondrion) or proteins. I found evidence that all of these pathways were especially enriched in WM OLs, especially in the context of high AD pathology donors. It is necessary to explain how each of these findings relates to senescence in other cell types to clarify its contribution to OL senescence in particular.

Elevation of the double-strand DNA break repair mechanisms is the first finding associated with cellular senescence. DNA damage is increasingly common in aging and can result in either senescence or apoptosis, seemingly depending on the magnitude

and severity of the damage[47]. This is a key point of senescence, the senescent phenotype resides somewhere “in limbo” between normal function and apoptosis, where the cell is still alive but no longer functioning as it properly should. This also highlights a challenge of identifying the senescent phenotype, namely that it is the aberrant expression of functions that are commonly present already within the cell. Thus, there is rarely a single gene or hallmark that can identify the senescent cell, rather it is a combination of reduced typical cell functions and aberrant elevation in others that defines the senescent cell type. The accumulation of DNA damage that is severe but not catastrophic can push the cell into this “limbo” where it is able to repair the damage to some extent, but not enough to resume proper functioning. The DDR requires a highly orchestrated series of events to properly repair the DNA breaks[163]. First, the damage site recruits the Ataxia-telangiectasia mutated (ATM) kinase to the site, which phosphorylates the histone H2AX (as an aside, this gamma-H2AX is commonly used as a senescence marker)[163]. Phospho-H2AX recruits the rest of the DNA repair machinery, resulting in methylation of histone 3 K9, which ultimately acetylates and activates ATM, beginning DNA repair.[163] This process requires the initial methylation of H3K9 to be reversed during the repair process to progress[163]. If the DDR is maintained, this methylation event is not reversed properly, which has multiple downstream effects[47,143,164]. First, it will result in degradation of methyltransferases that de-methylate histones[47]. Second, it will allow the unchecked phosphorylated ATM to continue phosphorylating proteins, including p53 and checkpoint kinase 1 and 2, drastically altering their activity[47]. Because I only have a single timepoint in my study, I cannot determine whether the elevated DDR in the high AD WM OLs is persistent, or whether it

was elevated due to some particular insult. Either these OLs are responding to new DNA damage, or they have persistently elevated expression akin to that seen in senescence.

The second finding in my WM OLs was elevated cytoplasmic HSP and chaperone protein expression in the high AD pathology context. Elevation of these transcripts suggests elevated chaperone production in response to elevated cytoplasmic protein misfolding, further insinuating overall cell stress. However, this could also be a result of elevated pathological protein (i.e. tau, amyloid) exposure. Protein misfolding can include denaturing and post-translational modifications, aggregation, and mislocalization[165], processes that are promoted by oxidative stress and increased pathological protein exposure. It is plausible that these elevated chaperone proteins are responding to elevated pathological aggregates or damaged proteins within the OL, a phenomenon that was unique to the high AD pathology WM. Similar to the DDR, elevated cytoplasmic chaperones are not a specific finding for senescence, and it is not possible to determine whether their elevation in my WM OLs is in response to an immediate stressor or aberrant expression. However, at a minimum I found evidence that specific cytoplasmic chaperones are elevated in the high AD pathology WM OLs.

I found consistent enrichment for cytokine activity and adaptive immunity pathways in my WM OLs. These immune pathways were significantly enriched in the old WM OLs relative to young WM OLs, as well as in WM OLs relative to GM OLs, implying the old WM OLs are exceptionally immune involved. I did find significant enrichment of cytokine and chemokine pathways in high ADNC GM OLs on CosMx as

well, providing some evidence that GM OLs may be contributing specifically to the pro-inflammatory milieu of the high AD pathology brain as well. With the previous information of upregulated cytoplasmic chaperones in these same OLs, seeing this elevation of cytokine-related pathways raises the question of whether this is a presentation of the senescence-associated secretory phenotype (SASP). The SASP is a well-characterized aspect of some senescent populations where senescent cells produce and secrete cytokines, typically in an abnormal and counter-productive manner, skewing the surrounding tissue towards a pro-inflammatory state[47]. Specifically seeing these cytokine pathways enriched in the old versus young, and high AD pathology donors aligns with what would be expected if this were senescence[143]. On a more qualitative level, I saw more expression of transcripts in the GO pathway “response to cytokine” in a manner where only a subset of the total old OLs expressed them (Figure 10C). This also adds some evidence to the idea of these OLs being senescent, as it would likely be only a subset of the total population that are truly senescent, impacting the other cells surrounding them. My CosMx data hints at a possible senescent subpopulation as well, with OL1 being enriched for cytokine pathways while OL2 is not (Figure 10J-K). However, considering OL1 comprises nearly half of all OLs identified, this would be a surprisingly high number of senescent OLs. It is unclear whether this is a true subtype of OL, or whether this is widespread senescence. Future studies will be needed to assess this.

The next finding was elevated ferritin, a proxy for elevated intracellular iron stores in the high AD pathology WM OLs. Iron accumulation has recently been implicated in fibrosis, senescence, and SASP in mice following injury, in multiple tissues including

lung and kidney[166]. This study identified persistent accumulation and maintenance of iron following injury in both a ferritin-bound and lysosomal labile state. Considering the OL has the largest stores of iron in the CNS[98], my finding of even higher levels of ferritin in the high AD pathology WM OLs is suggestive of iron accumulation in these cells beyond the “normal amount” present in younger or less stressed WM OLs. This accumulation of iron supports the idea of at least a subset of these WM OLs being senescent.

The final finding I identified that may support OL senescence is the elevation of autophagy pathways in the old WM OLs. This is challenging to isolate from the myelination-associated autophagy employed by OLs to complete myelination. However, by comparing the WM and GM OLs, there is some modest support for this claim as well. In Figure 10B, I show that autophagy and macroautophagy are enriched in WM OLs relative to GM OLs. However, when I assess various classic myelination genes like *MBP, MOG, MAG, PLP1*, and *MOBP*, I do not see much difference in the expression of these genes between WM and GM OLs. This may hint at the WM OLs doing autophagy processes that are beyond those necessary for myelination since the myelin transcripts themselves seem similar. However, this could also be a result of the type of myelin being made in WM versus GM. WM myelination is typically multiple concentric wrappings that ensheathe the axon, while GM myelination can be partial, single wrappings, full wrappings with gaps, or multiple loose wrappings with no compaction. Recall that compaction requires autophagy, so if the myelin is being produced in GM but not compacting, then there would be less autophagy-based activity present likely. This

needs to be further assessed in future studies to determine there is elevated autophagy independent of myelination in WM OLs.

Together, a potential senescent OL phenotype emerges with key instigating events of oxidative stress and pathological protein accumulation. Oxidative stress through hypoxia, iron accumulation, and abnormal metabolism causes DNA and protein damage. These processes promote the DDR and elevated chaperone protein production, respectively. In a healthy cell, these processes will adequately repair the damage and turn off. However, the AD brain is not healthy, and the pathological proteins produced and accumulated likely overwhelm the sequestering ability of chaperones, preventing it from adequately responding to the oxidative damage, preventing the DDR and chaperones from resolving the issue and remaining active. Abnormal and maintained expression of the DDR and misfolded proteins result in cytokine production and autophagy to sequester damaged mitochondria and proteins. All of these aspects work simultaneously to lead to a dysfunctional but still living OL that is no longer providing the insulating and trophic support to the axon it ensheathes. This potential senescent OL phenotype is summarized in the bottom half of Figure 14.

4.VII. Function of GM versus WM OLs

My last major question I answered was how the GM OL differed from the WM OL. The GM OL expressed significantly more synaptic transcripts than equivalent WM OLs. This finding was consistently supported by both snRNAseq. and CosMx. This was the primary difference between GM and WM OLs, although young WM OLs also showed significantly more synapse-related transcripts than old WM OLs. While the WM OL makes more myelin than GM OLs typically, I didn’t see a significant difference in

myelination transcripts between the two tissues, suggesting the GM OL produces comparable myelin transcript amounts to WM OLs.

In the context of the high AD pathology GM OLs, there was significant enrichment of immune pathways and chaperone proteins relative to no/low AD pathology, a finding similar to that found in WM OLs. However, the heat shock protein pathway specifically was no longer significantly enriched in GM OLs, hinting at a possible alternate UPR mechanism in GM OLs. Further investigation is needed to determine whether GM OLs (and younger WM OLs for that matter) are producing functional synapses, which direction these synapses “flow”, and how the OL is using these signals. My findings between WM and GM OLs are summarized in Figure 14.

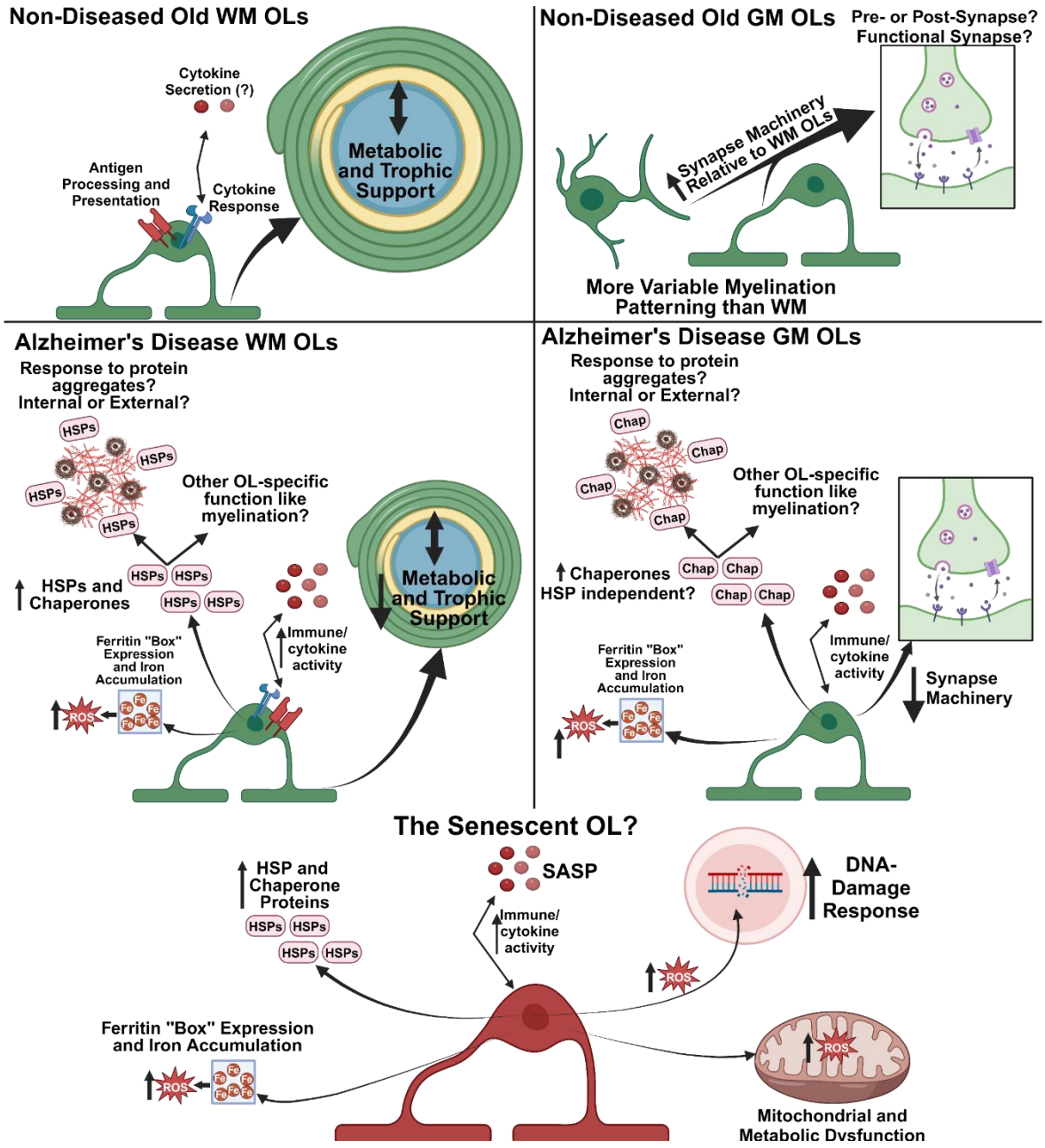

Figure 14. Cartoon schematic summarizing the findings from the snRNAseq. and CosMx data. The top half of this cartoon depicts the identified roles of WM OLs (left side) and GM OLs (right side) in the context of no/low ADNC pathology (top panels) and high ADNC pathology (bottom panels). The bottom portion of this cartoon summarizes the proposed phenotype of the senescent OL, potentially present in both WM and GM. This figure was made in BioRender.

4.VIII. Future Directions

Transcriptomic data is a phenomenal tool for identifying novel correlations and connections. However, the key limitation is that all findings are just that, correlations. Thus, all of the key findings in this thesis require follow-up and confirmatory studies. The findings of elevated ferritin, cytoplasmic chaperones, and immunological transcripts can be assessed using immunohistochemistry. This would first identify whether the transcripts being identified are being translated into functional protein, and confirm the resulting protein levels are being elevated. Numerous ferritin and iron-related stains have been developed, including assays for iron content (Prussian blue) and ferritin protein (*FTH* and *FTL* antibodies). It would be expected that high AD pathology WM OLs would show elevations in both iron content and ferritin protein levels relative to low AD pathology WM OLs. Similarly, antibody labeling of HSPs (in particular *HSPA1A, HSP90s,* and *HSPH1*) would confirm these proteins are elevated in the high AD pathology WM OLs. Finally, antibodies for cytokines and MHCs would identify whether high AD pathology WM OLs are producing these constructs, corroborating our transcriptomic findings.

Immunohistochemistry would be valuable to confirm the proposed synaptic functions of GM OLs as well. Antibodies specific to key components of the synapse (i.e. synaptotagmin, synapsin1, neurexin, nectin, neuroligin, etc.) would identify whether these elevated GM OL transcripts are forming complete synapses. Beyond this, unique antibodies to various neurotransmitters and their receptors would begin parsing out which neurotransmitters these OLs are involved with.

Beyond histological confirmatory studies, an unbiased gene clustering method would be invaluable for this dataset. Because OLs are understudied in general, and especially transcriptomically, there are few annotated pathways (GO or KEGG) unique to the OL. While some of the existing pathways were insightful and provided clues to potential unique functions, these pathways were prone to error or misidentification. This was most clearly displayed with our “unfolded protein response” GO pathway enrichment that is most likely cytoplasmic chaperone upregulation in reality. A way to work around this limitation is to use an unbiased gene expression clustering algorithm like weighted gene corollary network analysis (WGCNA) to group genes by similar expression and condition across a population of cells[167]. This method would identify clusters of genes that are expressed together within specific populations without relying on existing annotated pathways. By doing this, unique OL functionalities that do not “fit the mold” of other cell types will be identified, as well as unique OL genes that are being expressed in addition to a known pathway. This method would expand our understanding of OL-specific functionalities and begin to understand the unique OL transcriptomic landscape.

Beyond the snRNAseq., developing the methodology to extract more information from the CosMx dataset would be invaluable. A current issue with CosMx is its lack of viable neural membrane and cytoplasmic morphology markers, which drastically limits the ability of the segmentation algorithm to identify cell boundaries. Without proper cell boundaries, transcripts beyond the nucleus are impossible to localize to a particular cell, greatly limiting the utility of the spatial data. However, there are some methods that may still be informative with the current state of the CosMx data, in particular microstructure

cell variability and cell neighborhood studies. By microstructure variability, I mean the ability to identify if individual regions within the tissue have unique cell distributions and transcriptomic profiles relative to other regions. This would likely require substantial effort some “fishing”, as the technology to do this is in its infancy with this technology. Similarly, understanding which cell types are typically localized adjacent to each other could be useful information for understanding the microstructure of WM especially. Since WM is 70% OLs, understanding how the other cell types are distributed within these tissues would potentially yield useful information. Further, understanding where and how WM neurons are distributed would be interesting. As CosMx technology continues to develop, I suspect these methods will be more easily employed. In an ideal situation, proper neural membrane markers would be developed to label the cell boundaries. This would enable cytoplasmic transcripts to be localized as well as cell-to-cell interactions. A key potential strength of CosMx is the ability to apply -omics level gene coverage to an intact tissue slice, and to fully realize its potential the ability to identify cell type identity (transcriptomically) and the cell-to-cell interactivity of ALL cell types within the tissue is needed.

Now that I have identified a set of potential aspects that may represent the senescent OL, returning back to *in vitro* cell culture methods may be warranted. A key limitation of my cell culture experiments is that they were predicated on a couple studies that had identified plausible (but not definitive) senescent OL-lineage cells, especially reliant on rodent models. Without a clear senescent OL phenotype defined, I decided to employ the most commonly used senescence methods to attempt to detect senescent OLs. These methods were using etoposide or hydrogen peroxide to induce senescence

for 3 or 7 days, then using the beta-galactosidase assay as the primary readout. While I was able to induce senescence and detect it reliably in human meningeal fibroblasts, this was not the case with hiPSC-OLs. In hindsight, this is likely a result of the beta-galactosidase assay not being the right assay to detect OL senescence. I didn't find much regarding lysosomal accumulation in the transcriptomic data, which suggests beta-galactosidase may not be the right tool for the job. Using transcriptomic data as a guide, other more OL-centric assessments may be more lucrative in detecting senescence. In particular, I identified immune, cytoplasmic chaperones, DNA damage repair, and ferritin complex accumulation in OLs in the high AD complex. So, using qPCR or IHC to detect various transcripts within these pathways would be a reasonable way to identify if these cells are becoming senescent. Using an ELISA or similar to detect cytokines being secreted would be a very interesting study on how OLs may be responding to cellular stress.

Beyond the readout methods, using different senescence-inducing agents may be appropriate. Etoposide (DNA double strand breaking agent) and hydrogen peroxide (free radical generator, damaging lipid, protein, and DNA) were tried in my studies. Both seemed to result it similar senescence levels in fibroblasts but essentially resulted in death of the OLs. Using some sort of agent more biologically relevant like amyloid beta oligomers, tau protein, or cytokines may be an interesting avenue of study to assess whether these pathological proteins induce cytoplasmic chaperone production. This would add support to the idea of OLs responding to these proteins *in vivo*.

4.IX. Final Summary

In this thesis, I began with the hypothesis that human oligodendroglia could and would go senescent in the human brain. The initial approach to this question was to generate OPCs and OLs from human iPSCs to easily induce and assess whether the hiPSC-OLs would go senescent. While I was able to successfully generate hiPSC-OPCs and OLs, these cells did not go senescent but rather simply died. Because little is known about human oligodendroglia senescence, I decided the best course was to approach the question from a different angle. To this end, I generated the most comprehensive and entirely WM-focused snRNAseq. dataset to date. This dataset included WM from human donors in three groups, a young cohort (ages 27-50 at time of death), no/low ADNC pathology stage 70+ donors, and high ADNC pathology 70+ donors. I merged my OLs and OPCs with the Allen Institute's SEA-AD project focused on GM to identify how GM and WM OLs differ. Further, I generated a spatial transcriptomic dataset using Nanostring's CosMx platform on WM and GM samples from 6 donors included in both my WM and SEA-AD's GM samples to corroborate these findings and provide spatial information. In addition to showing these two technologies provide similar and comparable datasets, I found that GM OLs are producing more synaptic machinery than WM OLs. Further, I found three main OL subtypes by unique function, a myelination cluster, an immune cluster, and a synaptic cluster. Finally, I found evidence of age and AD-specific changes in OL transcription that together may provide a profile for what a senescent OL may look like, transcriptomically. This dataset will be highly valuable to other researchers and future studies beyond these important insights into OL biology.

Acknowledgements

I would like to thank the following people for their contributions on various aspects of this thesis. It takes a village to successfully execute these projects and their help was very much appreciated. First, I would like to thank my mentor, Dirk, for the help throughout my projects, giving advice and providing the resources I needed to succeed. Thank you to my committee for their support and guidance as well.

In Dirk's laboratory, I would like to thank Angela Wilson for helping me throughout the entire process. She was my point person for tissue sampling, 10x and Nanostring-based technologies, and moral support. I value her input immensely and would not have been able to complete these projects without her. I would also like to thank Mamatha Damodarasamy for her help. Her RNA work is fantastic and her help with Nanostring was invaluable. I would also like to thank Amanda Kirkland for her help with tissue sampling, sectioning, slide preparation, histology, and a multitude of other things she was integrally involved with. And, thank you to the rest of the Keene lab for their help and support throughout the years.

I would like to thank Scott Kennedy for his help with sequencing, analysis, and review and refinement of my thesis and manuscript. He was my primary sequencing person and has provided immense support along this project. Thank you to Brendan Kohrn and Cindy Reichel in Scott's lab as well, for their assistance on sequencing.

Thank you Jessica Young and Shannon Rose for their help with the cell culture aspects of this thesis. The lines used were all from them, and their guidance on the complex and fascinating world of stem cell biology was crucial to my success.

A special thanks to Jeremy Miller at the Allen Institute for his assistance and critique of the GM and WM omics analyses, as well as helping me troubleshoot and develop my pipelines and analyses. He went above and beyond to help, and I am very grateful for the assistance.

References

1. Azevedo, F. A. C. *et al.* Equal numbers of neuronal and nonneuronal cells make the human brain an isometrically scaled-up primate brain. *J. Comp. Neurol.* **513**, 532–541 (2009).
2. Herculano-Houzel, S., Mota, B. & Lent, R. Cellular scaling rules for rodent brains. *Proc. Natl. Acad. Sci. U. S. A.* **103**, 12138–12143 (2006).
3. Zhang, K. & Sejnowski, T. J. A universal scaling law between gray matter and white matter of cerebral cortex. *Proc. Natl. Acad. Sci. U. S. A.* **97**, 5621–5626 (2000).
4. Herculano-Houzel, S., Mota, B., Wong, P. & Kaas, J. H. Connectivity-driven white matter scaling and folding in primate cerebral cortex. *Proc. Natl. Acad. Sci. U. S. A.* **107**, 19008–19013 (2010).
5. Assaf, Y. & Pasternak, O. Diffusion Tensor Imaging (DTI)-based White Matter Mapping in Brain Research: A Review. *J. Mol. Neurosci.* **34**, 51–61 (2008).
6. Nave, K. A. & Werner, H. B. Myelination of the nervous system: Mechanisms and functions. *Annu. Rev. Cell Dev. Biol.* **30**, 503–533 (2014).
7. Bankston, A. N. *et al.* Autophagy is essential for oligodendrocyte differentiation, survival, and proper myelination. *Glia* **67**, 1745–1759 (2019).
8. Simons, M. & Nave, K. A. Oligodendrocytes: Myelination and axonal support. *Cold Spring Harb. Perspect. Biol.* **8**, 1–16 (2016).
9. Suzuki, K. Myelin: A Specialized Membrane for Cell Communication. *Nat. Educ.* **3**, 59 (2010).
10. Pan, S., Mayoral, S. R., Choi, H. S., Chan, J. R. & Kheirbek, M. A. Preservation of

a remote fear memory requires new myelin formation. *Nat. Neurosci.* (2020) doi:10.1038/s41593-019-0582-1.

11. Gibson, E. M. *et al.* Neuronal Activity Promotes Oligodendrogenesis and Adaptive Myelination in the Mammalian Brain. *Science (80-.).* **344**, (2014).
12. Yeung, M. S. Y. *et al.* Dynamics of oligodendrocyte generation and myelination in the human brain. *Cell* **159**, 766–774 (2014).
13. Kirby, B. B. *et al.* In vivo time-lapse imaging shows dynamic oligodendrocyte progenitor behavior during zebrafish development. *Nat. Neurosci.* **9**, 1506–1511 (2006).
14. Dawson, M. R. L., Polito, A., Levine, J. M. & Reynolds, R. NG2-expressing glial progenitor cells: An abundant and widespread population of cycling cells in the adult rat CNS. *Mol. Cell. Neurosci.* **24**, 476–488 (2003).
15. von Bartheld, C. S., Bahney, J. & Herculano-Houzel, S. The search for true numbers of neurons and glial cells in the human brain: A review of 150 years of cell counting. *J. Comp. Neurol.* **524**, 3865–3895 (2016).
16. Nave, K. A. Myelination and the trophic support of long axons. *Nat. Rev. Neurosci.* **11**, 275–283 (2010).
17. Mergenthaler, P., Lindauer, U., Dienel, G. A. & Meisel, A. Sugar for the brain: the role of glucose in physiological and pathological brain function. *Trends Neurosci.* **36**, 587–97 (2013).
18. Domènech-Estévez, E. *et al.* Distribution of monocarboxylate transporters in the peripheral nervous system suggests putative roles in lactate shuttling and myelination. *J. Neurosci.* **35**, 4151–4156 (2015).

19. Philips, T. *et al.* MCT1 Deletion in Oligodendrocyte Lineage Cells Causes Late-Onset Hypomyelination and Axonal Degeneration. *Cell Rep.* **34**, 108610 (2021).
20. Lee, Y. *et al.* Oligodendroglia metabolically support axons and contribute to neurodegeneration. *Nature* **487**, 443–448 (2012).
21. Looser, Z. J. *et al.* Oligodendrocyte–axon metabolic coupling is mediated by extracellular K+ and maintains axonal health. *Nat. Neurosci.* **27**, 433–448 (2024).
22. Chamberlain, K. A. *et al.* Oligodendrocytes enhance axonal energy metabolism by deacetylation of mitochondrial proteins through transcellular delivery of SIRT2. *Neuron* **109**, 3456-3472.e8 (2021).
23. Jang, M., Gould, E., Xu, J., Kim, E. J. & Kim, J. H. Oligodendrocytes regulate presynaptic properties and neurotransmission through bdnf signaling in the mouse brainstem. *Elife* **8**, 1–26 (2019).
24. Wilkins, A., Majed, H., Layfield, R., Compston, A. & Chandran, S. Oligodendrocytes promote neuronal survival and axonal length by distinct intracellular mechanisms: A novel role for oligodendrocyte-derived glial cell line-derived neurotrophic factor. *J. Neurosci.* **23**, 4967–4974 (2003).
25. Du, Y. & Dreyfus, C. F. Oligodendrocytes as providers of growth factors. *J. Neurosci. Res.* **68**, 647–654 (2002).
26. Richardson, W. D., Kessaris, N. & Pringle, N. Oligodendrocyte wars. *Nat. Rev. Neurosci.* **7**, 11–18 (2006).
27. Huang, W. *et al.* Origins and Proliferative States of Human Oligodendrocyte Precursor Cells. *Cell* **182**, 594-608.e11 (2020).
28. Chen, J.-F. *et al.* Enhancing myelin renewal reverses cognitive dysfunction in a

murine model of Alzheimer's disease. *Neuron* **109**, 2292-2307.e5 (2021).

29. Tepavčević, V. & Lubetzki, C. Oligodendrocyte progenitor cell recruitment and remyelination in multiple sclerosis: the more, the merrier? *Brain* **145**, 4178–4192 (2022).
30. Boyd, A., Zhang, H. & Williams, A. Insufficient OPC migration into demyelinated lesions is a cause of poor remyelination in MS and mouse models. *Acta Neuropathol.* **125**, 841–59 (2013).
31. Kaes, T. *Die Grosshirnrinde Des Menschen in Ihren Massen Und in Ihrem Fasergehalt*. (Fischer, 1907, 1907).
32. Bartzokis, G. Age-related myelin breakdown: A developmental model of cognitive decline and Alzheimer's disease. *Neurobiol. Aging* **25**, 5–18 (2004).
33. López-Otín, C., Blasco, M. A., Partridge, L., Serrano, M. & Kroemer, G. The Hallmarks of Aging. *Cell* **153**, 1194–1217 (2013).
34. López-Otín, C., Blasco, M. A., Partridge, L., Serrano, M. & Kroemer, G. Hallmarks of aging: An expanding universe. *Cell* **186**, 243–278 (2023).
35. Feldman, M. L. & Peters, A. Ballooning of myelin sheaths in normally aged macaques. *J. Neurocytol.* **27**, 605–614 (1998).
36. Wang, F. *et al.* Myelin degeneration and diminished myelin renewal contribute to age-related deficits in memory. *Nat. Neurosci.* (2020) doi:10.1038/s41593-020-0588-8.
37. Young, K. M. *et al.* Oligodendrocyte dynamics in the healthy adult CNS: Evidence for myelin remodeling. *Neuron* **77**, 873–885 (2013).
38. Belgrad, J., De Pace, R. & Fields, R. D. Autophagy in Myelinating Glia. *J.*

Neurosci. **40**, 256–266 (2020).

39. Dutta, D. J. *et al.* Regulation of myelin structure and conduction velocity by perinodal astrocytes. *Proc. Natl. Acad. Sci. U. S. A.* **115**, 11832–11837 (2018).
40. Hughes, A. N. & Appel, B. Microglia phagocytose myelin sheaths to modify developmental myelination. *Nat. Neurosci.* **23**, 1055–1066 (2020).
41. Safaiyan, S. *et al.* Age-related myelin degradation burdens the clearance function of microglia during aging. *Nat. Neurosci.* **19**, 995–998 (2016).
42. Nicaise, A. M. *et al.* Cellular senescence in progenitor cells contributes to diminished remyelination potential in progressive multiple sclerosis. *Proc. Natl. Acad. Sci. U. S. A.* **116**, 9030–9039 (2019).
43. Binamé, F., Pham-Van, L. D. & Bagnard, D. Manipulating oligodendrocyte intrinsic regeneration mechanism to promote remyelination. *Cell. Mol. Life Sci.* **78**, 5257–5273 (2021).
44. Leenders, F. *et al.* Navigating oligodendrocyte precursor cell aging in brain health. *Mech. Ageing Dev.* **220**, 111959 (2024).
45. Huang, W., Hickson, L. J., Eirin, A., Kirkland, J. L. & Lerman, L. O. Cellular senescence: the good, the bad and the unknown. *Nat. Rev. Nephrol.* **18**, 611–627 (2022).
46. Rai, T. S. & Adams, P. D. Lessons from senescence: Chromatin maintenance in non-proliferating cells. *Biochim. Biophys. Acta* **1819**, 322–31 (2012).
47. Hernandez-Segura, A., Nehme, J. & Demaria, M. Hallmarks of Cellular Senescence. *Trends Cell Biol.* **28**, 436–453 (2018).
48. Bussian, T. J. *et al.* Clearance of senescent glial cells prevents tau-dependent

pathology and cognitive decline. *Nature* **562**, 578–582 (2018).

49. Lenze, E. Dasatinib Plus Quercetin for Accelerated Aging in Mental Disorders - ID:NCT05838560. *ClinicalTrials.gov* https://clinicaltrials.gov/study/NCT05838560?intr=Dasatinib %2B Quercetin&rank=1 (2025).
50. Zhang, P. *et al.* Senolytic therapy alleviates Aβ-associated oligodendrocyte progenitor cell senescence and cognitive deficits in an Alzheimer's disease model. *Nat. Neurosci.* **22**, 719–728 (2019).
51. Gomez, P. T. *et al.* Aging and senescent fates of oligodendrocyte precursor cells in the mouse brain. *npj Aging* **10**, 1–7 (2024).
52. Alzheimer's Disease International. Dementia statistics. https://www.alzint.org/about/dementia-facts-figures/dementia-statistics/#:~:text=Someone in the world develops,will be in developing countries.
53. Alzheimer's Association. Alzheimer's disease facts and figures. (2024).
54. Rajan, K. B., Weuve, J., Barnes, L. L., Wilson, R. S. & Evans, D. A. Prevalence and incidence of clinically diagnosed Alzheimer's disease dementia from 1994 to 2012 in a population study. *Alzheimer's Dement.* **15**, 1–7 (2019).
55. Manly, J. J. *et al.* Estimating the Prevalence of Dementia and Mild Cognitive Impairment in the US: The 2016 Health and Retirement Study Harmonized Cognitive Assessment Protocol Project. *JAMA Neurol.* **79**, 1242–1249 (2022).
56. Mayo Clinic. Alzheimer's Disease. *Diseases and Conditions* https://www.mayoclinic.org/diseases-conditions/alzheimers-disease/symptoms-causes/syc-20350447#:~:text=Alzheimer's disease is the most,and the brain to

shrink. (2024).

57. Kramarow, E. A. Diagnosed Dementia in Adults Age 65 and Older: United States, 2022. *Natl. Health Stat. Report.* **2024**, 1–8 (2024).

58. Chen, G. F. *et al.* Amyloid beta: Structure, biology and structure-based therapeutic development. *Acta Pharmacol. Sin.* **38**, 1205–1235 (2017).

59. Sengupta, U., Nilson, A. N. & Kayed, R. The Role of Amyloid-β Oligomers in Toxicity, Propagation, and Immunotherapy. *EBioMedicine* **6**, 42–49 (2016).

60. Zhang, Y., Chen, H., Li, R., Sterling, K. & Song, W. Amyloid β-based therapy for Alzheimer's disease: challenges, successes and future. *Signal Transduct. Target. Ther.* **8**, 248 (2023).

61. Guo, T., Noble, W. & Hanger, D. P. Roles of tau protein in health and disease. *Acta Neuropathol.* **133**, 665–704 (2017).

62. Wang, Y. & Mandelkow, E. Tau in physiology and pathology. *Nat. Rev. Neurosci.* **17**, 5–21 (2016).

63. Torii, T. *et al.* Identification of Tau protein as a novel marker for maturation and pathological changes of oligodendrocytes. *Glia* **71**, 1002–1017 (2023).

64. Taddei, R. N. *et al.* Tau Oligomer-Containing Synapse Elimination by Microglia and Astrocytes in Alzheimer Disease. *JAMA Neurol.* **80**, 1209–1221 (2023).

65. Mandelkow, E. M. & Mandelkow, E. Biochemistry and cell biology of Tau protein in neurofibrillary degeneration. *Cold Spring Harb. Perspect. Biol.* **3**, 1–25 (2011).

66. Chen, S., Townsend, K., Goldberg, T. E., Davies, P. & Conejero-Goldberg, C. MAPT Isoforms: Differential Transcriptional Profiles Related to 3R and 4R Splice Variants. *J. Alzheimer's Dis.* **22**, 1313–1329 (2011).

67. Busche, M. A. & Hyman, B. T. Synergy between amyloid-β and tau in Alzheimer's disease. *Nat. Neurosci.* **23**, 1183–1193 (2020).

68. Matsuo, E. S. *et al.* Biopsy-derived adult human brain tau is phosphorylated at many of the same sites as Alzheimer's disease paired helical filament tau. *Neuron* **13**, 989–1002 (1994).

69. Köpke, E. *et al.* Microtubule-associated protein tau: Abnormal phosphorylation of a non-paired helical filament pool in Alzheimer disease. *J. Biol. Chem.* **268**, 24374–24384 (1993).

70. Thal, D. R., Rüb, U., Orantes, M. & Braak, H. Phases of Aβ-deposition in the human brain and its relevance for the development of AD. *Neurology* **58**, 1791–1800 (2002).

71. Serrano-Pozo, A. *et al.* Thal amyloid stages do not significantly impact the correlation between neuropathological change and cognition in the Alzheimer disease continuum. *J. Neuropathol. Exp. Neurol.* **75**, 516–526 (2016).

72. Matthews, K. Tau protein abnormalities correlate with the severity of dementia in Alzheimer's disease. *Nat. Clin. Pract. Neurol.* **2**, 178–178 (2006).

73. Braak, H., Alafuzoff, I., Arzberger, T., Kretzschmar, H. & Tredici, K. Staging of Alzheimer disease-associated neurofibrillary pathology using paraffin sections and immunocytochemistry. *Acta Neuropathol.* **112**, 389–404 (2006).

74. Braak, H. & Braak, E. Neuropathological stageing of Alzheimer-related changes. *Acta Neuropathol.* **82**, 239–259 (1991).

75. Franzmeier, N. *et al.* Functional brain architecture is associated with the rate of tau accumulation in Alzheimer's disease. *Nat. Commun.* **11**, 1–17 (2020).

76. Hyman, B. T. *et al.* National Institute on Aging-Alzheimer's Association guidelines for the neuropathologic assessment of Alzheimer's disease. *Alzheimer's Dement.* **8**, 1–13 (2012).

77. Moms, J. C. *et al.* The Consortium to Establish a Registry for Alzheimer's Disease (CERAD). Part I. Clinical and neuropsychological assesment of Alzheimer's disease. *Neurology* **39**, 1159–1159 (1989).

78. Mirra, S. S. *et al.* The Consortium to Establish a Registry for Alzheimer's Disease (CERAD): Part II. Standardization of the neuropathologic assessment of Alzheimer's disease. *Neurology* **41**, 479–479 (1991).

79. Bartzokis, G. *et al.* White matter structural integrity in healthy aging adults and patients with Alzheimer disease: A magnetic resonance imaging study. *Arch. Neurol.* **60**, 393–398 (2003).

80. Dean, D. C. *et al.* Association of amyloid pathology with myelin alteration in preclinical Alzheimer disease. *JAMA Neurol.* **74**, 41–49 (2017).

81. Migliaccio, R. *et al.* White matter atrophy in Alzheimer's disease variants. *Alzheimer's Dement.* **8**, (2012).

82. Rémy, F., Vayssière, N., Saint-Aubert, L., Barbeau, E. & Pariente, J. White matter disruption at the prodromal stage of Alzheimer's disease: Relationships with hippocampal atrophy and episodic memory performance. *NeuroImage Clin.* **7**, 482–492 (2015).

83. Lee, S. *et al.* White matter hyperintensities are a core feature of Alzheimer's disease: Evidence from the dominantly inherited Alzheimer network. *Ann. Neurol.* **79**, 929–939 (2016).

84. Bartzokis, G., Lu, P. H. & Mintz, J. Human brain myelination and amyloid beta deposition in Alzheimer's disease. *Alzheimer's Dement.* **3**, 122–125 (2007).

85. Duncan, I. D., Marik, R. L., Broman, A. T. & Heidari, M. Thin myelin sheaths as the hallmark of remyelination persist over time and preserve axon function. *Proc. Natl. Acad. Sci. U. S. A.* **114**, E9685–E9691 (2017).

86. De la Rosa, A. *et al.* Physical exercise in the prevention and treatment of Alzheimer's disease. *J. Sport Heal. Sci.* **9**, 394–404 (2020).

87. Faulkner, M. E. *et al.* Evidence of association between higher cardiorespiratory fitness and higher cerebral myelination in aging. *Proc. Natl. Acad. Sci.* **121**, 2017 (2024).

88. Tsuno, N. & Homma, A. What is the association between depression and Alzheimer's disease? *Expert Rev. Neurother.* **9**, 1667–1676 (2009).

89. Ownby, R. L., Crocco, E., Acevedo, A., John, V. & Loewenstein, D. Depression and Risk for Alzheimer Disease. *Arch. Gen. Psychiatry* **63**, 530 (2006).

90. Teissier, A. *et al.* Early-life stress impairs postnatal oligodendrogenesis and adult emotional behaviour through activity-dependent mechanisms. *Mol. Psychiatry* (2019) doi:10.1038/s41380-019-0493-2.

91. Sacchet, M. D. & Gotlib, I. H. Myelination of the brain in major depressive disorder: An in vivo quantitative magnetic resonance imaging study. *Sci. Rep.* **7**, 1–14 (2017).

92. Gabitto, M. I. *et al.* Integrated multimodal cell atlas of Alzheimer's disease. *Nat. Neurosci.* (2024) doi:10.1038/s41593-024-01774-5.

93. Depp, C. *et al.* Myelin dysfunction drives amyloid-β deposition in models of

Alzheimer's disease. *Nature* **618**, 349–357 (2023).

94. Sasmita, A. O. *et al.* Oligodendrocytes produce amyloid-β and contribute to plaque formation alongside neurons in Alzheimer's disease model mice. *Nat. Neurosci.* **27**, 1668–1674 (2024).

95. Blanchard, J. W. *et al.* APOE4 impairs myelination via cholesterol dysregulation in oligodendrocytes. *Nature* **611**, 769–779 (2022).

96. Xu, J. *et al.* Amyloid-beta peptides are cytotoxic to oligodendrocytes. *J. Neurosci.* **21**, 1–5 (2001).

97. Ferrer, I. *et al.* Involvement of oligodendrocytes in tau seeding and spreading in tauopathies. *Front. Aging Neurosci.* **11**, 1–16 (2019).

98. Quintana, C. *et al.* Study of the localization of iron, ferritin, and hemosiderin in Alzheimer's disease hippocampus by analytical microscopy at the subcellular level. *J. Struct. Biol.* **153**, 42–54 (2006).

99. Reinert, A., Morawski, M., Seeger, J., Arendt, T. & Reinert, T. Iron concentrations in neurons and glial cells with estimates on ferritin concentrations. *BMC Neurosci.* **20**, 1–14 (2019).

100. Bartzokis, G. *et al.* Brain ferritin iron may influence age- and gender-related risks of neurodegeneration. *Neurobiol. Aging* **28**, 414–423 (2007).

101. Cheli, V. T., Correale, J., Paez, P. M. & Pasquini, J. M. Iron Metabolism in Oligodendrocytes and Astrocytes, Implications for Myelination and Remyelination. *ASN Neuro* **12**, (2020).

102. Valko, M., Morris, H. & Cronin, M. T. D. Metals, toxicity and oxidative stress. *Curr. Med. Chem.* **12**, 1161–208 (2005).

103. Connor, J. R. & Menzies, S. L. Relationship of iron to oligodendrocytes and myelination. *Glia* **17**, 83–93 (1996).

104. Bartzokis, G. Alzheimer's disease as homeostatic responses to age-related myelin breakdown. *Neurobiol. Aging* **32**, 1341–1371 (2011).

105. Dietschy, J. M. & Turley, S. D. Cholesterol metabolism in the central nervous system during early development and in the mature animal. *Journal of Lipid Research* vol. 45 1375–1397 at https://doi.org/10.1194/jlr.R400004-JLR200 (2004).

106. Morell, P. & Jurevics, H. Origin of cholesterol in myelin. *Neurochem. Res.* **21**, 463–470 (1996).

107. MOREIRA, P. I. *et al.* Oxidative Stress and Neurodegeneration. *Ann. N. Y. Acad. Sci.* **1043**, 545–552 (2005).

108. Wiggins, R. C. Myelin development and nutritional insufficiency. *Brain Res.* **257**, 151–75 (1982).

109. Torvik, A. The Pathogenesis of Watershed Infarcts in the Brain. *Stroke* **8**, 299–301 (1983).

110. Toubasi, A. A. *et al.* Watershed regions are more susceptible to tissue microstructural injury in multiple sclerosis. *Brain Commun.* **6**, 1–13 (2024).

111. Goldsmith, H. S. Alzheimer's Disease: A Decreased Cerebral Blood Flow to Critical Intraneuronal Elements Is the Cause. *J. Alzheimers. Dis.* **85**, 1419–1422 (2022).

112. Govindpani, K. *et al.* Vascular dysfunction in Alzheimer's disease: A prelude to the pathological process or a consequence of it? *J. Clin. Med.* **8**, 1–57 (2019).

113. Zhou, J. NG2 glia regulate brain innate immunity via TGF-β2/TGFBR2 axis. *IBRO Reports* **6**, S34 (2019).

114. Kirby, L. *et al.* Oligodendrocyte precursor cells present antigen and are cytotoxic targets in inflammatory demyelination. *Nat. Commun.* **10**, 1–20 (2019).

115. Zeis, T., Enz, L. & Schaeren-Wiemers, N. The immunomodulatory oligodendrocyte. *Brain Res.* **1641**, 139–148 (2016).

116. Falcão, A. M. *et al.* Disease-specific oligodendrocyte lineage cells arise in multiple sclerosis. *Nat. Med.* **24**, 1837–1844 (2018).

117. Zveik, O., Rechtman, A., Brill, L. & Vaknin-Dembinsky, A. Anti- and pro-inflammatory milieu differentially regulate differentiation and immune functions of oligodendrocyte progenitor cells. *Immunology* **171**, 618–633 (2024).

118. Timmler, S. & Simons, M. Grey matter myelination. *Glia* **67**, 2063–2070 (2019).

119. Tomassy, G. S. *et al.* Distinct Profiles of Myelin Distribution Along Single Axons of Pyramidal Neurons in the Neocortex. *Science (80-.).* **344**, 319–324 (2014).

120. Kang, S. H. *et al.* Degeneration and impaired regeneration of gray matter oligodendrocytes in amyotrophic lateral sclerosis. *Nat. Neurosci.* **16**, 571–579 (2013).

121. Douvaras, P. & Fossati, V. Generation and isolation of oligodendrocyte progenitor cells from human pluripotent stem cells. *Nat. Protoc.* **10**, 1143–1154 (2015).

122. Vetter, R. & Iber, D. Precision of morphogen gradients in neural tube development. *Nat. Commun.* **13**, 1145 (2022).

123. Carballo, G. B., Honorato, J. R., de Lopes, G. P. F. & Spohr, T. C. L. de S. e. A highlight on Sonic hedgehog pathway. *Cell Commun. Signal.* **16**, 11 (2018).

124. Huff, T. C. *et al.* Vitamin C regulates Schwann cell myelination by promoting DNA demethylation of pro-myelinating genes. *J. Neurochem.* **157**, 1759–1773 (2021).
125. Bechler, M. E. A Neuron-Free Microfiber Assay to Assess Myelin Sheath Formation. in 97–110 (2019). doi:10.1007/978-1-4939-9072-6_6.
126. Lee, S. *et al.* A culture system to study oligodendrocyte myelination processes using engineered nanofibers. *Nat. Methods* **9**, 917–922 (2012).
127. de Faria, O., Gonsalvez, D. G., Nicholson, M. & Xiao, J. Activity-dependent central nervous system myelination throughout life. *J. Neurochem.* **148**, 447–461 (2019).
128. Ravanelli, A. M. *et al.* Sequential specification of oligodendrocyte lineage cells by distinct levels of Hedgehog and Notch signaling. *Dev. Biol.* **444**, 93–106 (2018).
129. Barber, H. M., Ali, M. F. & Kucenas, S. Glial Patchwork: Oligodendrocyte Progenitor Cells and Astrocytes Blanket the Central Nervous System. *Front. Cell. Neurosci.* **15**, (2022).
130. Casper, K. B. & McCarthy, K. D. GFAP-positive progenitor cells produce neurons and oligodendrocytes throughout the CNS. *Mol. Cell. Neurosci.* **31**, 676–684 (2006).
131. Mabie, P. C. *et al.* Bone Morphogenetic Proteins Induce Astroglial Differentiation of Oligodendroglial–Astroglial Progenitor Cells. *J. Neurosci.* **17**, 4112–4120 (1997).
132. LLeonart, M. E., Artero-Castro, A. & Kondoh, H. Senescence induction; a possible cancer therapy. *Mol. Cancer* **8**, 3 (2009).
133. Zhang, J., Yu, H., Man, M.-Q. & Hu, L. Aging in the dermis: Fibroblast

senescence and its significance. *Aging Cell* **23**, e14054 (2024).

134. Schmitt, C. A., Wang, B. & Demaria, M. Senescence and cancer — role and therapeutic opportunities. *Nat. Rev. Clin. Oncol.* **19**, 619–636 (2022).
135. Hines, J. H. Evolutionary Origins of the Oligodendrocyte Cell Type and Adaptive Myelination. *Front. Neurosci.* **15**, (2021).
136. Mitroi, D. N., Tian, M., Kawaguchi, R., Lowry, W. E. & Carmichael, S. T. Single-nucleus transcriptome analysis reveals disease- and regeneration-associated endothelial cells in white matter vascular dementia. *J. Cell. Mol. Med.* **26**, 3183–3195 (2022).
137. Elkjaer, M. L. *et al.* Single-Cell Multi-Omics Map of Cell Type–Specific Mechanistic Drivers of Multiple Sclerosis Lesions. *Neurol. Neuroimmunol. Neuroinflammation* **11**, (2024).
138. Chancellor, K. B. *et al.* Altered oligodendroglia and astroglia in chronic traumatic encephalopathy. *Acta Neuropathol.* **142**, 295–321 (2021).
139. Buyanova, I. S. & Arsalidou, M. Cerebral White Matter Myelination and Relations to Age, Gender, and Cognition: A Selective Review. *Front. Hum. Neurosci.* **15**, 662031 (2021).
140. Nelson, P. T. *et al.* LATE-NC staging in routine neuropathologic diagnosis: an update. *Acta Neuropathol.* **145**, 159–173 (2023).
141. Armstrong, R. A. When to use the Bonferroni correction. *Ophthalmic Physiol. Opt.* **34**, 502–508 (2014).
142. Benjamini, Y. & Hochberg, Y. Controlling the False Discovery Rate: A Practical and Powerful Approach to Multiple Testing. *J. R. Stat. Soc. Ser. B Stat. Methodol.*

57, 289–300 (1995).

143. Pluquet, O., Pourtier, A. & Abbadie, C. The unfolded protein response and cellular senescence. A Review in the Theme: Cellular Mechanisms of Endoplasmic Reticulum Stress Signaling in Health and Disease. *Am. J. Physiol. Physiol.* **308**, C415–C425 (2015).
144. Hetz, C. The unfolded protein response: controlling cell fate decisions under ER stress and beyond. *Nat. Rev. Mol. Cell Biol.* **13**, 89–102 (2012).
145. Saibil, H. Chaperone machines for protein folding, unfolding and disaggregation. *Nat. Rev. Mol. Cell Biol.* **14**, 630–642 (2013).
146. Park, S.-H. *et al.* The cytoplasmic Hsp70 chaperone machinery subjects misfolded and endoplasmic reticulum import-incompetent proteins to degradation via the ubiquitin-proteasome system. *Mol. Biol. Cell* **18**, 153–65 (2007).
147. Hoter, A., El-Sabban, M. E. & Naim, H. Y. The HSP90 Family: Structure, Regulation, Function, and Implications in Health and Disease. *Int. J. Mol. Sci.* **19**, (2018).
148. Hughes, A. N. & Appel, B. Oligodendrocytes express synaptic proteins that modulate myelin sheath formation. *Nat. Commun.* **10**, 1–15 (2019).
149. Gautier, H. O. B. *et al.* Neuronal activity regulates remyelination via glutamate signalling to oligodendrocyte progenitors. *Nat. Commun.* **6**, 8518 (2015).
150. Schirmer, L. *et al.* Oligodendrocyte-encoded Kir4.1 function is required for axonal integrity. *Elife* **7**, (2018).
151. Livesey, M. R. *et al.* Maturation and electrophysiological properties of human pluripotent stem cell-derived oligodendrocytes. *Stem Cells* **34**, 1040–1053 (2016).

152. Balusu, S. *et al.* MEG3 activates necroptosis in human neuron xenografts modeling Alzheimer's disease. *Science (80-.).* **381**, 1176–1182 (2023).

153. Hernández, D. E. *et al.* Axonal degeneration induced by glutamate excitotoxicity is mediated by necroptosis. *J. Cell Sci.* **131**, (2018).

154. McKenzie, I. A. *et al.* Motor skill learning requires active central myelination. *Science (80-.).* **346**, 318–322 (2014).

155. Michaud, M. *et al.* Proinflammatory Cytokines, Aging, and Age-Related Diseases. *J. Am. Med. Dir. Assoc.* **14**, 877–882 (2013).

156. Heppner, F. L., Ransohoff, R. M. & Becher, B. Immune attack: The role of inflammation in Alzheimer disease. *Nat. Rev. Neurosci.* **16**, 358–372 (2015).

157. Sahara, N. *et al.* Molecular chaperone-mediated tau protein metabolism counteracts the formation of granular tau oligomers in human brain. *J. Neurosci. Res.* **85**, 3098–3108 (2007).

158. Koren, J. *et al.* Chaperone signalling complexes in Alzheimer's disease. *J. Cell. Mol. Med.* **13**, 619–630 (2009).

159. Evans, C. G., Wisén, S. & Gestwicki, J. E. Heat Shock Proteins 70 and 90 Inhibit Early Stages of Amyloid β-(1–42) Aggregation in Vitro. *J. Biol. Chem.* **281**, 33182–33191 (2006).

160. Cheli, V. T., Correale, J., Paez, P. M. & Pasquini, J. M. Iron Metabolism in Oligodendrocytes and Astrocytes, Implications for Myelination and Remyelination. *ASN Neuro* **12**, 1759091420962681 (2020).

161. Koperdanova, M. & Cullis, J. O. Interpreting raised serum ferritin levels. *BMJ* h3692 (2015) doi:10.1136/bmj.h3692.

162. Liu, J.-L., Fan, Y.-G., Yang, Z.-S., Wang, Z.-Y. & Guo, C. Iron and Alzheimer's Disease: From Pathogenesis to Therapeutic Implications. *Front. Neurosci.* **12**, (2018).

163. Giglia-Mari, G., Zotter, A. & Vermeulen, W. DNA Damage Response. *Cold Spring Harb. Perspect. Biol.* **3**, a000745–a000745 (2011).

164. Schwab, N., Grenier, K. & Hazrati, L. N. DNA repair deficiency and senescence in concussed professional athletes involved in contact sports. *Acta Neuropathol. Commun.* **7**, 1–23 (2019).

165. Brettschneider, J., Del Tredici, K., Lee, V. M. Y. & Trojanowski, J. Q. Spreading of pathology in neurodegenerative diseases: A focus on human studies. *Nat. Rev. Neurosci.* **16**, 109–120 (2015).

166. Maus, M. *et al.* Iron accumulation drives fibrosis, senescence and the senescence-associated secretory phenotype. *Nat. Metab.* **5**, 2111–2130 (2023).

167. Langfelder, P. & Horvath, S. WGCNA: an R package for weighted correlation network analysis. *BMC Bioinformatics* **9**, 559 (2008).